DESIGN, SIMULATION, AND FABRICATION OF LOW-COST CHIPLESS
RFID TAGS

A THESIS SUBMITTED TO
THE GRADUATE SCHOOL OF NATURAL AND APPLIED SCIENCES
OF
MIDDLE EAST TECHNICAL UNIVERSITY

BY

ELİF ÇETİN

IN PARTIAL FULFILLMENT OF THE REQUIREMENTS
FOR
THE DEGREE OF MASTER OF SCIENCE
IN
ELECTRICAL AND ELECTRONICS ENGINEERING

NOVEMBER 2019

Approval of the thesis:

DESIGN, SIMULATION, AND FABRICATION OF LOW-COST CHIPLESS RFID TAGS

submitted by **ELİF ÇETİN** in partial fulfillment of the requirements for the degree of **Master of Science in Electrical and Electronics Engineering Department, Middle East Technical University** by,

Prof. Dr. Halil Kalıpçılar
Dean, Graduate School of **Natural and Applied Sciences**   _____

Prof. Dr. İlkay Ulusoy
Head of Department, **Electrical and Electronics Eng.**   _____

Assoc. Prof. Dr. Özgür Ergül
Supervisor, **Electrical and Electronics Eng., METU**   _____

Examining Committee Members:

Prof. Dr. Özlem Aydın Çivi
Electrical and Electronics Eng., METU   _____

Assoc. Prof. Dr. Özgür Ergül
Electrical and Electronics Eng., METU   _____

Assoc. Prof. Dr. Lale Alatan
Electrical and Electronics Eng., METU   _____

Prof. Dr. Çiğdem Seçkin Gürel
Electrical and Electronics Eng., Hacettepe University   _____

Prof. Dr. Asım Egemen Yılmaz
Electrical and Electronics Eng., Ankara University   _____

Date: 29.11.2019

I hereby declare that all information in this document has been obtained and presented in accordance with academic rules and ethical conduct. I also declare that, as required by these rules and conduct, I have fully cited and referenced all material and results that are not original to this work.

Name, Surname: Elif Çetin

Signature:

ABSTRACT

DESIGN, SIMULATION, AND FABRICATION OF LOW-COST CHIPLESS RFID TAGS

Çetin, Elif
Master of Science, Electrical and Electronics Engineering
Supervisor: Assoc. Prof. Dr. Özgür Ergül

November 2019, 93 pages

In this thesis, low-cost chipless radio-frequency-identification (RFID) tags are investigated. These types of tags are proposed and developed to replace barcodes in item-level tagging. In addition to the standard methods using printed circuit boards (PCBs), chipless RFID tags are suitable to be fabricated via low-cost inkjet printing. In these low-cost fabrications, tags are printed on photopapers via commercial inkjet printers loaded with silver-based inks. Various tag designs are simulated via the multilevel fast multipole algorithm (MLFMA) and their radar-cross-section (RCS) values are rigorously studied to developed superior designs for high performance identifications.

This study particularly focuses on frequency-based chipless RFID tag designs, where data is encoded via resonators. Existences of the resonators induce resonance peaks at the backscattered RCS response of the tag such that the data is encoded in binary notation depending on the resonators' absence or presence. In other words, tags having different ID words generate different signatures in the RCS spectrum. To construct an RFID system, RCS responses are collected in an ID library, while the tags that yield poor RCS responses are removed from the library based on an elimination rule. In addition to the conventional tags, novel array strategies are investigated to increase the reliability and readability of the tags at the cost of reduced compactness.

Furthermore, novel hourglass structures, which have more compact forms and enhanced RCS performances in comparison to the standard structures, are investigated. Finally, fabricated tags are tested in anechoic chamber by using various calibration techniques. While satisfactory results are obtained with PCB-based tags, improvements are needed to construct RFID systems involving inkjet-printed tags.

ÖZ

DÜŞÜK MALİYETLİ MİKROÇİPSİZ RFID ETİKETLERİNİN TASARIM, BENZETİM VE ÜRETİMLERİ

Çetin, Elif
Yüksek Lisans, Elektrik ve Elektronik Mühendisliği
Tez Danışmanı: Doç. Dr. Özgür Ergül

Kasım 2019, 93 sayfa

Bu tezde, düşük maliyetli çipsiz radyo frekanslarında tanımlama (RFID) etiketleri incelenmiştir. Bu tür etiketlerin ürün etiketlemede barkodların yerini almaları beklenmektedir. Bu etiketler, standart baskı devre kart (PCB) üretimlerine ek olarak, düşük maliyetli inkjet baskı tekniği ile de üretilmeye uygundur. Bu tür düşük maliyetli üretimlerde, etiketler fotoğraf kağıtlarına gümüş bazlı mürekkeple doldurulan ticari yazıcılarla basılırlar. Farklı etiket tasarımlarının benzetimleri çok seviyeli hızlı çokkutup yöntemi (MLFMA) ile gerçekleştirilmiş ve etiketlerin radar kesit alanı (RCS) tepkilerinin detaylı bir şekilde incelenmesiyle yüksek performanslı tanımlama kabiliyetine sahip etiket tasarımları geliştirilmiştir.

Bu çalışmada, özellikle veri kodlamasını rezonatörler vasıtasıyla gerçekleştiren frekans tabanlı çipsiz RFID etiketler üzerine odaklanılmıştır. Rezonatörlerin varlıklarının etikete ait RCS eğrilerinde tepeler meydana getirmesiyle, veriler rezonatörlerin varlığı veya yokluğu durumuna göre ikili sistemde kodlanmaktadır. Başka bir deyişle, farklı kimliklere sahip etiketler farklı RCS tepkileri vermektedir. Bir RFID sisteminin kurulabilmesi için, kimliklere ait RCS eğrileri bir kütüphanede toplanmakta ve uygun olmayan RCS tepkisine sahip olan etiketler bir eleme kuralına göre elenmektedir. Standart yapılara ek olarak, etiketlerin güvenilirliği ve okunabilirliğini artırmak amacı ile, yüzey alanının genişlemesi pahasına yenilikçi dizi

stratejileri incelenmiştir. Ek olarak, standart yapılara göre daha kompakt olan ve iyileştirilmiş RCS performansına sahip olan kum saati şeklinde yenilikçi etiket yapıları da incelenmiştir. Son olarak, üretilen etiketler yankısız odada çeşitli kalibrasyon tekniklerinin kullanılmasıyla test edilmiştir. Test sonuçları PCB yöntemi kullanılarak basılan etiketler için tatmin edici olsa da, inkjet yöntemi kullanılarak üretilmiş etiketlerin geliştirilmesine ihtiyaç duyulmaktadır.

Anahtar Kelimeler: Radyo Frekanslarında Tanımlama, Düşük Maliyetli Çipsiz RFID, Spektral İmza Tanımlaması, İnkjet Basım

To my beloved family…

ACKNOWLEDGEMENTS

TABLE OF CONTENTS

LIST OF TABLES

TABLES

LIST OF FIGURES

FIGURES

xviii

LIST OF ABBREVIATIONS

ABBREVIATIONS

Auto-ID	Automatic Identification
EFIE	Electric-Field Integral Equation
IC	Integrated Circuit
ID	Identity
MGA	Model Generation Algorithm
MLFMA	Multilevel Fast Multipole Algorithm
PCB	Printed Circuit Board
PPM	Pulse Position Modulation
RA	Receiver Antenna
RCS	Radar Cross Section
RF	Radio Frequency
RFID	Radio Frequency Identification
SAW	Surface Acoustic Wave
TA	Transmitter Antenna
VNA	Vector Network Analyzer

CHAPTER 1

INTRODUCTION

In the context of this study, identification refers to constructing a relationship between a physical item, which can be a stationary or a moving object, and its information that is networked to a computer database. The information of stationary items is directly accessible from database. However, more advanced concepts are required for moving items. Automatic identification (Auto-ID) is a well-known method, which was developed in order to identify moving items [1]. Auto-ID is mainly used for tracing and distinguishing items and it is commonly employed in supply chains where contactless data transmission is needed [2]. Auto-ID concepts have been proposed to satisfy identification process requirements that exceed human abilities [3]. In general, there are two commonly used contactless ID technologies: (i) Barcodes and (ii) radio-frequency identification (RFID) [4].

1.1. Barcodes

Evolution of Auto-ID technologies has started with barcodes. This well-known technology encodes the information typically into black and white parallel stripes as shown in Figure 1.1. Characters or numbers of the data are represented by varying width of the stripes. The first commercial use of barcodes was occurred in 1966 even if they were firstly introduced in 1950 by Woodland and Silver [5]. The data on the barcode is read via special optical scanners. Although there are diverse types of barcodes, they can be classified into two sub-categorizes: 1D and 2D (also known as QR codes [6]). Barcode labels have favorable properties, including their low-costs, small sizes, and light weights. Also, barcodes systems are easily implemented due their inexpensive and simple photosensor-based readers. Today, billions of barcode labels are in use for identification purposes [6].

Figure 1.1. A barcode tag

Barcodes are commonly employed in production, transportation, and library systems [7]. However, the main drawback of them is that they should be placed in the direct line of sight of readers that limits their reading operation. For example, barcodes are insufficient for fast moving items, such as products on conveyor belt systems.

1.2. Radio-Frequency Identification

RFID systems have become major tools in many applications involving the identification and tracking of living and nonliving objects, particularly in the areas of healthcare, manufacturing, transportation, and security [3]. RFID is the abbreviation of radio-frequency identification, since radio-frequency (RF) waves are used to encode and transfer data wirelessly during the identification of the items [3]. In the literature, RFID technology has attracted much attention due to its wide range of application areas, which open a new chapter to contactless identification systems. Such systems provide efficient, fast, and practical identification for supply chain managements, while eliminating physical sight requirements [8]. RFID tags appeared in 1930s for identifying airplanes in IFF systems by the U.S. government; however, they were firstly presented in 1948 [9]. RFID gained its popularity in 2003 thanks to Wal-Mart, one of the largest retailers, which replaced barcode tags of products with item-level RFID tags to efficiently solve their inventory management problems [10, 11]. The acceptance of RFID systems by such large institutions has lowered their costs and further developed the technology. Today, 600 billions RFID tags are sold per year and the cost of each tag is only about 4 cents [12]. They are most commonly used in supply chains, transportation, logistic, personal tracking, communication, medical services, security, and document tracking. Table 1.1 provides a general comparison of RFID and barcode systems.

Figure 1.2. An RFID tag

The most important advantage of RFID tags over barcode tags is that they do not have to be in line of sight of the readers since RFID is based on communication via RF waves instead of optical beams.

In general, an RFID system consists of two main elements: (i) A tag and (ii) a reader [3]. The reader contains transmitter antenna (TA) and receiver antenna (RA), and an RF circuitry. It is directly connected to a host computer that controls the whole system via its user interface. The reader is basically a transceiver structure. The interrogator signal is generated and transmitted while the received signal reflected from the tag is captured and decoded at the same time. The RFID tag usually consists of a coupling antenna and an integrated circuit (IC) chip to encode the information indicating the item as shown in Figure 1.2 [13, 14]. RFID tags can be categorized into three groups; active, semi-active, and passive tags depending on their power sources. An active tag generally has its own power source, e.g., a battery that runs the IC chip when the interrogator signal reaches the tag. On the contrary, passive tags need external power supplies to activate their circuits. In such a system, interrogator signal energy is often used as a power source in the tag [3]. Semi-passive tags are hybridizations of passive and active tags. In this thesis, passive tags are particularly focused, since they are more common and they also demonstrate all advantages of the RFID technology, including being energy-efficient and friendly to environment.

Table 1.1. *RFID versus barcodes*

Parameter	Barcode	RFID
Data capacity (byte)	1−100	Up to 128k
Security level	Low	High
Dirt and damage durability	Low	High
Line of sight	Needed	Not needed
Speed	Low	Fast
Read range	0−50 cm	0−5 m
Re-writable	No	Yes
Multiple interactions	No	Yes
Cost	Very low (0.01$)	Medium (0.10$−1.00$)

The operation of a passive RFID system can be described as follows [15].

● The identification procedure starts with the transmission of an interrogation signal (with data and clock information) to the tag from the reader via integrated TA.

● When the signal is captured by the antenna of the tag, the IC chip is activated with the received signal energy.

● The IC encodes the information to an RF signal. Then, the modulated signal is transmitted back to the reader.

● The reader receives the modulated signal by RA. With the help of the host computer, data is decoded and the information of the tag is determined.

Despite its great advantages, the cost has still been the main problem in RFID systems since the price of the tags should be lowered down to meet the expectations of labelling

low-cost items as well. Using paper or plastic substrates is not sufficient to reduce the cost of the conventional RFID tags, particularly due to the IC chips located on the tags [16]. In order to overcome this bottleneck, chipless RFID tags have been proposed and developed. The main motivation of this thesis is presenting effective and low-cost chipless RFID tags.

1.3. Outline of the Thesis

The organization of this thesis is as follows.

In Chapter 2, the basic concept of chipless RFID technology is presented in detail. Also, the main elements of a chipless RFID system, data encoding methods, and tag identification techniques are discussed. Lastly, the simulation environment used in this study is presented.

In Chapter 3, U-shaped chipless RFID tags, which are commonly used in the literature, are introduced. Simulation results of the designed tags are also presented. Moreover, a block diagram of constructing a chipless RFID library and the design methodology are shown in detail.

In Chapter 4, novel array strategies for U-shaped tags are presented. The performances of the designed chipless RFID tags depending on various parameters are also discussed.

In Chapter 5, a novel type of hourglass-shaped chipless RFID tags is proposed in order to enhance the performance. Simulation results for different hourglass-shaped tags are presented.

In Chapter 6, fabrications of chipless RFID tags using PCB and inkjet printing technology are considered in detail. Also, a sensitivity analysis for the printed tags is presented. Finally, measurement techniques for chipless tags are investigated, followed by the presentation of initial measurement results for different tags.

Chapter 7 concludes the thesis, with the emphasis on future work.

CHAPTER 2

CHIPLESS RFID

In this chapter, general aspects of chipless RFID tags are discussed. First, some milestone studies in the literature are reviewed to describe the state-of-the-art. Then, system parameters for chipless tags, as well as basic concepts of data encoding and tag identification are presented.

2.1. Definition

As contactless identification systems gain popularity, their capabilities and costs have become major issues, especially considering large volume of production in all areas of science and society. Although barcodes are the most affordable ones among all auto-ID technologies, they are not sufficient to meet expectations in terms of accuracy and effectiveness [17]. In order to obtain an efficient solution, RFID systems have been particularly focused. These systems do not only accelerate reading processes, but also eliminate the need for line of sight between readers and tags. On the other hand, the developed RFID systems have had to be revised to reduce their costs, particularly contributed by IC chips. For this purpose, chipless RFID tags have become innovative solutions for contactless identification technologies. As their names state, these tags do not contain any IC chip to encode data. This way, chipless RFID tags provide advantages of both conventional RFID tags and barcodes at the same time [7]. Due to their longer read range, accuracy, and faster identification processes, they are superior to barcodes. At the same time, they have advantages over the conventional RFID tags with their inexpensive costs. It is even possible to reduce the price of a chipless RFID tag to 0.4 cent [18]. Most of the chipless RFID tag designs are fully printable and the tags are environmentally friendly because of the elimination of IC chips.

For chipless RFID systems, there are many different data encoding methods; however, they can be classified into three basic categories: Time-based (time domain reflectometry), frequency-based (spectral signature), and phase-based [19].

2.2. Literature Review

Hartmann et al. presented the first chipless RFID design in [20]. The proposed tag structure is fabricated with surface acoustic wave (SAW) technology and it is a type of time-based chipless RFID tag. The data is encoded with respect to pulse position modulation (PPM) via acoustic reflectors on the tag. The reader sends pulses and receives the echoes reflected from the tag. Each one of the acoustic reflectors generates pulses at specific time delays as soon as the interrogator signal reaches the tag. In the overall tag response, the pulse positions specify the encoded data since each pulse represents 1-bit information.

Chipless RFID tag proposed by Shretha was a printable delay-based tag [21]. The design converts the SAW-based tags into microstrip concept, where the data is encoded via transmission-line-based structures. It is indicated that the transmission line is equivalent to an LC circuit that corresponds to time delay. Therefore, it is possible to generate different time delays by varying the L and C parameters, which are controlled by the length of the transmission line. Similar to the SAW-based tags, time delays from the incoming signal encodes the data. Depending on the length of the line, it is possible to create different ID codes.

Space filling curves were proposed by Jalaly et al. and they form the basis for frequency-based chipless RFID tags [22]. These types of tags encode the binary data by generating resonances via Peano and Hilbert space filling curves, which can be considered as frequency-selective surfaces [23]. In the proposed design, each surface resonator encodes each bit individually. Then, resonances are observed as peaks in the frequency spectrum, and this phenomenon is called spectral signature. Basically, radar-cross-section (RCS) values indicate the spectral signatures of the tags.

Capacitively tuned dipoles are versions of spectral signature-based chipless RFID tags. In the study presented in [24], data is stored via dipole antennas having specific resonance frequencies and the overall tag structure is named as RF barcode. Varying dipole lengths control the resonance frequencies. This leads to separate resonances in the spectrum since each dipole corresponds to 1-bit information. Similar to the space filling curves, these resonances represent the bits of the binary data. Depending on the absence or presence of a dipole, the bit information is either 0 or 1. The proposed structure in [24] is one of the first fully printable chipless tag design.

Multi-resonator-based chipless RFID tags proposed by Preradovic et al. encode information via spiral-shaped resonators [25]. Depending on the resonators' existence or absence, spectral signature is formed. The proposed structure has an important place in the chipless RFID literature since it provides a basis for various resonator-based chipless tags and the corresponding concept is now commonly used. The presented tag structure is able to achieve 35-bit data capacity [26]. On the contrary to different spectral signature-based tags, the tag encodes the data in both phase and magnitude, increasing the accuracy of the system. Also, the proposed design brings another advantage, i.e., different ID combinations can be obtained via very small modifications on a printed tag by shortening the resonators.

A stub-loaded chipless RFID tag was introduced by Balbin et al. and it is based on the concept of phase signature encoding by three individual elements [27]. The 3-bit tag design is a square patch antenna array having high impedance load at the reader end. Depending on the resonance frequencies of the antennas, the data is encoded in the magnitude response while inducing a shift at the phase response. The shift is controlled by the length of the load, which results in distinct phase responses in the backscattered signal. It is possible to obtain different ID combinations by adding or removing a load stub. The proposed design is useful in industrial applications thanks to its low-cost and printable properties.

A chipless RFID tag design proposed by Vena et al. has recently become popular in the literature [28]. U-shaped resonators used in the tags have significant resonance performances considering the backscattered signal spectrum. Since, the resonators also have a phase shifter behavior, data can be encoded both in amplitude and phase, increasing the efficiency and reliability of the system and also enabling higher capacity via hybrid coding techniques [29−31]. Also, it is possible to switch any specific encoded bit between 0 and 1 by making basic adjustments on the tag, such as short circuiting, based on the absence/presence principle. This reduces the amount of time to change the layout for tags with different IDs.

The chipless tag design proposed in [28] has some mutual-coupling problems between resonators due to the array structure. In order to reduce such coupling effects, a re-arrangement method for neighboring array elements were proposed in [31]. Such rearrangements strongly affect the peaks and dips in the RCS response. Specifically, dips (representing "0") become more visible, while the peaks (representing "1") become more stable and uniformly distributed. The study also proposed bended resonators for array structures to improve the RCS uniformity, which also leads to more detectable dips of 0 bits. A spiral-shaped capacitive-loaded dipole array structure ensures an average magnitude level along with low bandwidth. Performances of different resonators were also examined in [31]. Based on many calculations, it is shown that there is a trade-off between achievable capacity and read range. Depending on the requirements of the application, one of the proposed resonator types can be selected for a tag design.

2.3. Why Should Chipless RFID Tags Be Used?

Important advantages of chipless RFID tags and related systems can be listed as follows.

- They are low-cost, e.g., a tag can be fabricated even for 0.4 cents [12].
- They can easily be fabricated since they are fully printable.
- Depending on the size of the tag, high data capacity can be achieved.

- They do not need direct line of sight with the reader, as opposed to barcodes.

- Generating different ID combinations can be achieved without major modifications on the layout. Thus, they are suitable for tagging vast numbers of objects.

- Read range is relatively longer than the range in barcode systems.

- Eliminating IC chips leads to easier recycling processes, and makes the fabricated tags environmentally friendly.

- They can be used in both encoding end sensing applications, e.g., for temperature, humidity, and light.

2.4. System Structure

An RFID system is composed of two major components, i.e., reader and ID tags [3].

2.4.1. Tag

A chipless RFID tag is placed on the object to be identified. There is not any power source placed on the tag to execute the data encryption process. The tag harvests the energy of the incoming RF signal and reflect a signal back to the reader. As mentioned above, the state-of-the-art chipless RFID tags encode information usually via multi-resonator structures, which are mainly used to generate the spectral signatures corresponding to the IDs. Hence, the main task of a tag is to capture the incoming signal and reflect it with an embedded signature. There is a tremendous amount of resonator-based chipless RFID tag designs, while U-shaped resonators are particularly focused in this work.

2.4.2. Reader

A chipless RFID reader is very similar to a regular RFID reader detailed in [3]. The reader structure consists of two sub-modules: Transceiver and controller. The transceiver is the connection between tags and the controller. The transceiver module used in this study is composed of a signal generating circuitry and two antennas. In chipless RFID systems, data is encoded in multiple frequencies covering wide

frequency bands, as opposed to the regular RFID systems. Therefore, the signal generator sweeps the frequency over the operating band and the generated signal is called the interrogation signal. There are two antennas placed on input and output. The interrogation signal is transmitted via the output antenna. After the reflection from a tag, ID-encoded backscattered signal is captured by the input antenna. Then, the collected data is sent to the controller for decryption.
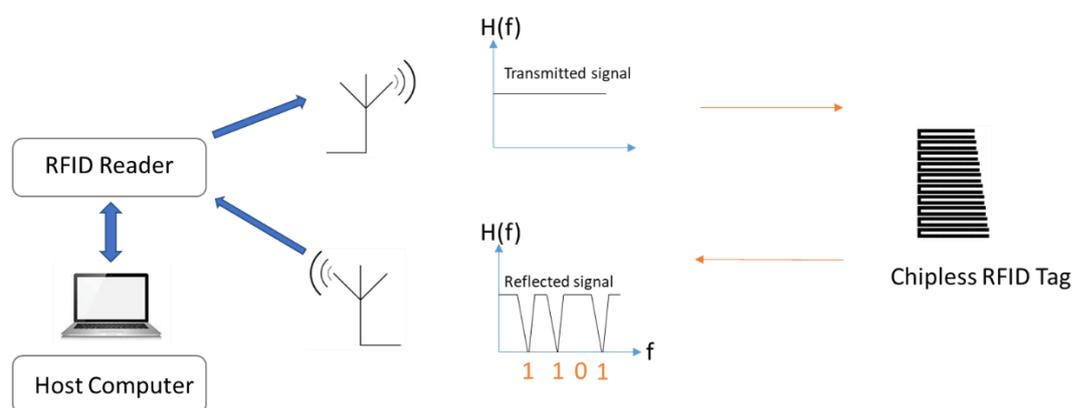
Figure 2.1. Chipless RFID system diagram

The controller module links the user with the data on the tag via a user interface. It runs the whole system and arranges the transmitting and receiving sequences. After receiving a signal, the response of the signal is decoded via detection algorithms so that the ID code is determined. The controller also has an access to an ID library to match the ID code with the information about the object.

2.5. Identification Procedure

In this study, frequency-coded chipless RFID systems are investigated, in which the ID codes are embedded in the frequency spectrum. Such systems utilize resonator structures for different frequencies in order to assign ID codes to tags. In a chipless RFID system described in Figure 2.1, the transmitter antenna starts the sequence by sending interrogation signals at different frequencies. When an interrogation signal reaches the tag, the multi-resonator structure on the tag reflects the incoming signal.
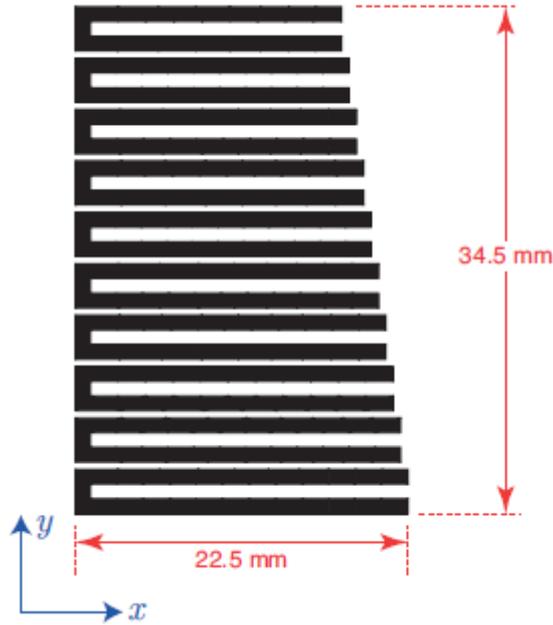
Figure 2.2. 10-bit U-resonator-based chipless RFID tag

The reader analyzes the spectrum of the received backscattered signal and decodes the ID code embedded on the tag by identifying the resonance frequencies [16].

2.6. Data Encoding

Encoding method for the tag designs investigated in this study is based on the principle of presence/absence of resonators [16]. Specifically, resonating elements encode the data into the frequency spectrum by creating resonances. This method is considered as binary coding since each resonator represents one bit of an ID word. In other words, each bit of the data is coded with a U-resonator on the tag with a specific length [28]. In this research, a chipless RFID tag with 10-bit data capacity shown in Figure 2.2 is studied in detail. Presence of a resonator on the tag indicates the logical "1" bit. Thus, the tag presented in Figure 2.2 actually corresponds to the ID word '1111111111'. Likewise, absence of a resonator implies the "0" bit. Considering 10 bits, there are $2^{10} - 1 = 1023$ different ID combinations.

(a)   (b)
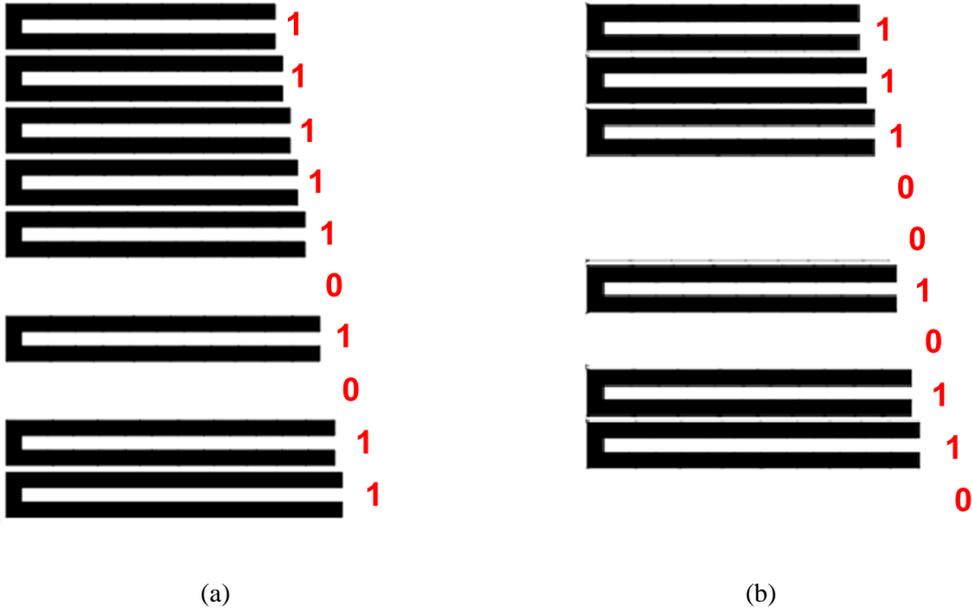
Figure 2.3. (a) Tag encoding '1101011111' word, and (b) tag encoding '0110100111' word

In order to obtain different ID words, the resonators are deleted from the full tag structure as shown in Figure 2.3 to alter the desired bits from "1" to "0". For example, Figure 2.3(a) presents the tag configuration corresponding to the ID word '1101011111', whereas Figure 2.3(b) presents the tag with the ID word '0110100111'.

2.7. Identification of Tags

As described in Section 2.6, ID codes can be embedded in spectrum signatures. The data is encoded into the backscattered wave spectrum via resonating elements that resonate at certain frequencies depending on their arm lengths [32, 33]. In chipless RFID systems, RCS is mainly used to detect these resonances and distinguish tags. Specifically, these resonances can be observed as peaks in the RCS spectrum. In general, the backscattered RCS defines how much power is scattered from the tag back to the reader [34]. Each component generates a resonance peak at a specific frequency, i.e., when the arms of the resonator correspond to $\lambda/4$, where λ is the wavelength of the interrogation signal [32]. Hence, tags with different IDs have distinct backscattered

RCS responses with respect to frequency. Depending on their responses, tags can be distinguished from each other and the corresponding ID codes can be identified.

2.8. Simulation Environment

In this study, simulations of chipless RFID tags are performed via the electric-field integral equation (EFIE) formulation. For discretization, the Rao-Wilton-Glisson functions are employed on the triangulated surfaces. Matrix equations are obtained with the method of moments. Then, the multilevel fast multipole algorithm (MLFMA) is employed to iteratively solve the matrix equations [35]. The algorithm accelerates the solutions by decreasing the complexity, while providing accurate results. After computing the electric current density coefficients, far-field electric intensity is calculated to obtain the backscattered RCS. In the simulation environment, tags are located on the x-y plane and they are excited by plane waves having different polarization types, such as linear and circular. The frequency range depends on the design; however, the sampling rate is fixed to 20 MHz for all designs.

CHAPTER 3

U-SHAPED CHIPLESS RFID TAGS

Tags with U-shaped resonators are commonly used structures for chipless RFID systems due to their highly frequency selective performances and flexibility [28−31]. In this research, tags with 10-bit U-shaped resonators are particularly investigated. Further information can be found in [36−38].

3.1. Tag Design

Frequency-based chipless RFID tags encode data into spectrum signatures and there are diverse approaches for this purpose. Multiple planar resonator structures on a tag generate such unique signatures, as a very common method in the literature [25−31]. For these tags, resonating elements create different responses depending on the frequency of the incoming signal. In this thesis, U-shaped structures are used as resonating elements, following the approach proposed by Vena et al. [28].

As shown in Figure 3.1, U-shaped resonators are folded versions of simple dipole structures. Resonance occurs when quarter of the wavelength of a polarized incoming signal is equal to the physical length of the resonator arms. In this case, a minimum current distribution occurs at the open ends of the resonator while the maximum current is induced at the short-circuited ends [32]. We note that the corresponding dipole also has minimum current distribution at its tips and maximum current at the center. Figure 3.2 shows the surface current densities on a dipole and U-shaped resonator that are excited similarly. Despite similarities, capacitive effects, due to folding, between the arms of the U-shaped resonator enhance the resonance and the corresponding quality factor [33]. Also, the U-shaped resonators have better frequency-selective characteristics.
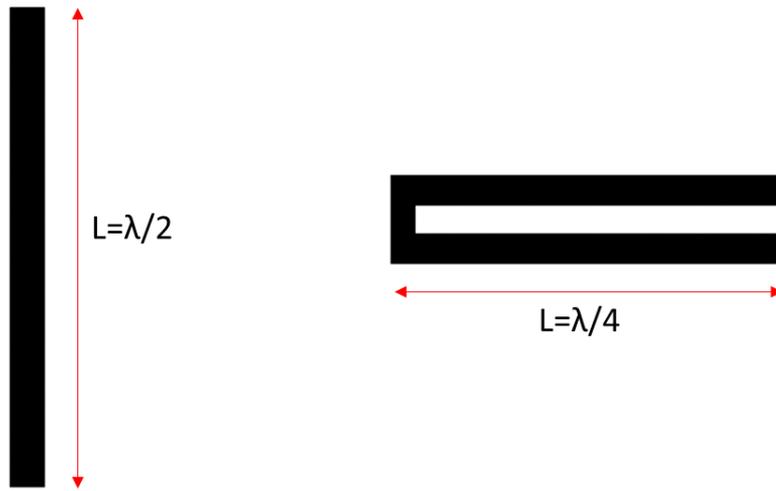
17

Figure 3.1. Dipole and U-shaped resonator
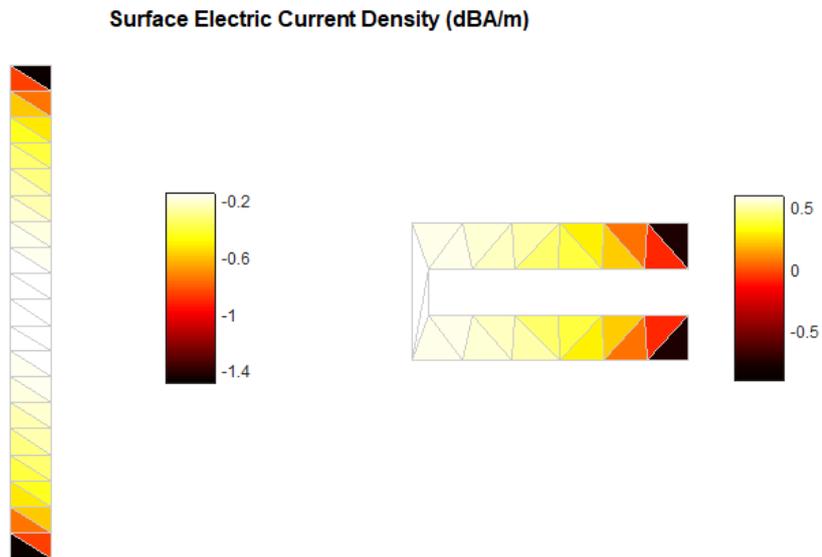
Figure 3.2. Surface electric current density induced on a dipole and the corresponding U-shaped resonator

18

ID words are generated by using U-resonators to form the tag structures. Different combinations of resonator elements lead to unique signatures in the frequency spectrum of the backscattered signal. This kind of multi-resonator-based tags are very favorable as they provide extensible data capacity that can be expanded only by increasing the number of resonators. The 10-bit tag geometry is shown in Figure 2.2 and not repeated here. The geometry covers an area of approximately 7.76 cm^2.

3.2. Simulation Results (10-Bit Tag)

In Figure 3.3, the backscattered RCS response of the 10-bit chipless tag (when all resonators exist) for circular polarization is shown. For comparison, RCS of each resonator (when it is individually excited) of the tag is also plotted. It can be observed that all resonances occur in the 3−4.2 GHz band. Individual peaks are easily detectable in the overall response of the tag, which is crucial to generate clearly distinguishable ID codes. Also, it can be inferred that coupling effects between the resonators are almost negligible in terms of resonance frequencies. On the contrary, the magnitudes of the peaks are visibly affected by the couplings. Figure 3.4 depicts the RCS responses of the tag for different polarizations. In addition to the circular polarization (CC), linear polarizations (XX and YY, based on the orientation of the tag in Figure 2.2) are considered. Depending on the application, one of the polarizations may be more practical than the others. However, in the following discussions, we often focus on the circular polarization as the general case.

3.2.1. Deletion Results

An RFID system should be able to provide many different ID words for tagging different items. The data capacity of the system corresponds to the number of different items to be tagged. In a conventional RFID system, different ID combinations are generated via IC chips. Although the geometry is the same for all tags, the IC chips provide the unique identities. On the contrary, ID encoding should be done via geometry for chipless tags.

Figure 3.3. RCS response of the 10-bit tag for circular polarization
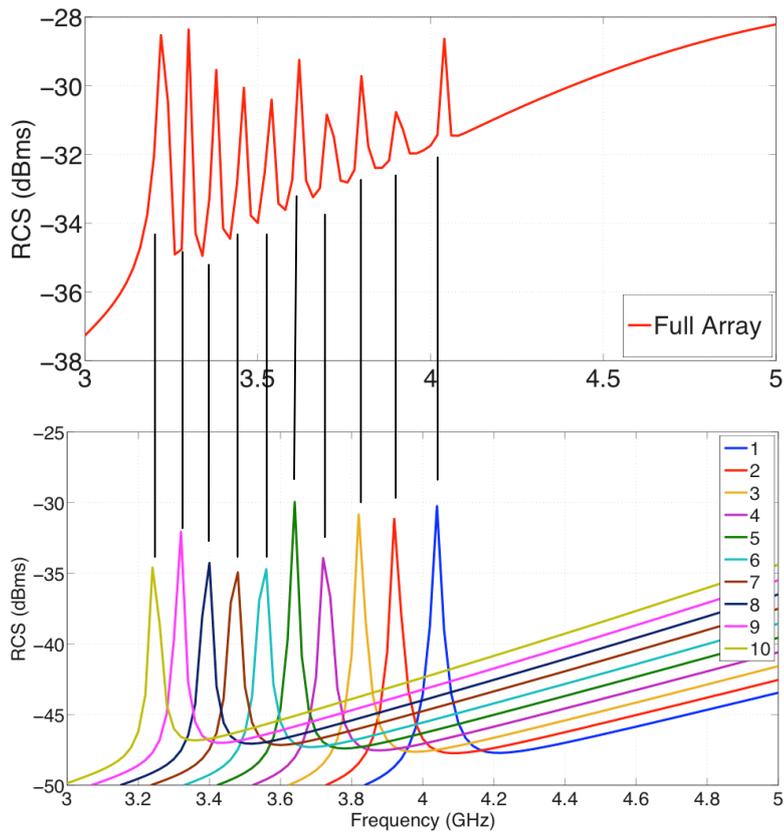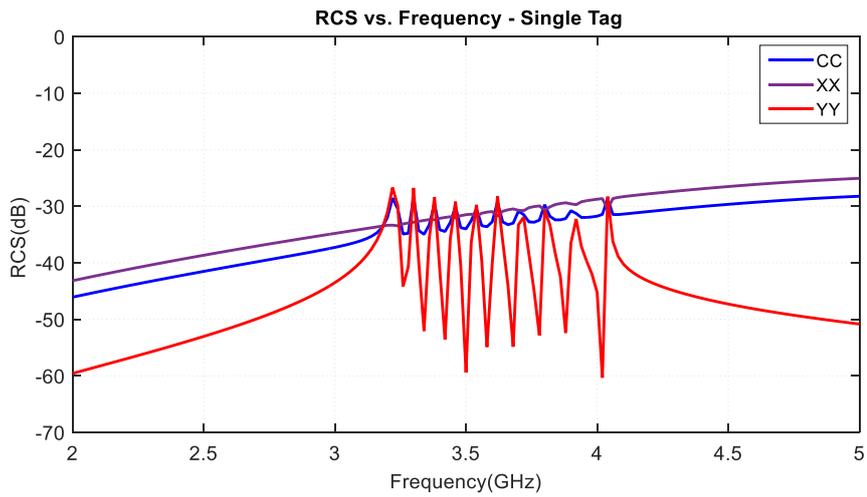

Figure 3.4. RCS response of the 10-bit tag for different polarizations

20

For multi-resonator-based chipless tags, the encoding approach is based on the principle of absence or presence of resonators, which is performed by removing resonators from the existing design [36, 38]. Specifically, ID words are reproduced from the master tag that includes all resonators. For the 10-bit chipless tag, the master tag has all 10 U-shaped resonators and its ID word is '1111111111'. And, for example, if the 5th bit is to be set to "0", its corresponding resonator should be removed from the master tag. Then, the corresponding ID word is '1111101111'. Consequently, the corresponding peak in the backscattered RCS spectrum disappears.

In the chipless RFID strategy followed in this study and discussed so far, least significant technique is employed for binary coding. In this technique, bits are placed from right to left and the corresponding resonators are ordered from the shortest to the longest. For multi-resonator-based chipless RFID tags, the data encoding is very straightforward and ID words can easily be obtained. For these reasons, the considered tag design is very suitable for RFID applications.

3.2.1.1. Single-Bit Deletions

RCS responses for single resonator deletions are shown in Figure 3.5. Each one of the resonators is removed from the tag one by one and the RCS response is calculated for each case. It can be observed that the RCS curves are plotted in a range from -38 dBsm to -28 dBsm. For each scenario, it is easily observed that the corresponding peak of the deleted resonator disappears from the RCS response. However, the electromagnetic couplings between the resonators, have significant impacts on the responses of neighboring resonators, which result in deformations on the undeleted peaks. Particularly, from top to bottom, each one of the deleted resonators affects the amplitude level of the next resonator's peak as a result of coupling.
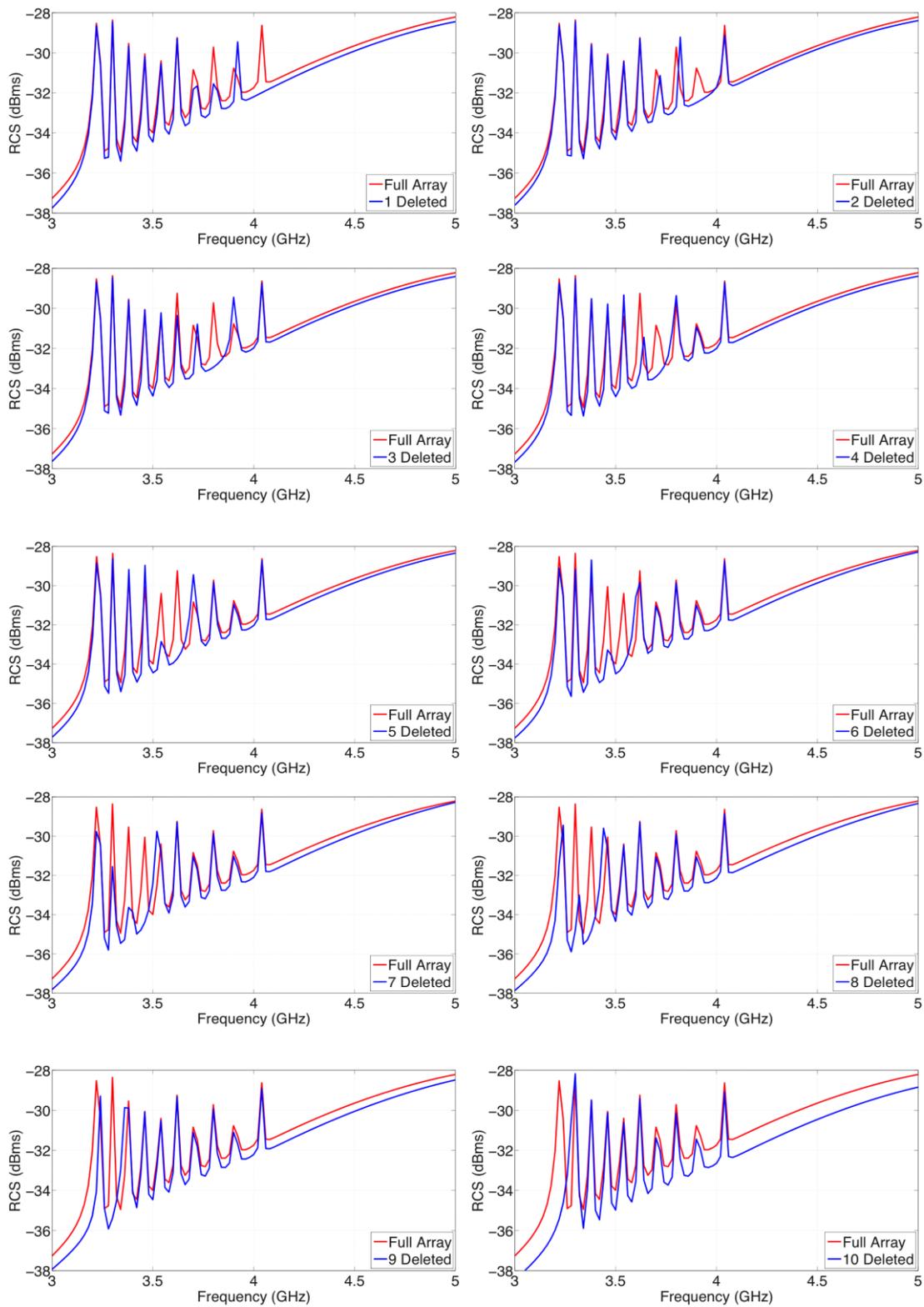
Figure 3.5. RCS results for single-bit deletions

22
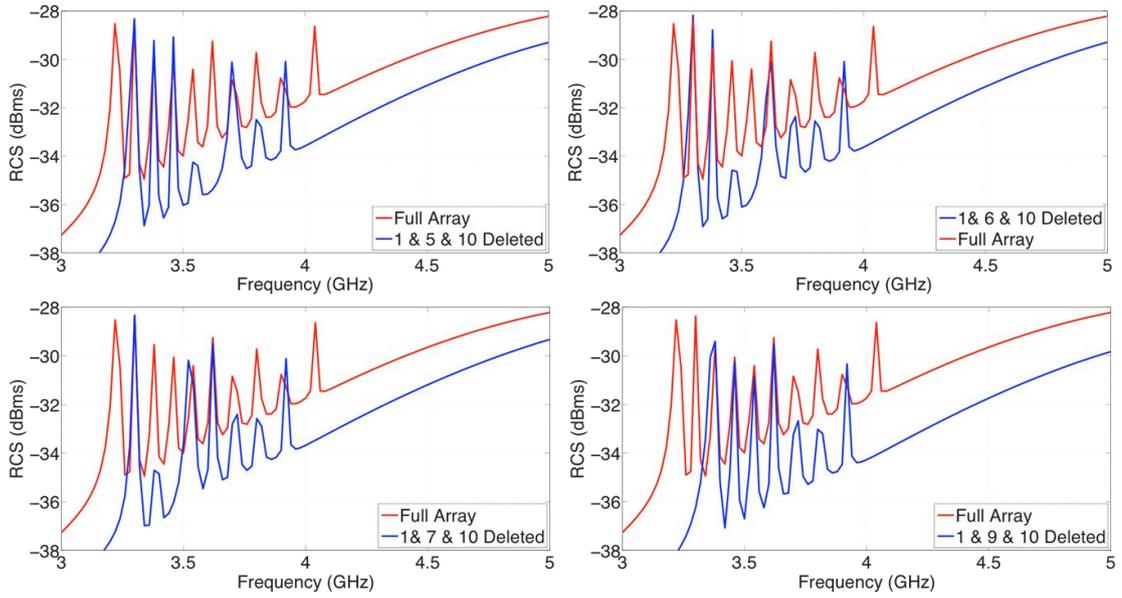
Figure 3.6. RCS results for three-bits deletions

3.2.1.2. Three-Bit Deletions

Figure 3.6 presents sample results of RCS responses for three-bit deletions. For all scenarios, the first and the last bits are always extracted. In addition, depending on the trial, the third deleted bit is selected as 5, 6, 7, and 9. As opposed to single-bit deletions, RCS levels are reduced due to the decreased numbers of reflecting elements. Moreover, deletion of a bit affects the next bit as observed in single-bit deletions, while several peaks remain at their high positions. On the other hand, peaks with high amplitude levels are not strongly affected. It is remarkable that, despite negative effects due to the coupling between resonators, the bits corresponding to the remaining resonators are clearly observed in all cases.

3.2.1.3. Cascaded Deletions

Now, we consider cascaded deletions to observe the effects of subsequent removals of resonators. In the first trial, bits 2, 3, 4, and 5 are deleted consecutively, while the first resonator is always extracted.

23
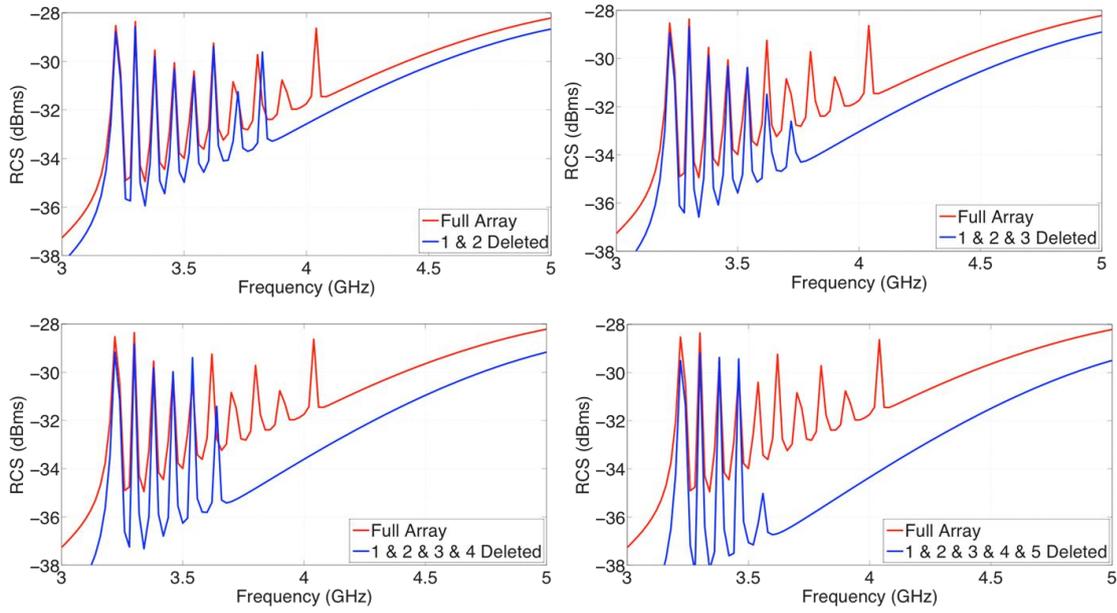
Figure 3.7. RCS results for cascaded bit deletions
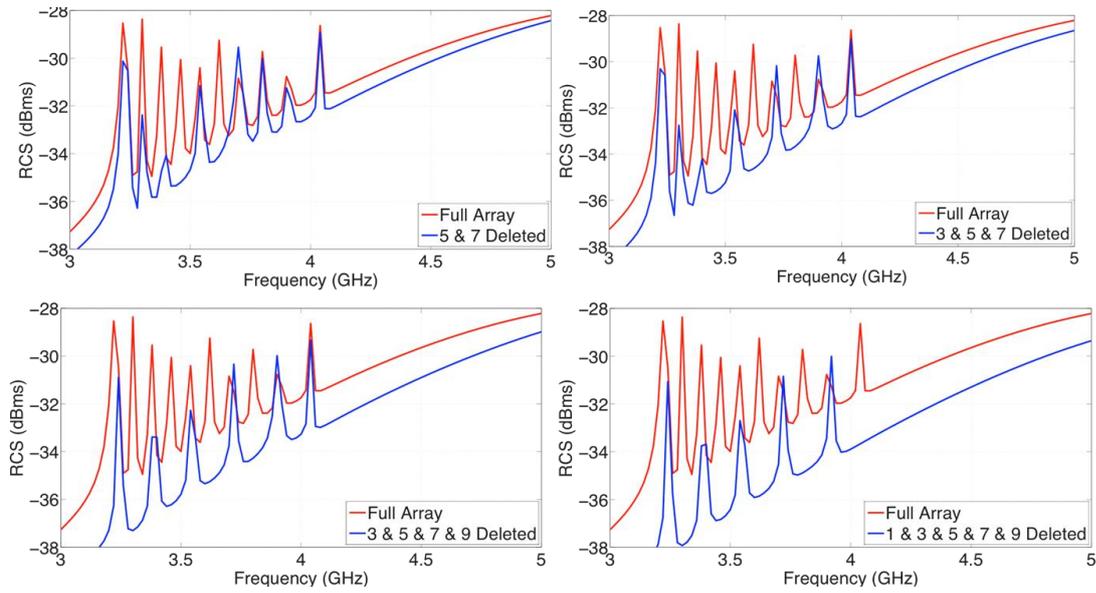
Figure 3.8. RCS results for cascaded bit deletions

Figure 3.7 shows that the base RCS level decreases as more resonators are removed. In all results, the resonance related to the smallest undeleted bit seems to be affected

24
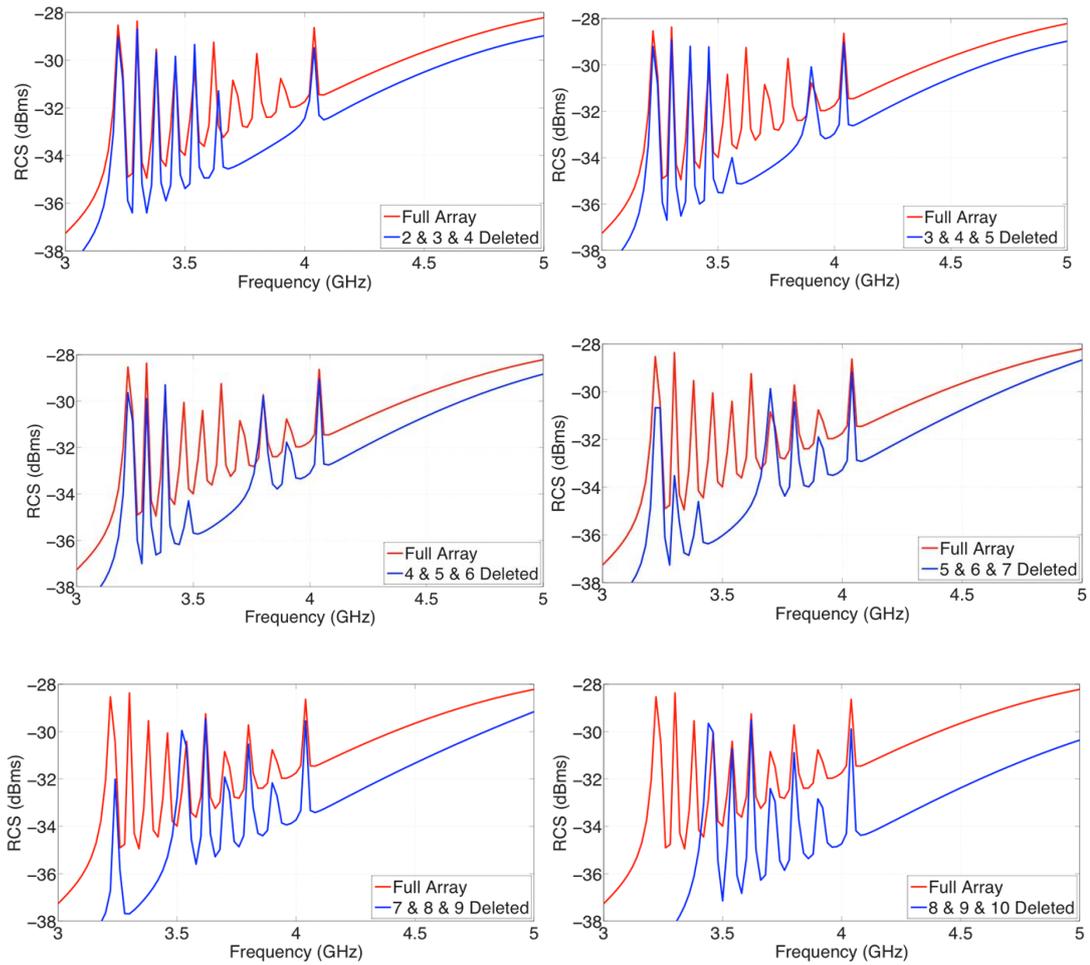
Figure 3.9. RCS results for three-bit block deletions

significantly, while the remaining resonances keep their strong characteristics.

In the second set of trials, 1, 3, 7, and 9 are removed subsequently while 5 is always missing. The plots in Figure 3.8 displays the reduced values of the base RCS, as well as remarkably decreased peaks. Once again, deleted bits strongly affect the resonances of the next peaks, leading to quite low levels, particularly when five resonators are removed from the tag.

25
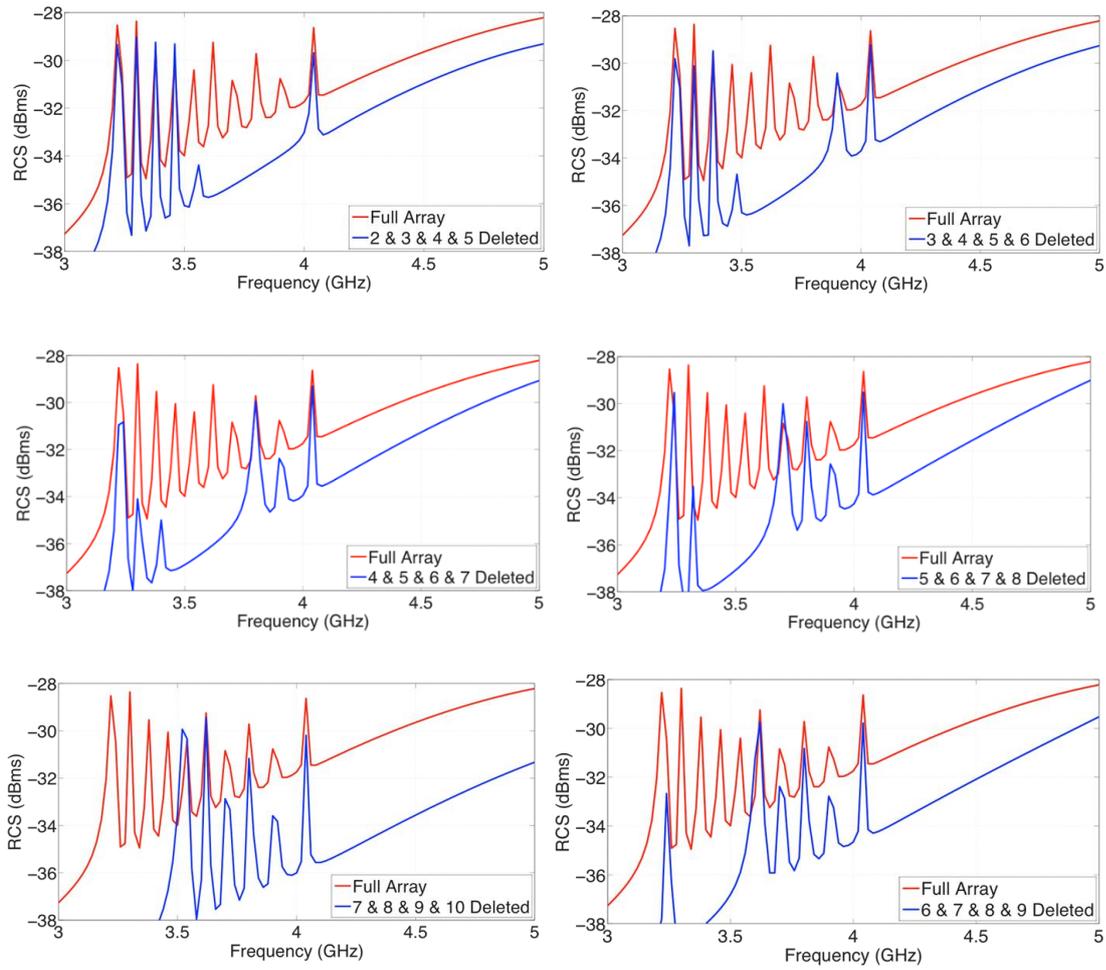
Figure 3.10. RCS results for four-bit block deletions

3.2.1.4. Block Deletions

In Figure 3.9, we consider sample trials of three-bit block deletions. Deleting larger labelled bits significantly decreases the RCS level since the corresponding resonators cover larger physical areas. Similarly, in each case, the amplitude of the first undeleted peak is affected drastically. Figures 3.10 and 3.11 present the RCS results for four-bit and five-bit deletions. The general RCS level decreases greatly when deleting a five-bit block, while the amplitudes of the peaks are still at sufficient levels to be detected.

26
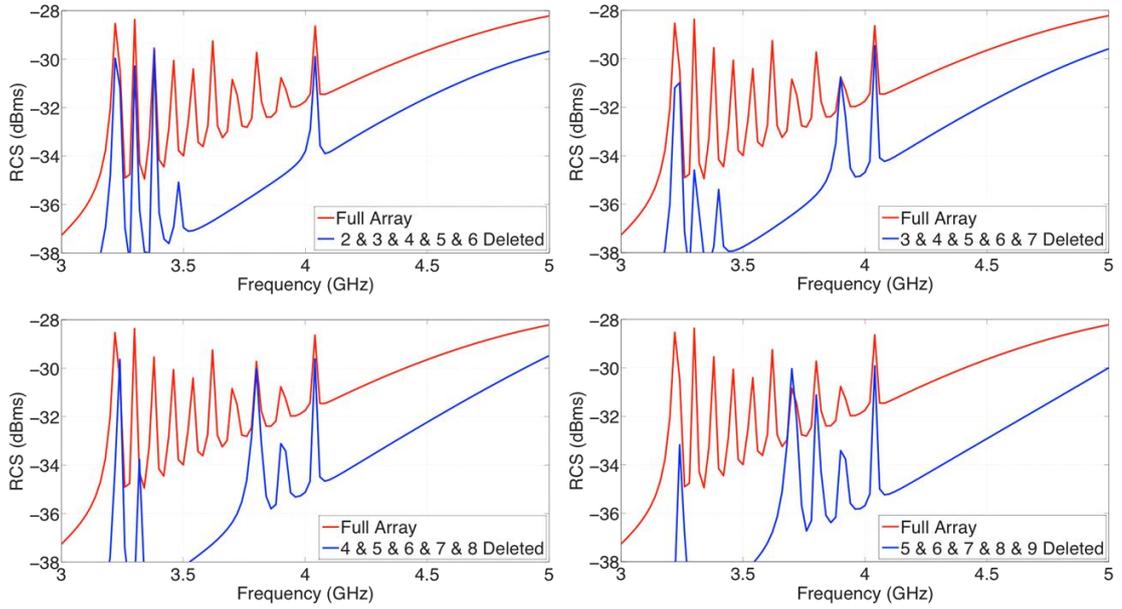
Figure 3.11. RCS results for five-bits block deletions

3.2.2. Comments on the Results

Considering the bit-deletion results, the most important observation is the strong characteristics of all existing and missing peaks in the RCS responses that enable the detection of the encoded ID words. In other words, undeleted resonators generate peaks well above the base RCS levels such that data is encoded as desired. Deleting a resonator decreases the reflecting area of the tag. Thus, the average level of the RCS response drops with the deleted resonators, although undeleted peaks are still recognizable. We note that the RCS level is affected particularly when deleting longer resonators.

According to the results, the most important issue is related to the undeleted resonators located next to the deleted resonators. Specifically, if a resonator $i < 10$ is removed while $(i + 1)$ (corresponding the next resonator) remains, then the peak related to $(i + 1)$ is significantly affected. This seems to be due to the unbalanced current distributions on the $(i + 1)$th resonator due to the absence of the ith resonator. On the other hand, if a resonator $i > 2$ is removed, $(i − 1)$ is less affected since this actually

27

improves the balance of metals (considering resonator sizes) on the two sides of (i − 1). Cross investigations support these arguments. For instance, the deletion of the block {3,4,5} has disastrous effect on the 6th bit while a balanced deletion of bits 3, 5, and 7 has a less significant impact on the 6th resonance.

Following the discussion above, we note that generating and using some ID words can be risky for accurate and reliable identifications. Thus, they should be removed directly from the generated ID set as detailed in Section 3.3. For instance, if the RCS signature of a tag is very similar to the signature of another tag, one of them should be excluded from the set in order to prevent misidentification. This elimination can be done automatically (Section 3.3) or manually, e.g., given a pair of IDs like

$$[.,.,.,1,0,.,.,.,.,.]$$

$$[.,.,.,0,0,.,.,.,.,.]$$

one of them can be eliminated to avoid misidentification, based on our observations above. Alternatively, distances between resonators could be increased at the cost of enlarging the areas covered by the tags, leading to a trade-off between size and efficiency.

3.3. Generating ID Library

Figure 3.12 shows a block diagram to generate a library of chipless RFID tags for a reliable system. Some main stages are as follows.

- The process starts with a master tag, which has all resonator elements and corresponds to the ID word '1111111111' for the 10-bit case.
- The master tag geometry is modelled via Siemens NX software and it is discretized with triangular meshes. Then, the discretized model of the geometry is exported.
- Tags encoding different IDs are generated from the discretized model of the master tag via an automatic model generation algorithm (MGA).

28

- For each generated tag, full-wave simulations are performed via MLFMA. Coefficients of the electric current density are calculated at each frequency in the interested band. Far-field electric field intensity values are calculated by using the current coefficients.
- Backscattered RCS response of each tag under interest is obtained from far-field electric field intensity values. Depending on similarity checks described below, the tag and its RCS response are added into the ID library or they are stored in the reserve collection.
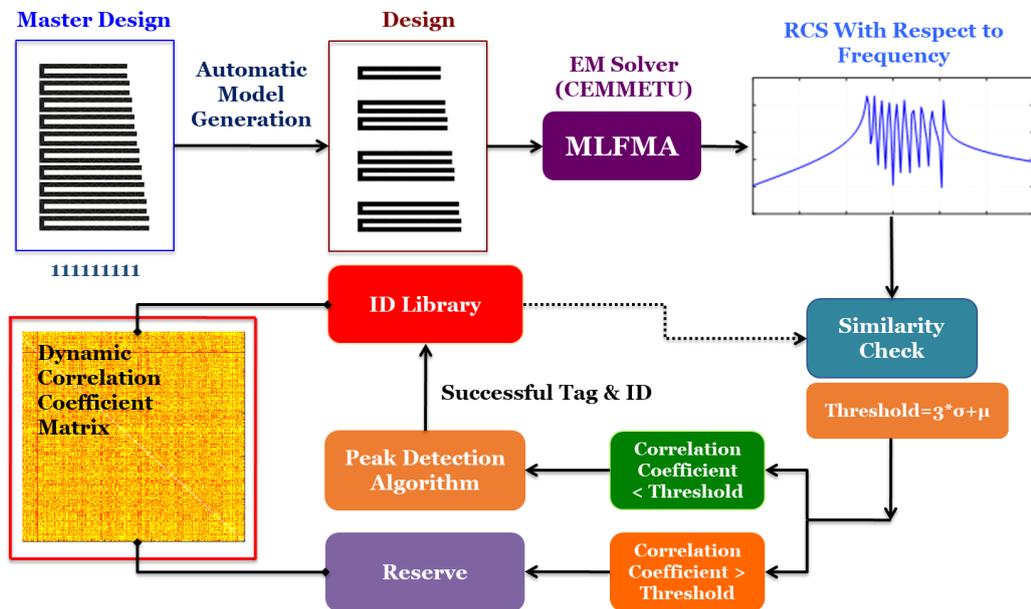
Figure 3.12. Block diagram of generating an ID library for a reliable RFID system

In order to prevent possible misidentifications, tags having similar responses should be avoided within the same library. Elimination is performed by evaluating correlations between different tags and numerically assessing the similarity between them. After calculating the correlation coefficient (R) for each tag pair, a 2-D matrix is constructed. In this study, the correlation coefficient is calculated as

29

$$R_{AB} = \frac{\sum_{i=1}^{n}(A_i - \bar{A})(B_i - \bar{B})}{\sqrt{\left(\sum_{i=1}^{n}(A_i - \bar{A})^2\right)\left(\sum_{i=1}^{n}(B_i - \bar{B})^2\right)}}, \tag{3.1}$$

where A and B represent the calculated RCS values (over the operation frequency band) of the first and second tags, respectively [45], while $\bar{A}$ and $\bar{B}$ are the corresponding mean values of RCS, and n is the number of the frequency samples.

In order to discard tags with similar responses, a threshold value is determined as $3\sigma + \mu$, where σ is the standard deviation value and μ is the mean value of the correlation coefficient matrix. The 3σ value basically represents the control limit that defines the statistical quality of the included tags. The standard deviation is calculated as [39]

$$\sigma = \sqrt{\frac{\sum_{i=1}^{n}(A_i - \bar{A})^2}{n-1}}. \tag{3.2}$$

Then, the elimination is performed as

$$\text{Elimination rule:} \quad \begin{cases} R < \mu + 3\sigma & \text{keep in the library} \\ \\ \text{otherwise} & \text{remove from the library.} \end{cases} \tag{3.3}$$

After all eliminations, the remaining tags in the library are used in the RFID system. At the same time, the eliminated tags are reserved for future applications.

At the reader side of an RFID system, the backscattered RCS response of a tag is processed via a peak detection algorithm, which scans the RCS response and detects peaks and missing peaks to determine the ID word. In Figure 3.13, a possible outcome of a peak detection algorithm is shown where '*' represents the detected peak values.
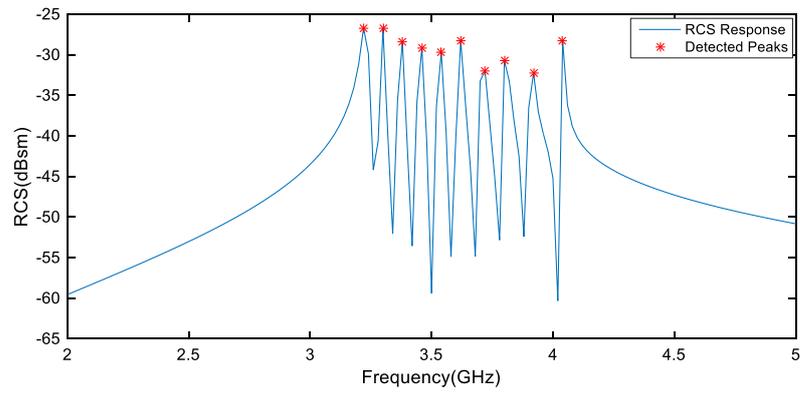
Figure 3.13. Outcome of the peak detection algorithm for ID word '1111111111'
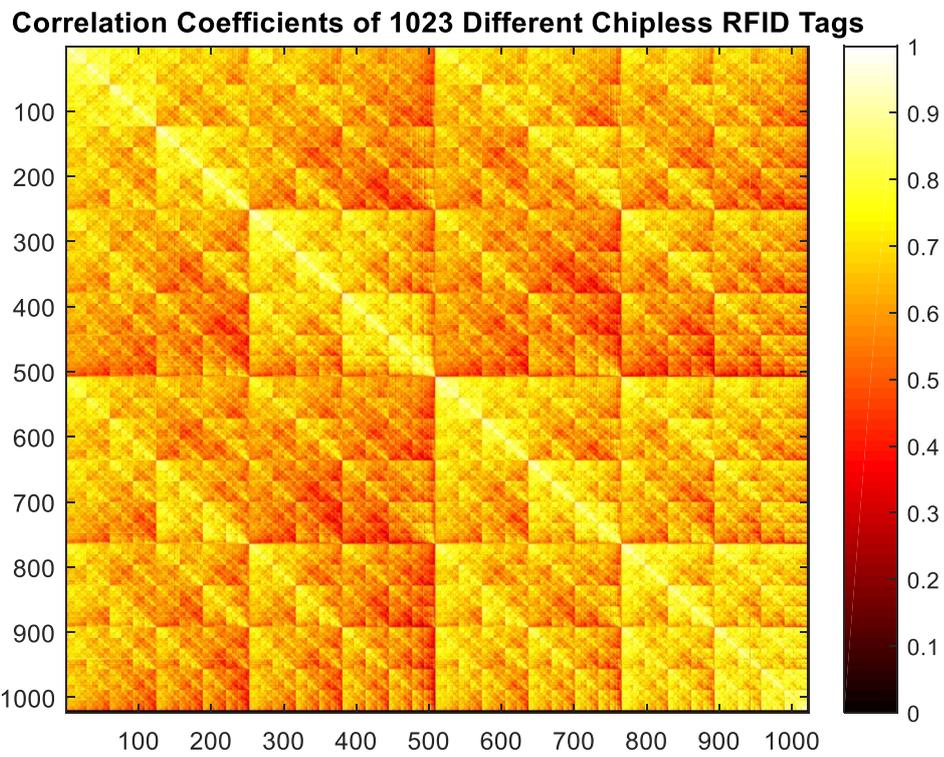
Figure 3.14. Correlation coefficient matrix for the 10-bit tag structure

3.3.1. ID Library of the 10-bit Chipless RFID System

Correlation coefficient matrix for the 10-bit chipless tag is computed as described above in order to form an ID library for the designed system. First, RCS responses of all possible tags are obtained via MLFMA. Then, by using these values, correlation coefficients are calculated. The resulting correlation matrix is shown in Figure 3.14. The matrix entries are represented by colors red to yellow corresponding to correlation values from 0 to 1. Then, using the matrix and the 3σ rule, the candidate tags are sorted in order to discard redundant ones that may lead to misreading. The constructed ID library consists of 890 highly distinguishable tags, while 133 tags are discarded and placed in the reserve database.

3.4. Remarks

In this chapter, chipless RFID tags with U-shaped resonators are analyzed. These types of tags are easily implemented for data encoding. Simulation results indicate that tags with different ID words can easily be constructed. Moreover, a design methodology for constructing an RFID library is discussed. A high-quality ID library is generated for the 10-bit tag structure to demonstrate both the suitability of the design methodology and the effectiveness of the design based on U-shaped resonators.

CHAPTER 4

ARRAY STRATEGIES

In this chapter, array strategies for chipless RFID tags are discussed. Arrays obtained by following various strategies are compared with each other to reach suitable designs for effective RFID systems.

4.1. Motivation

Chipless RFID systems are considered to be more suitable for practical identification and tracking applications due to their low-cost implementations compared to other state-of-the-art systems. However, chipless RFID tags may suffer from readability and reliability issues and a chipless RFID tag should provide sufficient RCS levels to achieve long reading ranges as much as possible in order to have an advantage over a barcode. In addition, peak sensing is the main principle of an RFID recognition. Therefore, the difference between a resonance peak level and the average RCS level should also be sufficiently large to reduce the risk of misidentification.

Performance of a chipless RFID system can be enhanced by arranging multiple tags into an array structure, while this brings a trade-off between size and performance [36], [37]. Inkjet printing technique can be particularly suitable to fabricate these kinds of arrays since it is an additive fabrication process. In this chapter, many different array scenarios are studied for developing enhanced performance for chipless RFID tags.

4.2. Simulation Results

Figures 4.1 to 4.7 show geometrical drawings of various arrays of the 10-bit structure as well as their RCS responses for linear (XX and YY) and circular (CC) polarizations.
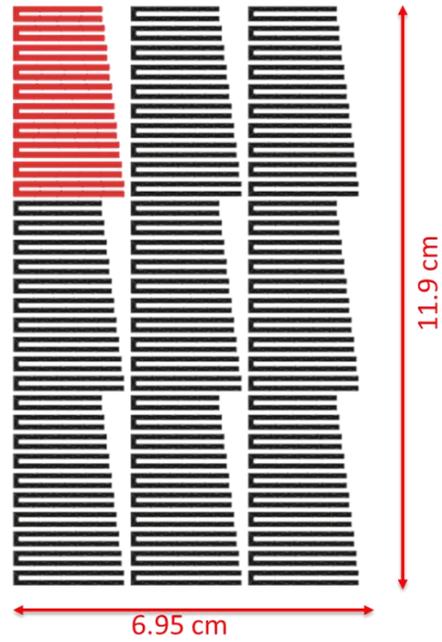
33

Figure 4.1. RCS of the D11 tag with ID word '1111111111'
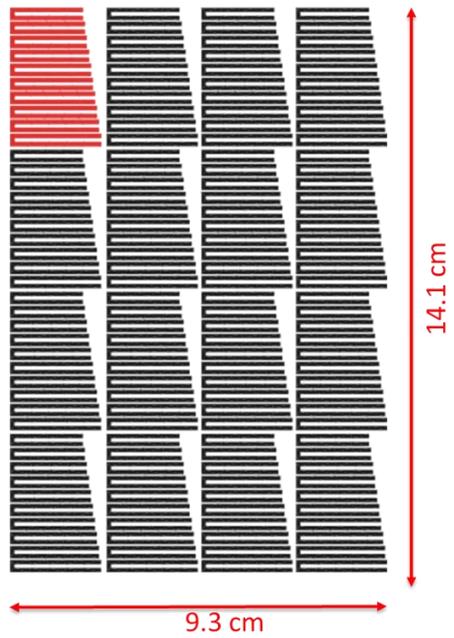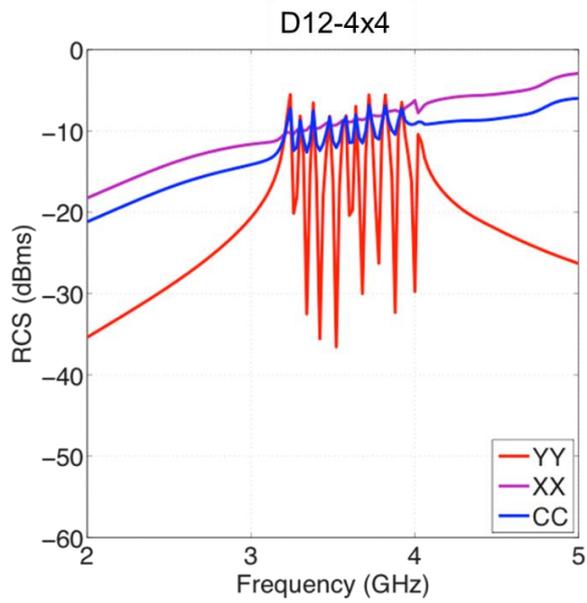
Figure 4.2. RCS of the D12 tag with ID word '1111111111'

34
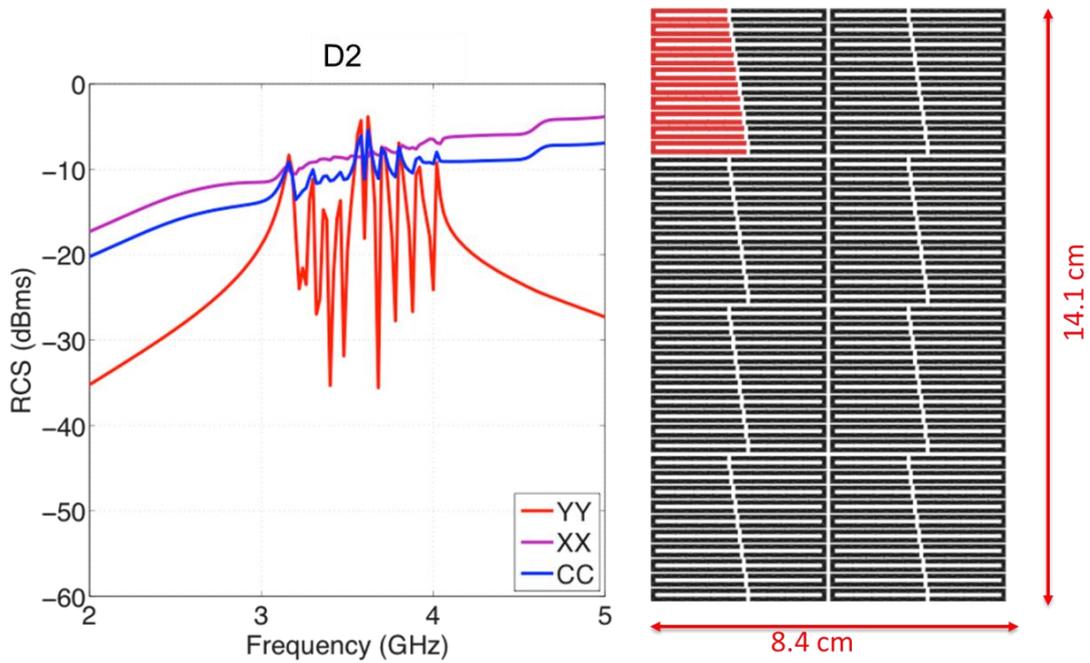
Figure 4.3. RCS of the D2 tag with ID word '1111111111'

These arrays are selected as examples based on many simulations involving other configurations. In general, results show that array configurations improve the performance in comparison to the single tag considered in Chapter 3.

Figures 4.1 and 4.2 show RCS results for the regular arrangements of 3x3 (D11) and 4x4 (D12) elements. For linear polarizations, the RCS level increases by 15 dB for the D11 tag and 20 dB for the D12 tag with respect to the RCS of a single 10-bit element. On the other hand, the peak-to-dip differentiation deteriorates as a consequence of couplings between the individual tags in the array. Among different polarization options, YY provides the best results for the arrays, i.e., it leads to much better peak-to-dip differentiation in comparison to XX or CC. It is remarkable that RCS level increases when using the XX option, while the differentiation becomes almost zero.
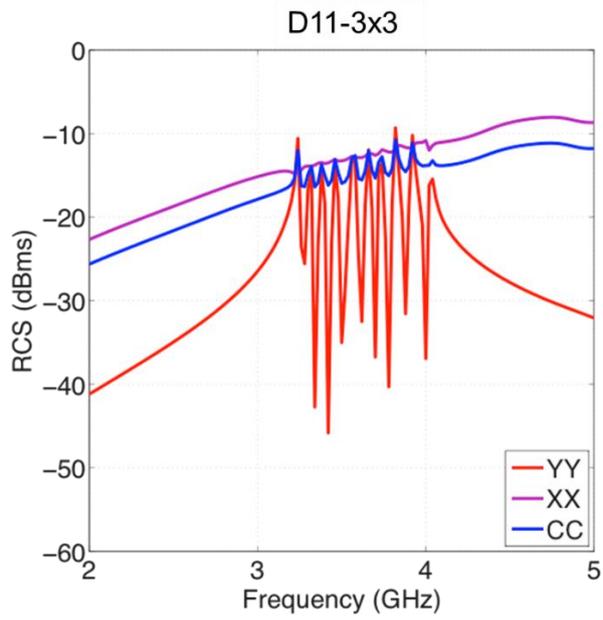
Figure 4.4. RCS of the D31 tag with ID word '1111111111'
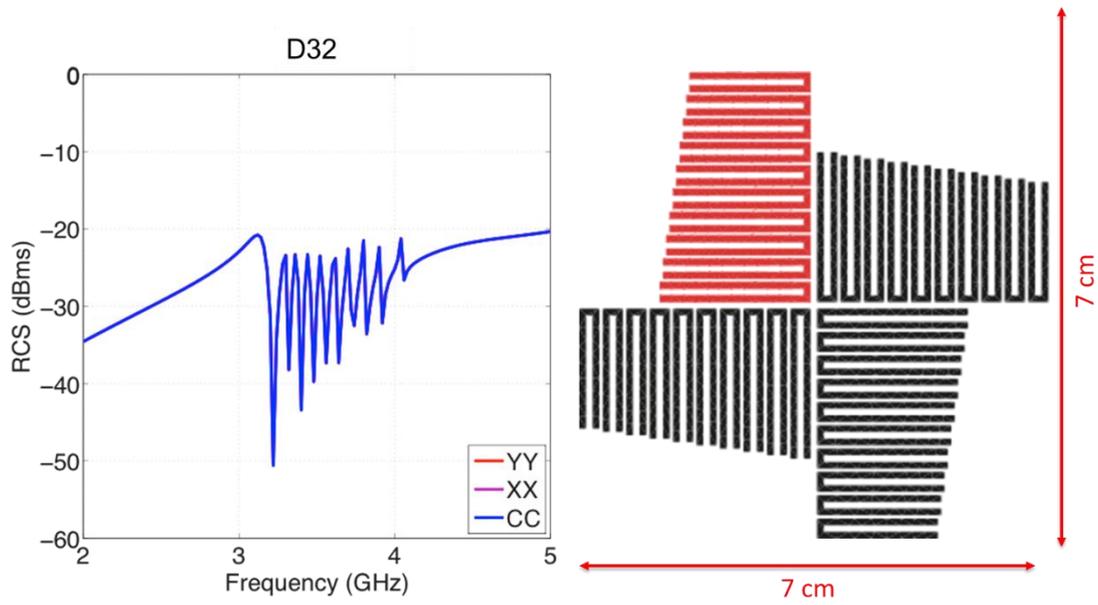
Figure 4.5. RCS of the D32 tag with ID word '1111111111'
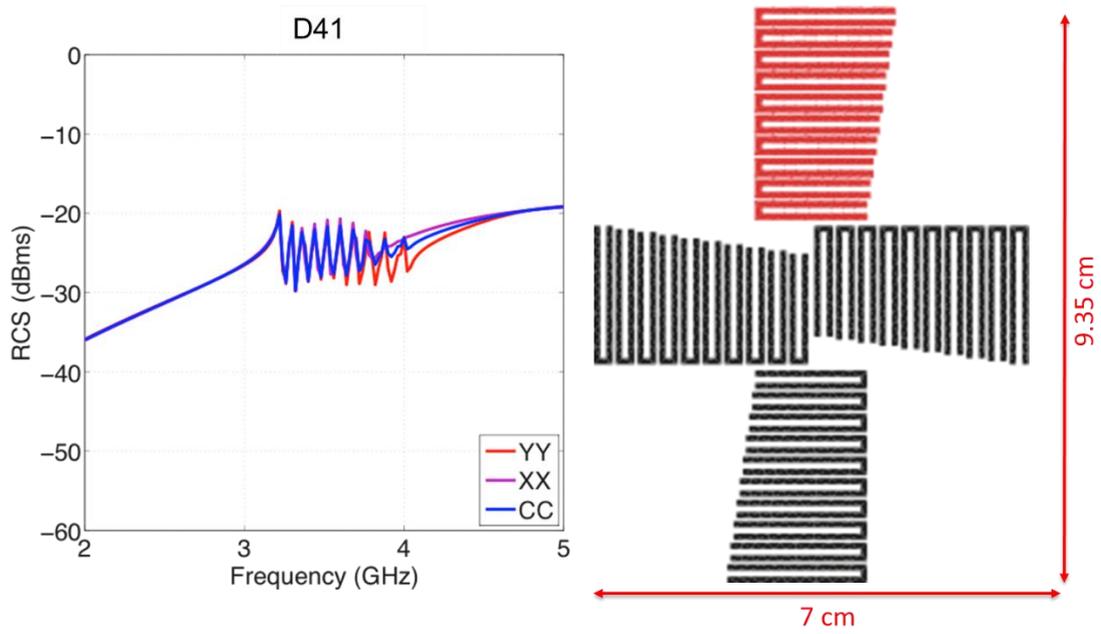
Figure 4.6. RCS of the D41 tag with ID word '1111111111'
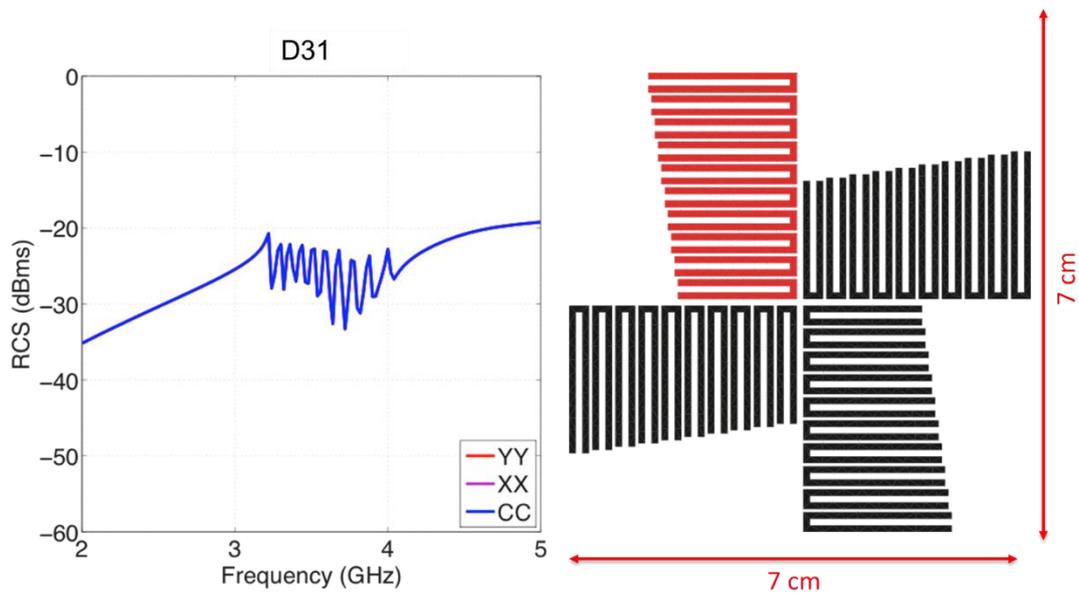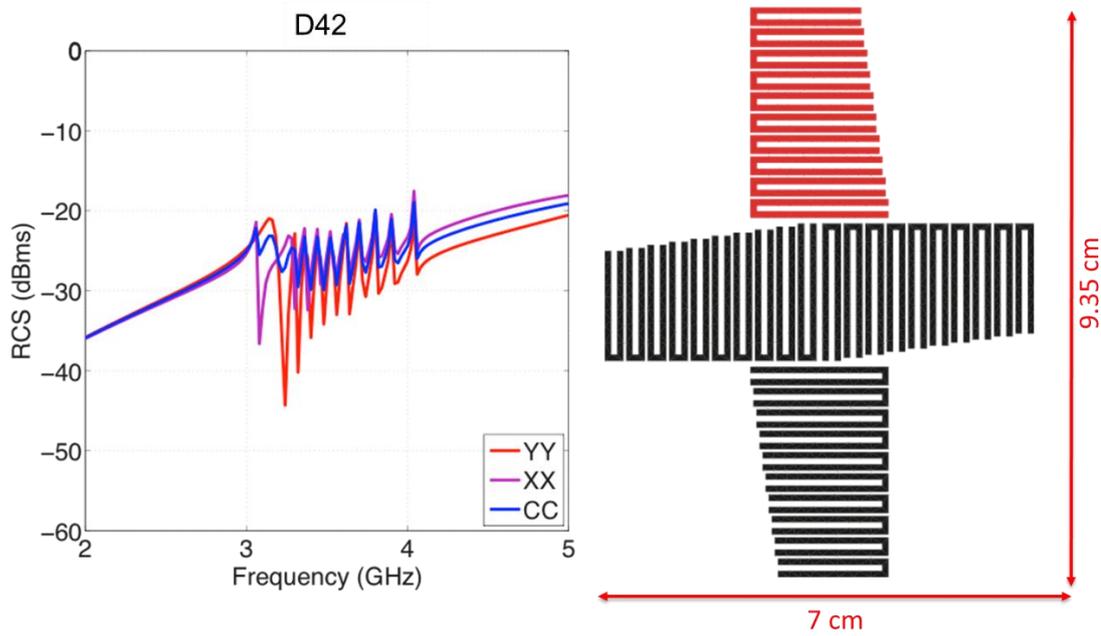

Figure 4.7. RCS of the D42 tag with ID word '1111111111'

37
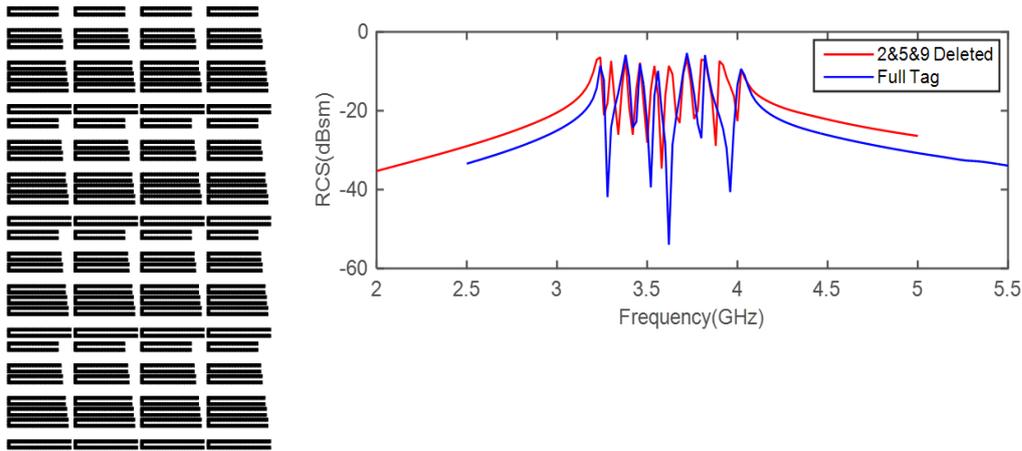
Figure 4.8. RCS of the D12 tag with ID word '1011101101'

Figure 4.3 presents the RCS results for a compact arrangement of 4x4 elements (D2). The RCS responses indicate that the D2 configuration increases the RCS level by 15−25 dB for linear polarizations. On the other hand, a relatively irregular RCS curve is obtained in terms of peak distribution for YY. Also, the minimum peak-to-dip difference value is 12 dB for this polarization.

D31 and D32 arrays are rotational arrangements of four elements with full symmetry. As one may expect, Figures 4.4 and 4.5 show that these tags provide exactly the same RCS response for different polarizations. Moreover, the RCS level increases by 5 dB in comparison to the single element, whereas the peak-to-dip difference is minimum 8 dB for all polarizations.

The last pair of configurations are cross-shaped arrangements, namely D41 and D42, shown in Figures 4.6 and 4.7. These tags also provide similar RCS responses for different polarizations. For the YY polarization, the RCS level increases by 8 dB, whereas the peak-to-dip difference is 8 dB.

Figures 4.8 to 4.10 present RCS responses of arrays D12, D2, and D32 when bits {2,5,9} are deleted (in all individual tags), in comparison to the full versions (when all bits exist) for the YY polarizations. We observe that the RCS peaks corresponding

38
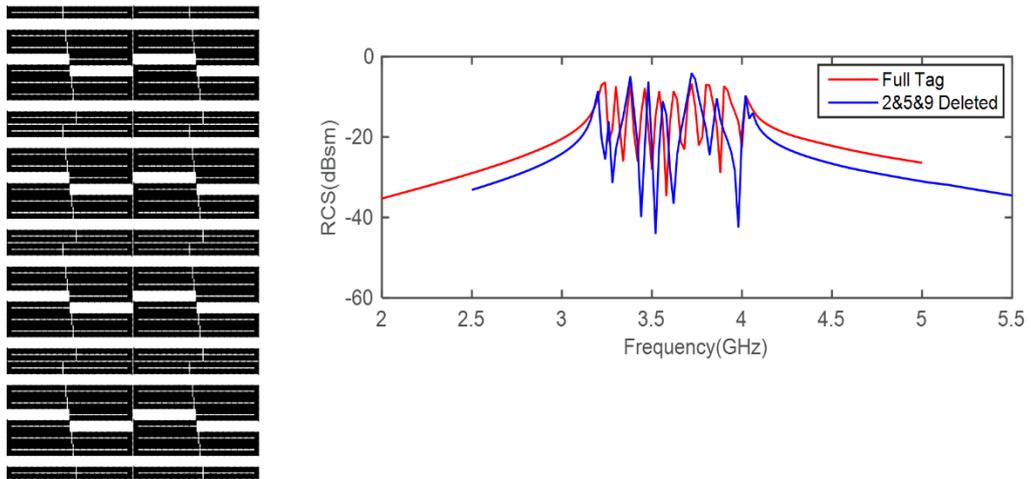
Figure 4.9. RCS of the D2 tag with ID word '1011101101'
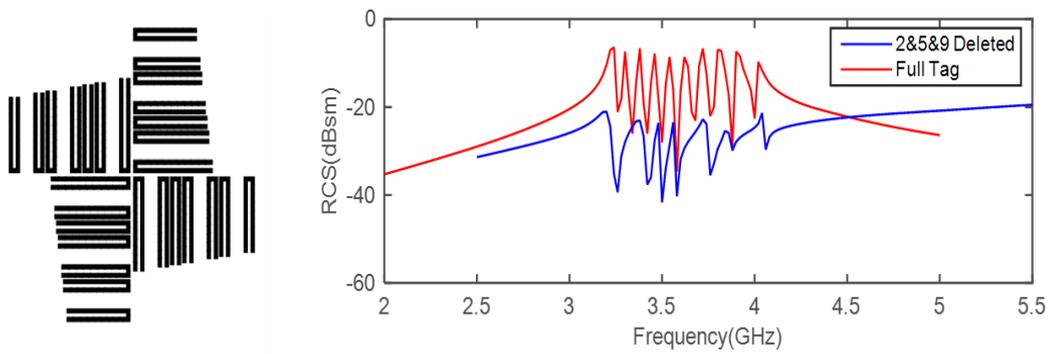
Figure 4.10. RCS of the D32 tag with ID word '1011101101'

to the deleted bits clearly disappear so that the RFID tags can be successfully identified.

4.2.1. Comments on the Results

For a quantitative comparison of different array configurations shown in Figures 4.1 to 4.7, Table 4.1 lists the mean RCS and peak-to-dip differentiation values for the single tag, as well as for the four different array configurations. The mean RCS is obtained by considering the frequency range from 2.75 GHz to 4.25 GHz. The peak-

to-dip differentiation is found by considering consecutive peak-to-dip pairs and selecting the worst case. The values are given for three polarization options, i.e., XX, YY, and CC. In addition, the surface areas covered by the structures are listed in Table 4.1.

Table 4.1. *Results for different array configurations*

		Mean (dBsm)			Peak-to-dip difference (dB)		
Structure	Size (cm^2)	XX	YY	CC	XX	YY	CC
Single	7.8	-31	-41	-33	0.1	18	2
D11	84	-14	-21	-16	0.1	11	2
D12	131	-9	-17	-12	0.1	10	3
D2	119	-9	-18	-11	0.1	12	0.5
D31	49	-26	-25	-25	4	7	7
D32	49	-26	-26	-26	10	10	10
D41	66	-24	-24	-24	2	5	2
D42	66	-25	-27	-25	6	8	2

Considering the presented values in Table 4.1, important observations are as follows.

- In general, XX leads to better (higher) mean values in comparison to YY and CC, especially for the D12 and D2 arrays. On the other hand, very small differentiation values make most designs impractical.
- Considering differentiation, the best polarization option seems to be YY. The exceptions are D31 and D32 arrays, which perform the same for all polarizations due to their rotational symmetry. Considering all performances,

D32 is more suitable than others if polarization cannot be controlled in the used RFID system.

- Assuming that the YY polarization is used, the best results (considering both mean and differentiation) are obtained with D12 and D2. On the other hand, these arrays occupy 131 cm^2 and 119 cm^2 areas, respectively. If compactness is also critical, the D32 array seems to be the best option with reasonable mean and differentiation values while using only 49.0 cm^2.

4.2.2. Quality Factor

While RCS plots provide important information on the RCS characteristics of the array, we further compare them quantitatively [36]. For a selected interval of frequency containing all resonances, i.e., [3.0, 4.2] GHz in our case, we compute

$$Q = M + \sum_{i=1}^{10} (P_i - M), \tag{4.1}$$

where M is the mean value (over dB values) of the RCS in the interval, while P_i for $i = 1, 2, \dots, 10$ represents the peak values (in dB) at resonances. A large value of Q indicates good array performance with both large mean RCS (M) and large peak-to-mean separation ($P_i - M$). Table 4.2 lists the values of Q for both linear (YY) and circular polarizations, as well as the size of each array, in contrast to values for a single element. Comparing the results for the linear polarization, performances of the first three arrays in comparison to other four (circular) are remarkable. Obviously, increasing the number of elements in the array improves the performance. Interestingly, these larger arrays (D11, D12, and D2) perform better than circular ones (D31, D32, D41, and D42) even for circular polarization. Among circular arrays, any of them can be used in terms of performance, while D31 and D32 come to forefront with their better compactness. Among D11, D12, and D2, Figure 4.3 shows that D2

does not provide good results in terms of the distinguishability of the peaks (even though this is not visible in Q value). D11 and D12 seem to be very suitable in terms of base and peak RCS values, while their selection depends on the trade-off between the performance and compactness.

Table 4.2. *Q factor values of the proposed array configurations*

Structure	Size (cm^2)	Q (dB) Linear	Q (dB) Circular
Single Element	7.8	-29.8	-29.6
D11	84	-12.7	-12.6
D12	131	-7.62	-8.00
D2	119	-8.93	-8.34
D31	49	-22.7	-22.7
D32	49	-22.6	-22.6
D41	66	-22.3	-22.3
D42	66	-22.5	-22.2

4.3. Reduced Tags

Similar array configurations are carried out for reduced sized tags, which are based on the original structure. The first reduced tag, namely R1, shifts of the operating frequency band to 3.5−5 GHz as shown in Figure 4.11. On the other hand, the R2 tag almost doubles the frequency bandwidth and operates in the 3−5 GHz band as shown in Figure 4.12. As shown in the results, R1, R2, and their array forms provide good RCS responses while occupying smaller areas in comparison to the original design presented so far.

Figure 4.11. RCS of the R1 tag with ID word '1111111111'

Figure 4.12. RCS of the R2 tag with ID word '1111111111'

Figure 4.13. RCS of the R1-D12 tag with ID word '1111111111'

Figure 4.14. RCS of the R1-D5 tag with ID word '1111111111'
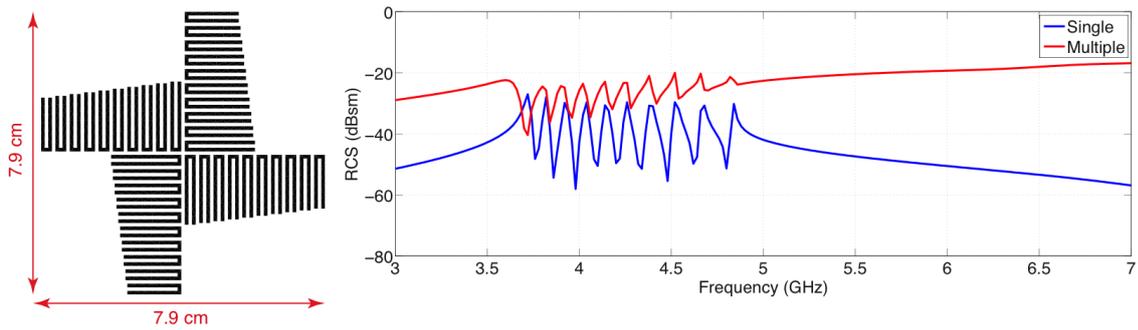
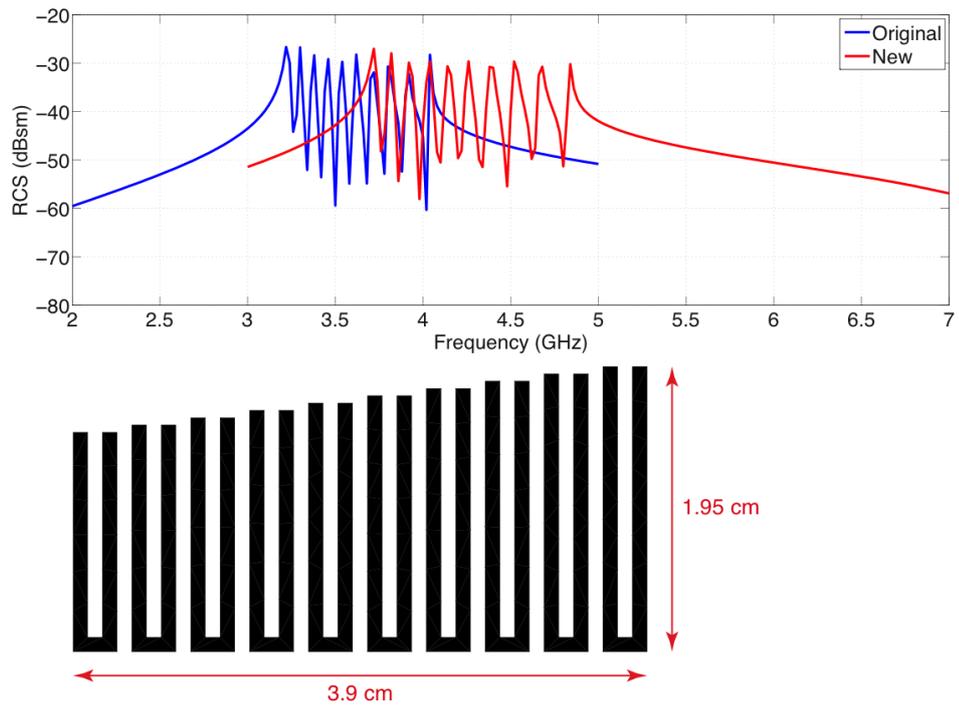Figure 4.15. RCS of the R1-D32 tag with ID word '1111111111'

44
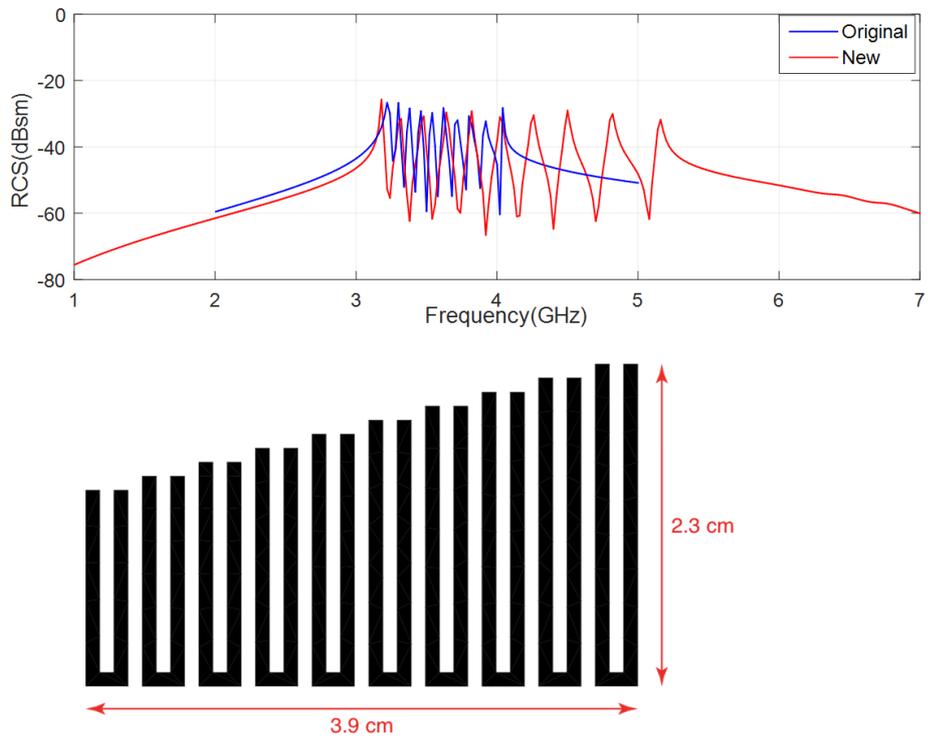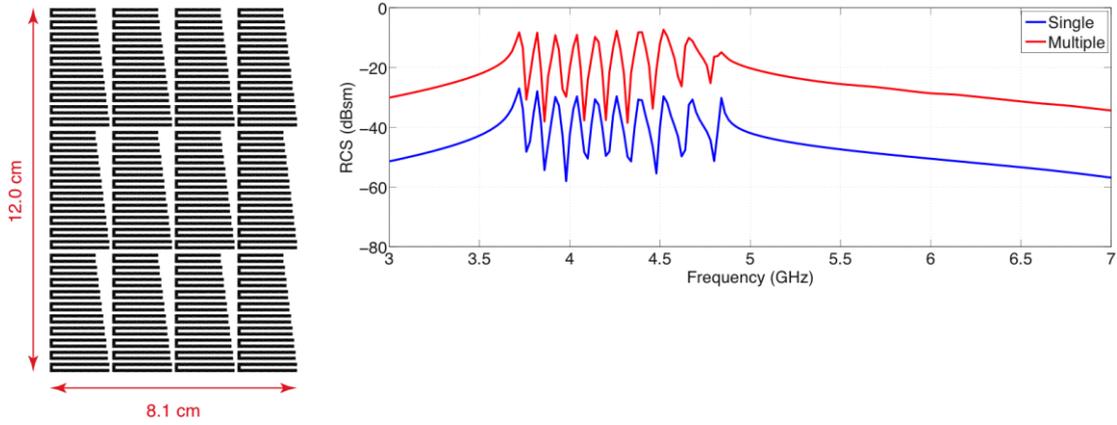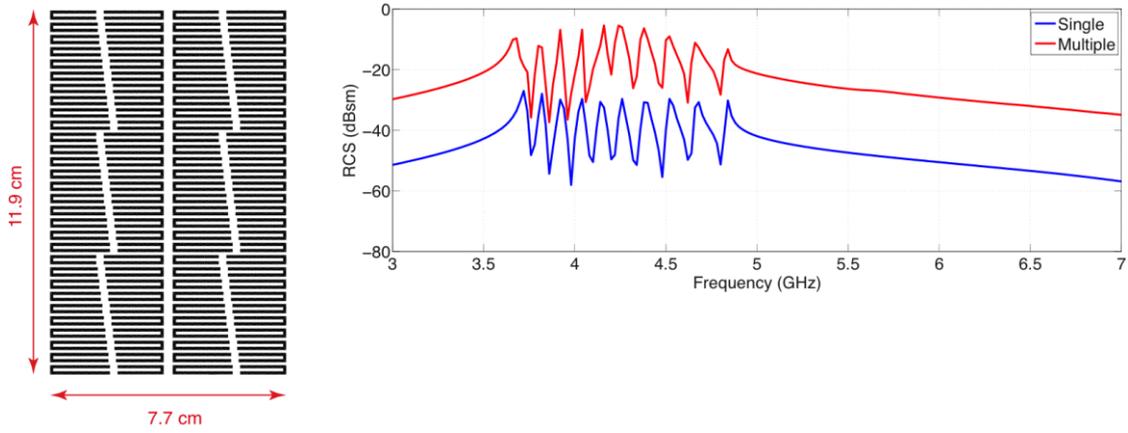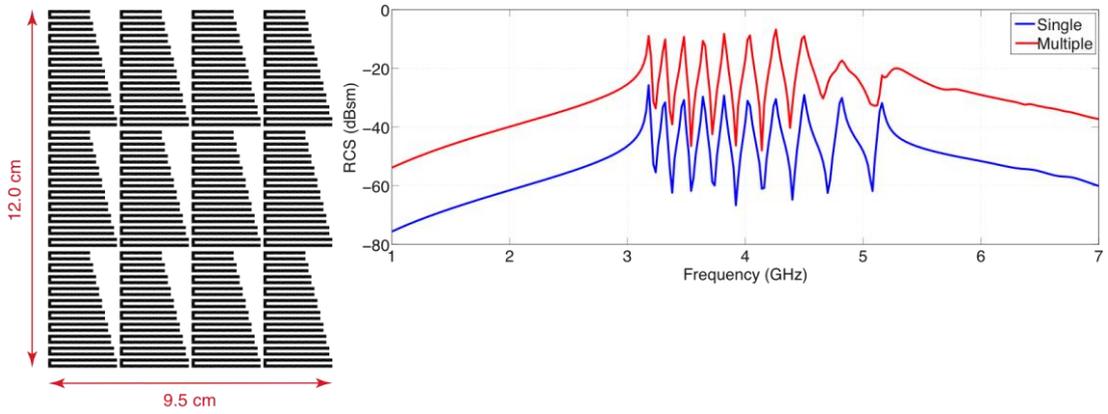
Figure 4.16. RCS of the R2-D12 tag with ID word '1111111111'
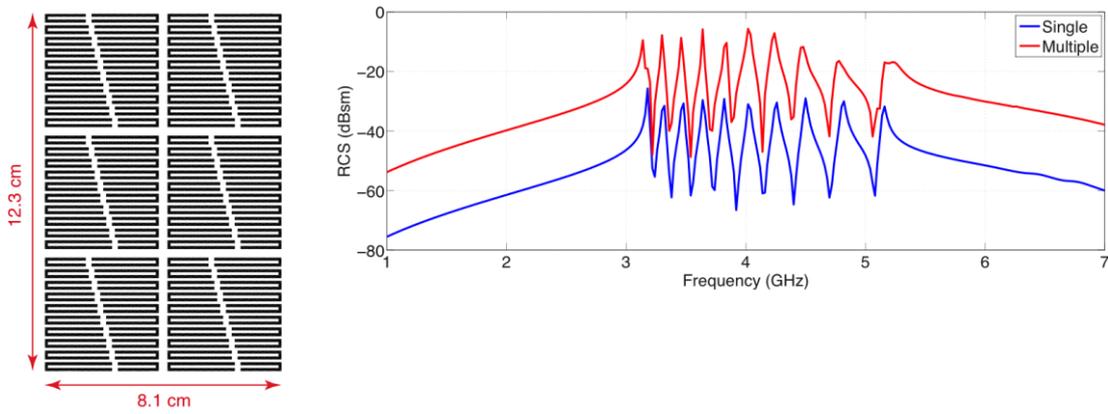
Figure 4.17. RCS of the R2-D5 tag with ID word '1111111111'
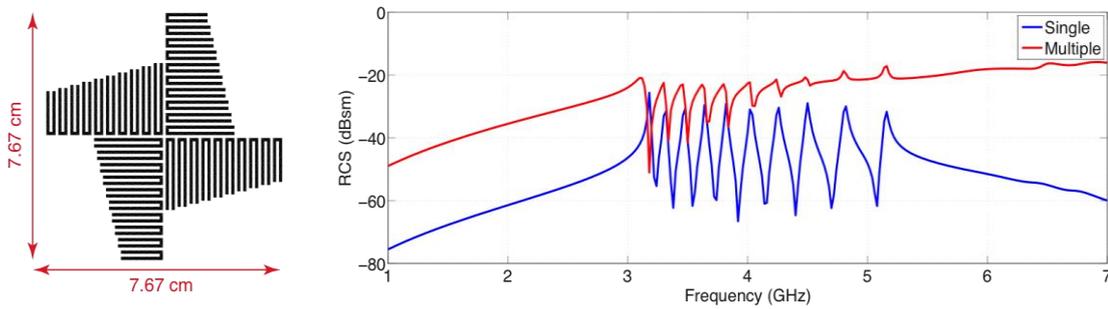
Figure 4.18. RCS of the R1-D32 tag with ID word '1111111111'

45

For both R1 and R2, different array configurations are tested in order to observe improvements in the RCS responses. Figure 4.13−4.15 and Figure 4.16−4.18 show examples for arrays arrangements of R1 and R2, respectively, when the YY polarization is used. The results are generally similar to these obtained with the original design, while they clearly show that different designs can be generated depending on the given frequency range.

4.4. Remarks

In this chapter, array configurations of U-shaped resonators for building effective chipless RFID tags are analyzed. Combining multiple tags as arrays can be useful for improving the related RFID systems, while the selected strategy is extremely important for readability and reliability performances, as well as for compactness. Numerical simulations, a few of which are presented in this thesis, show that the backscattered RCS can significantly be affected due to couplings between individual tags. Based on the numerical results and Q factor values, new strategies can further be developed to design more effective array-based tags.

CHAPTER 5

HOURGLASS-SHAPED CHIPLESS RFID TAGS

In this chapter, an innovative chipless RFID tag design, which is able to encode 20-bit data, is proposed. It is optimized to enhance RCS levels while being small-sized for practical use in real-life RFID systems.

5.1. Motivation

Considering different aspects, a chipless RFID tag design should use relatively narrow frequency bands, lead to highly distinguishable variations, and be compact while producing sufficient RCS level. In addition, fabrication limitations can bring extra constraints. In our previous works [36], we showed that array configurations may be necessary if available designs are to be used, while the resulting structures are naturally large.

5.1.1. New Tag Design

In this study, we present novel structures involving nested U-shaped resonators, such as depicted in Figure 5.1, which can provide desired RCS levels while being relatively compact. Resonator shapes, dimensions, and distances between them are designed parametrically to achieve the abovementioned desired properties. The tag design encoding 10-bit data with ID word '1111111111' (master tag) is shown in Figure 5.1.

5.1.1.1. 10-bit Tag Results

Figure 5.2 shows the RCS response of the new 10-bit tag for linear and circular polarizations. Based on the RCS responses, our observations are as follows.

- Considering distinctive appearance of the peaks relative to dips in the RCS response, the tag design provides superior readability and distinguishability.
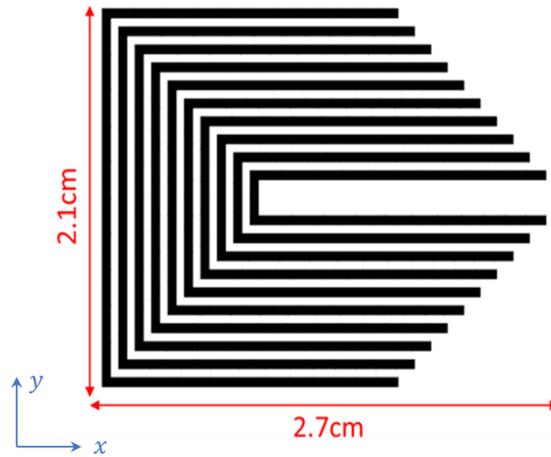
Figure 5.1. 10-bit nested-U-resonator-based tag with ID word '1111111111'
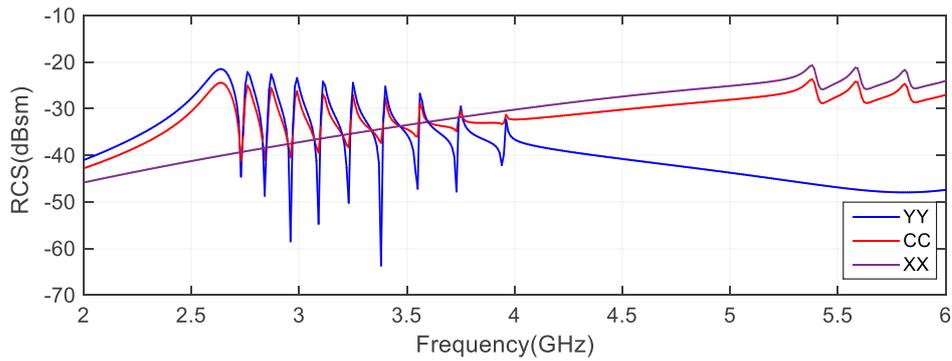
Figure 5.2. RCS of the tag in Figure 5.1 with ID word '1111111111'

- U-shaped resonators located on the tag resonate at different frequencies for the XX and YY polarizations, as opposed to the standard tag discussed in Chapter 3. If the tag is rotated by 90 degrees, the RCS responses for the XX and YY polarizations are also interchanged. We note that the resonance peaks for the XX and YY polarizations are all visible for the circular polarization since this polarization is the superposition of the linear polarizations.

- The proposed tag (21 mm × 27 mm) is more compact than the original one (23 mm × 34.5 mm) although both of them encode 10-bit data.

5.1.2. Array Configurations of the New Tag

In Chapter 2, the importance of the readability and reliability of a chipless RFID tag are discussed. In order to improve the readability, the RCS levels should be at relatively high levels such that the peaks can be detected. Chipless tags are fully passive structures, thus environmental factors that bring extra losses and cause many reflections may significantly affect the RCS responses of the tags. At the same time, the reliability, i.e., accurate identification, mainly depends on peak-to-dip difference levels, since adjacent peak and dip pairs should be well-separated to avoid mixing 0 and 1 bits. According to the results presented in Chapter 4, array configurations can be suitable for enhancing readability and reliability. Hence, a similar array methodology can be employed on the new 10-bit tag, without losing its advantages in terms of compactness. Figures 5.3, 5.5, 5.7, and 5.9 demonstrate the geometries of various array configurations that are discussed below.

5.1.2.1. Simulation Results

The first scenario depicted in Figure 5.3 is face-to-face (hourglass) configuration. Figure 5.4 shows the corresponding RCS response for different polarizations. For linear polarizations, the overall RCS level increases by 10 dB in comparison to the single tag. On the other hand, the RCS level is improved by 5 dB for the circular polarization. In general, the YY polarization leads to higher peak-to-dip differences in comparison to the XX and circular polarizations, especially at higher frequencies.

Figure 5.5 presents the geometry of a side-by-side arrangement, while Figure 5.6 shows the corresponding RCS responses. For all polarizations, the RCS level increases by 3 dB.

Figures 5.7 and 5.9 present two configurations where the tags are arranged vertically. The corresponding RCS results are shown in Figures 5.8 and 5.10, respectively. For both types and all polarizations, the RCS level increases by 3 dB with respect to the RCS of the single tag. On the other hand, peak-to-dip difference levels are not affected significantly.

Figure 5.3. Face-to-face arrangement of the new 10-bit tag with ID word '1111111111'

Figure 5.4. RCS of the face-to-face arrangement of the new 10-bit tag with ID word '1111111111'

Figure 5.5. Side-by-side arrangement of the new 10-bit tag with ID word '1111111111'

50

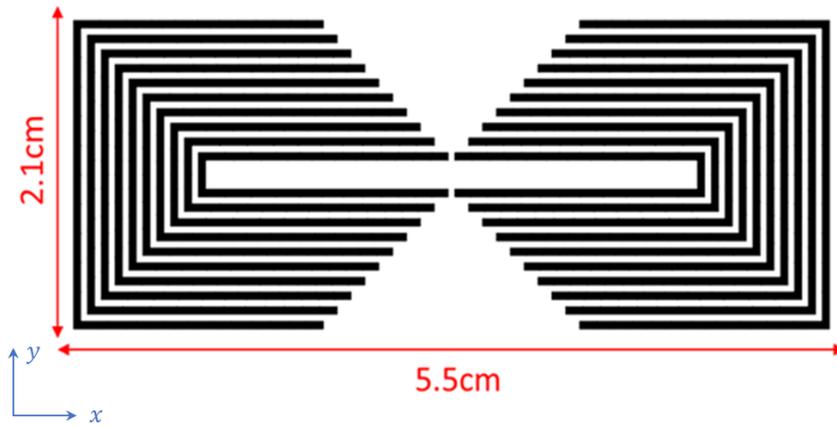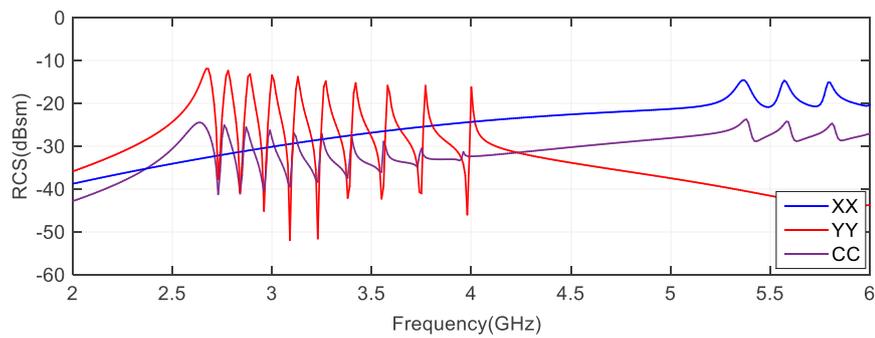Figure 5.6. RCS of the side-by-side arrangement of the new 10-bit tag with ID word '1111111111'

Figure 5.7. Vertical arrangement of the new 10-bit tag with ID word '1111111111'

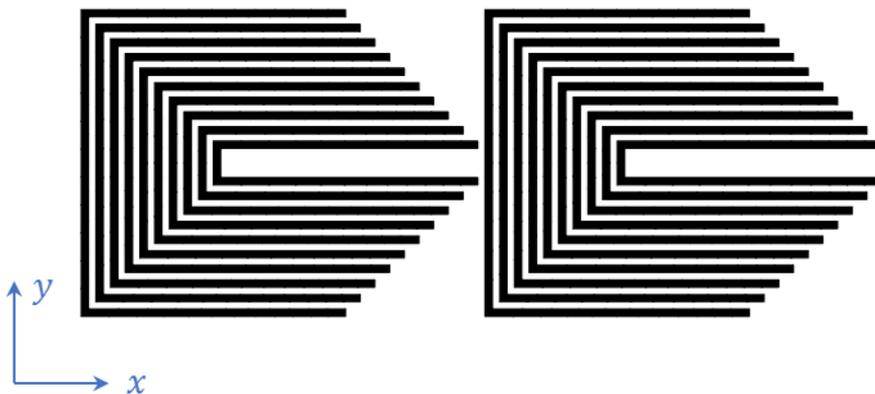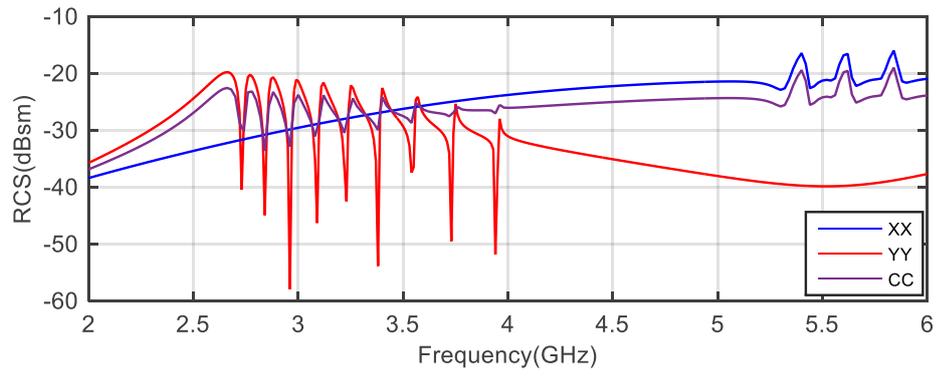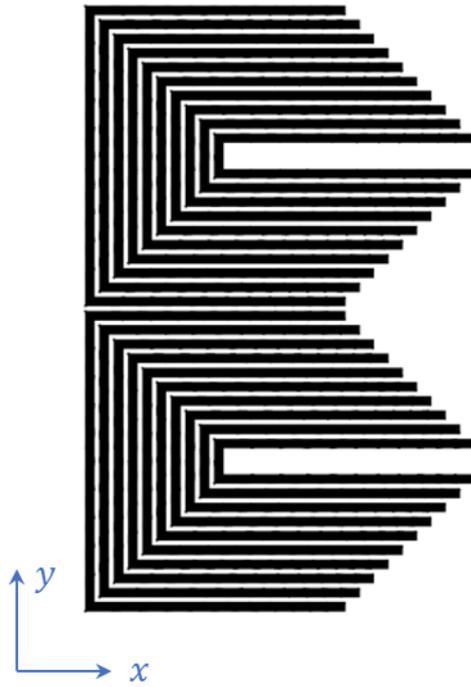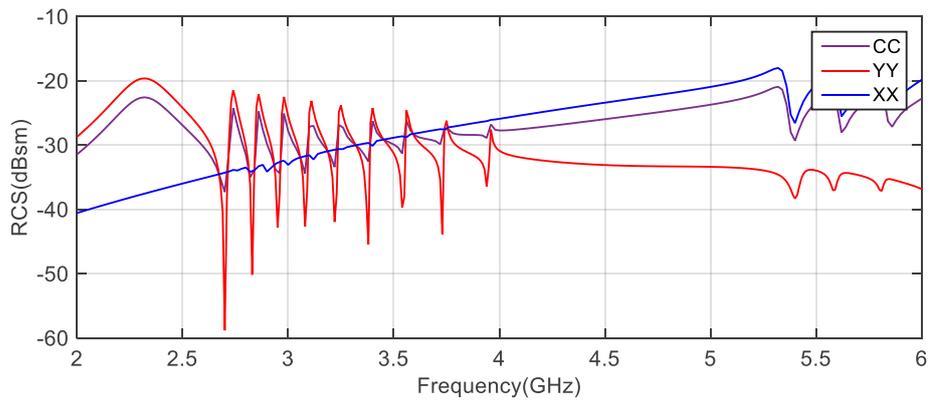Figure 5.8. RCS of the vertical arrangement of the new 10-bit tag with ID word '1111111111'
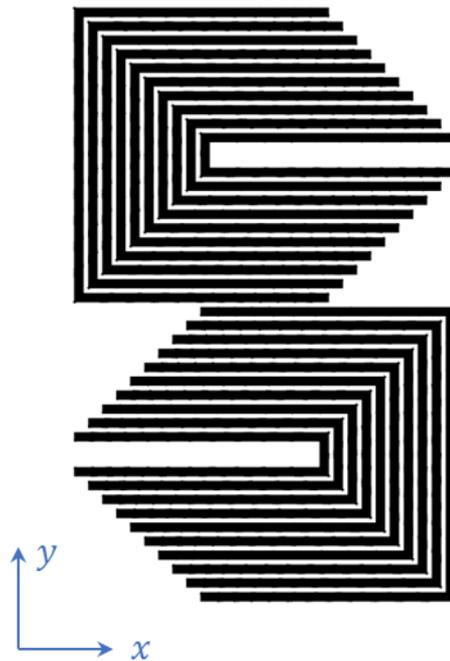
Figure 5.9. Vertical (mirrored) arrangement of the new 10-bit tag with ID word '1111111111'
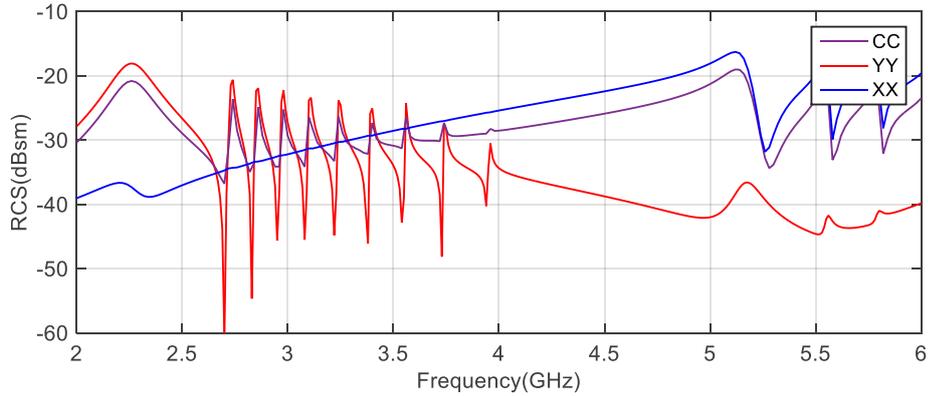
Figure 5.10. RCS of the vertical (mirrored) arrangement of the new 10-bit tag with ID word '11111111111'

Summarizing all results for the arrays, the best RCS level is clearly provided by the hourglass configuration, even though all configurations have the same number of elements. Moreover, the hourglass configuration is highly effective on separating peaks from dips leading to improved distinguishability. All these favorable properties seem to be due to positive effects of mutual couplings between the symmetrically located tags. We further note that the hourglass tag has a much more compact size (21 mm × 55 mm) than the competitive D1 tag (103.9 mm × 87.5 mm) although they provide the same data capacity and similar RCS quality.

Similar to D31 and D32 tags proposed in Chapter 4, a rotational array configuration is employed on the hourglass tag design, leading to a plus-shaped tag. Figure 5.11 presents the geometric model of the tag. The original hourglass tag has a stronger response for the Y polarization, as a typical behavior of U-shaped resonators. On the other hand, the plus-shaped tag has equal responses to X and Y polarizations due to its symmetric structure. Figure 5.12 shows the RCS plots, where the RCS responses to linear polarizations are exactly same due to full symmetry. Moreover, the RCS response is improved for the circular polarization in comparison to the hourglass tag.
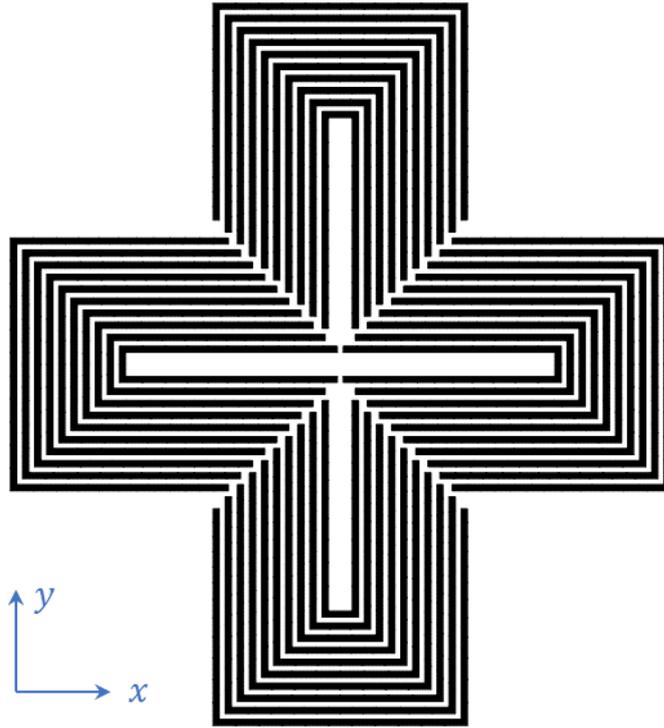
Figure 5.11. 10-bit plus-shaped tag with ID word '1111111111'
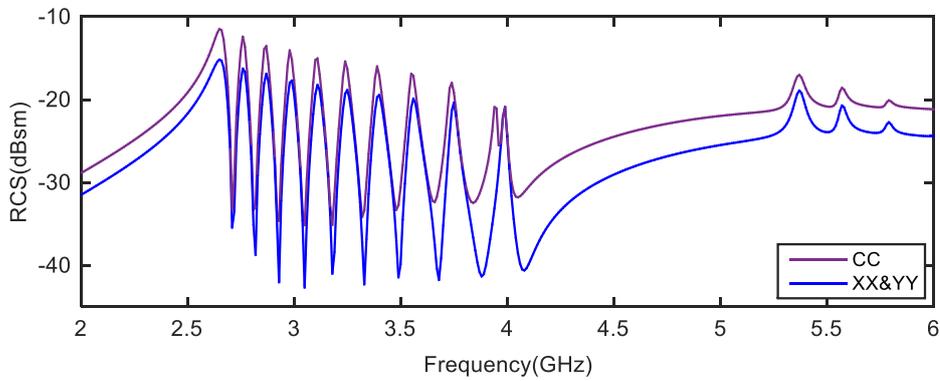
Figure 5.12. RCS of the plus-shaped 10-bit tag with ID word '1111111111'

On the other hand, the plus-shaped tag covers wider area compared to the hourglass tag. Thus, for systems using X or Y polarizations individually, the hourglass tag can be more suitable.
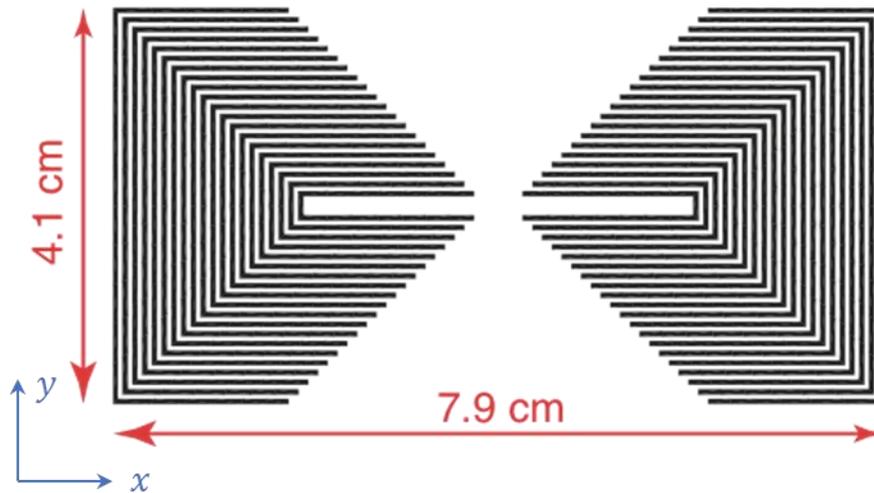
Figure 5.13. 20-bit hourglass tag with ID word '11111111111111111111'
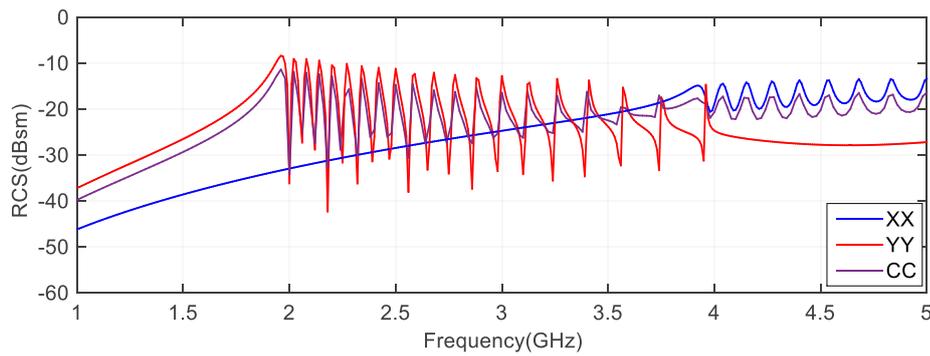
Figure 5.14. RCS curve of 20-bit hourglass tag with ID word '11111111111111111111'

5.1.3. 20-Bit Hourglass Tag

Chipless RFID tags become more attractive when they provide high data capacity in compact forms. For this purpose, small-sized forms of the hourglass tag with 20-bit data capacity are developed. Figure 5.13 presents the geometric model of a designed tag shown for ID word '11111111111111111111'.
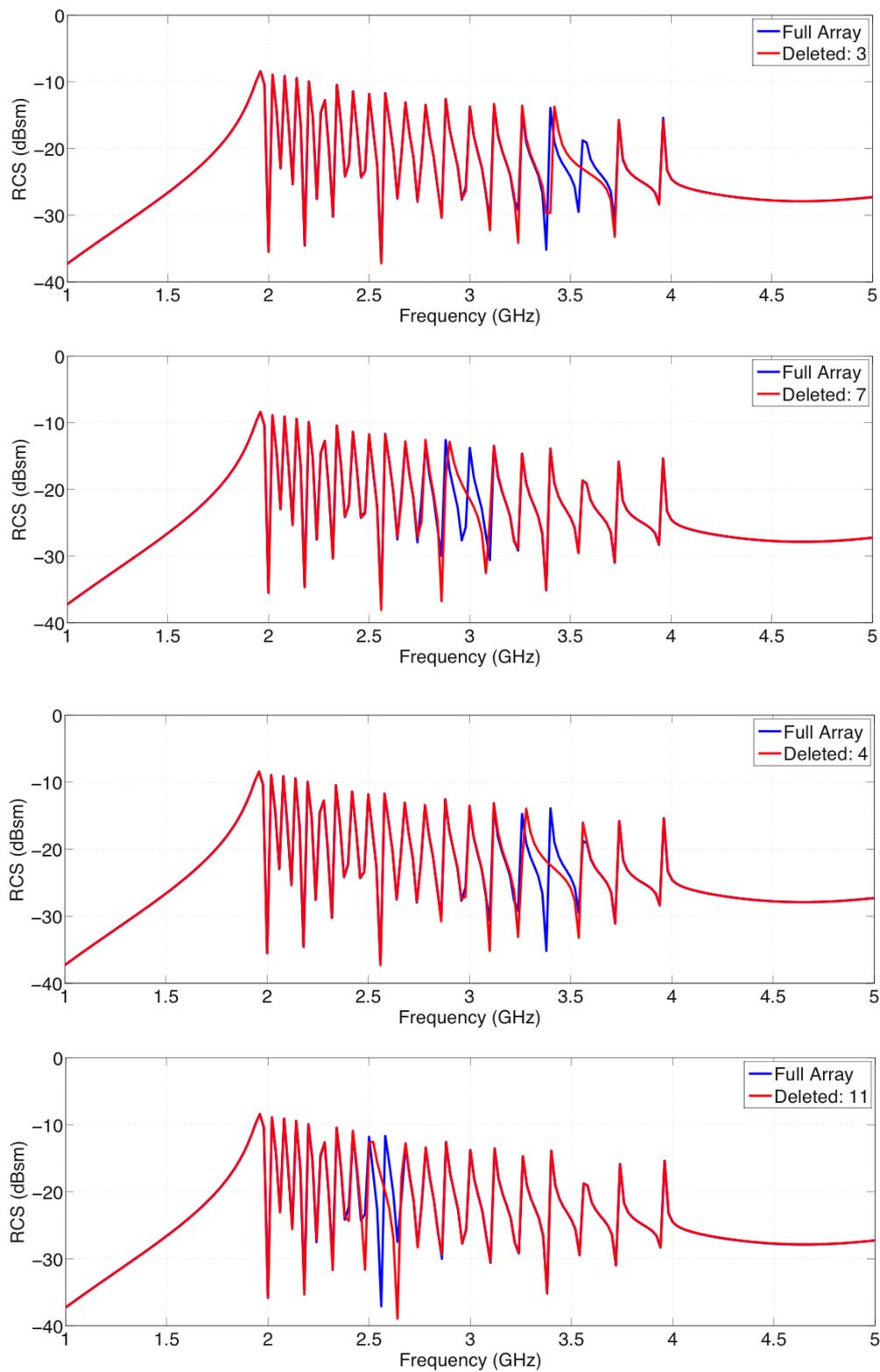
Figure 5.15. RCS results for single-bit deletions

56
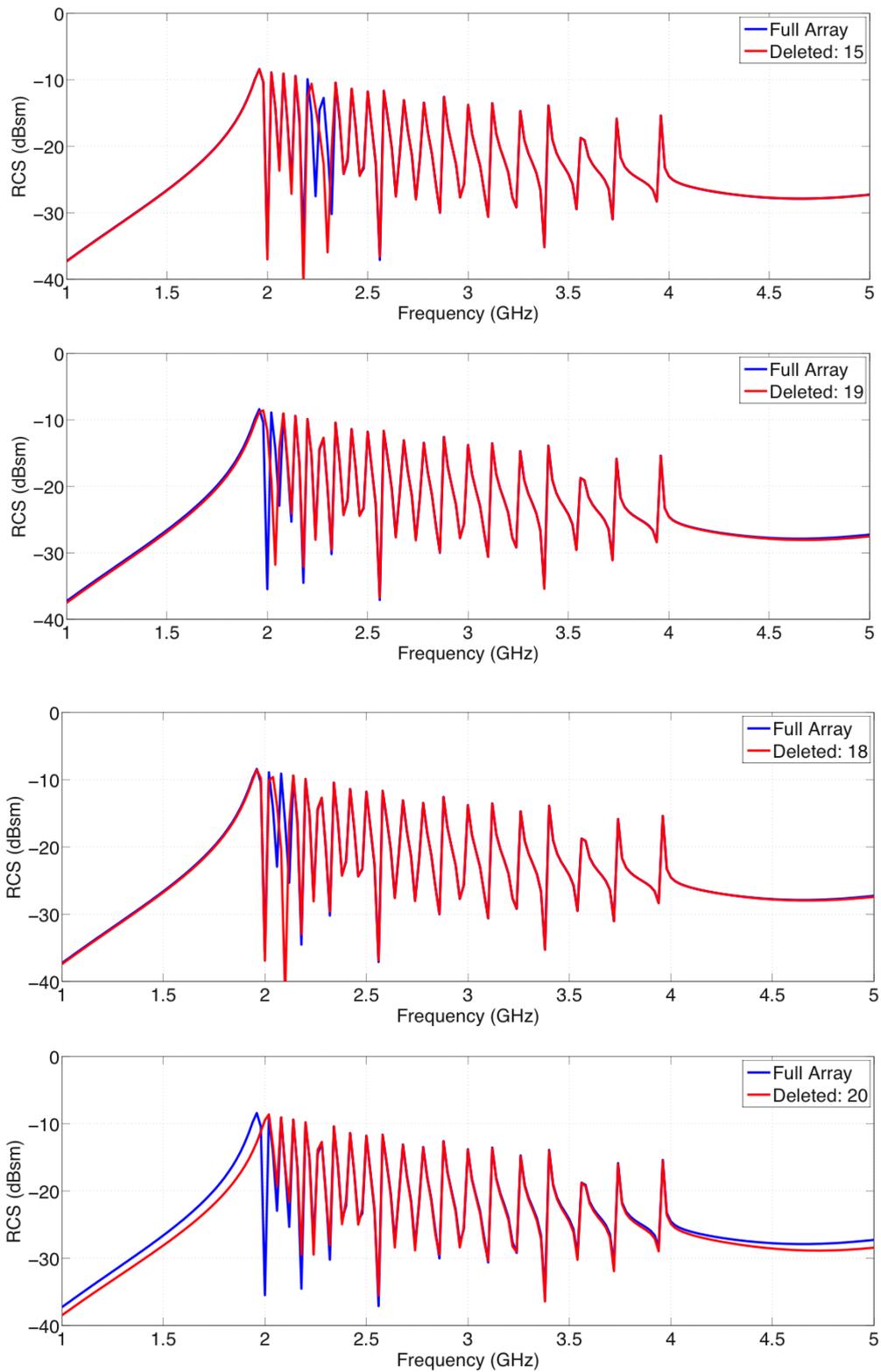
Figure 5.16. RCS results for single-bit deletions
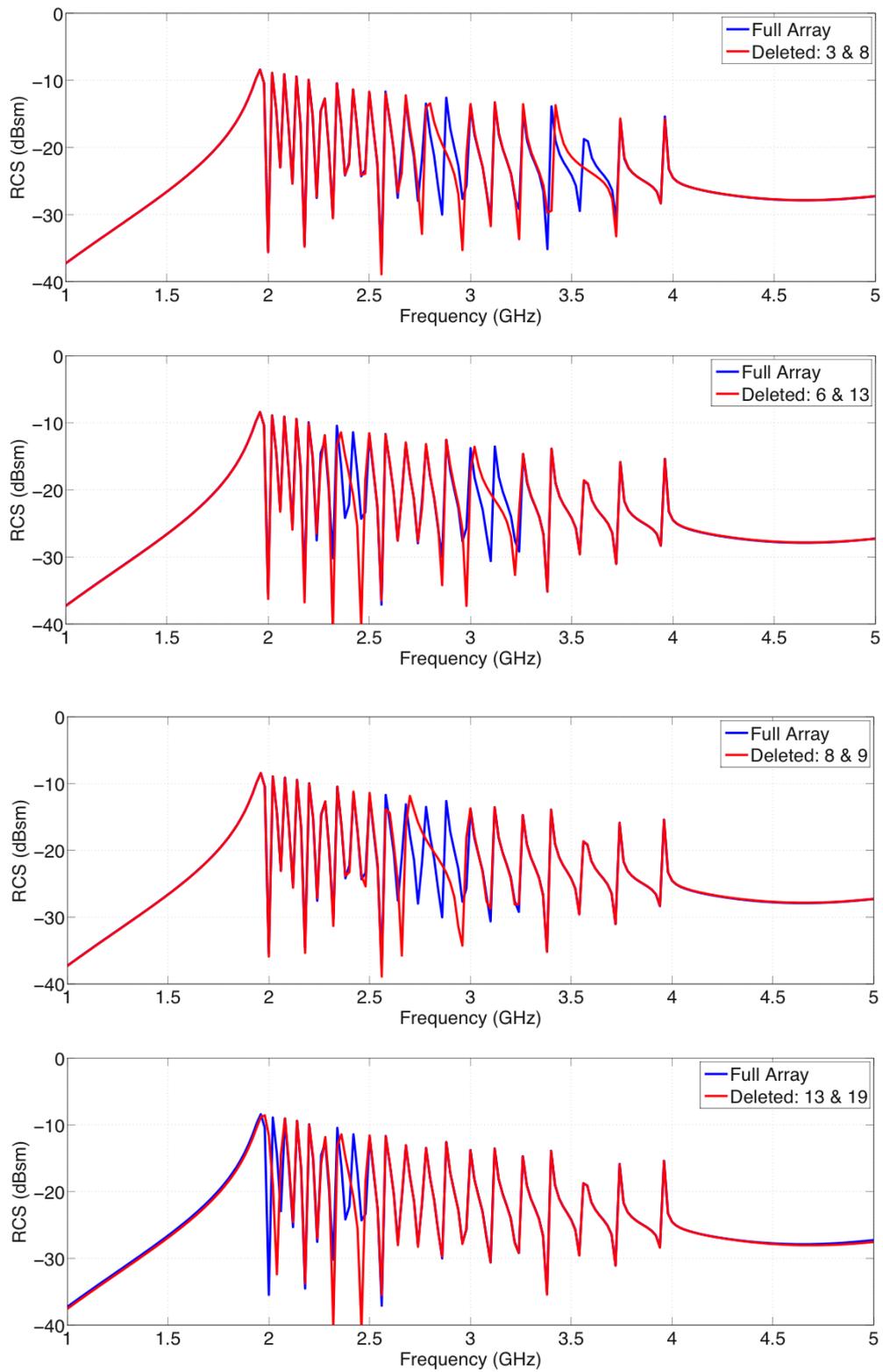
Figure 5.17. RCS results for three-bit deletions

58
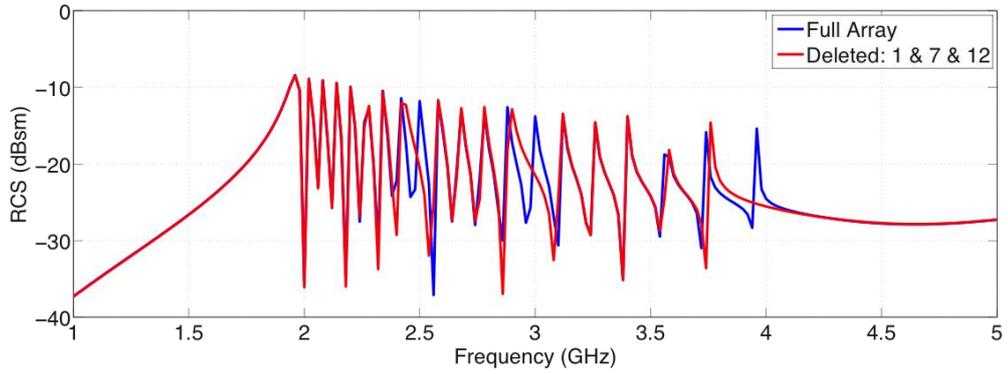
Figure 5.18. RCS results for three-bit deletions
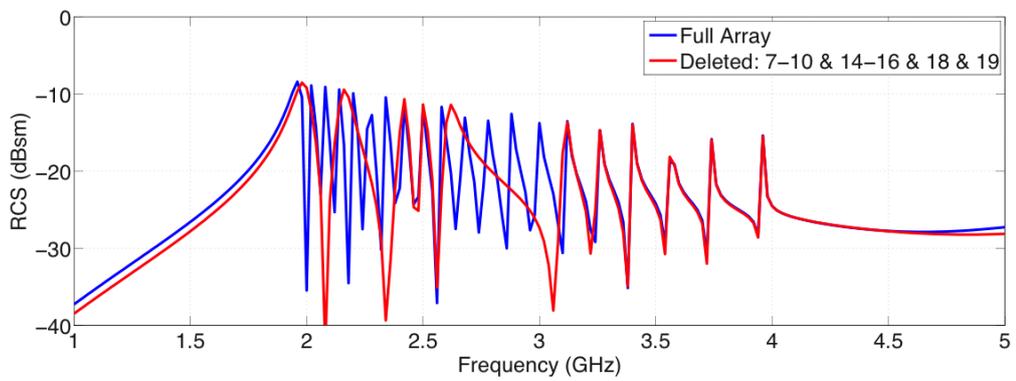
Figure 5.19. RCS results for six-bit deletions

5.1.3.1. Simulation Results

For linear and circular polarizations, RCS responses of the 20-bit tag in Figure 5.13 are shown in Figure 5.14. As one may expect, the resonance bands are wider in comparison to bands of the 10-bit tag, while all resonances for the YY polarization are still located in the 2−4 GHz. Also, each resonance peak is easily detected in the RCS response. Figures 5.15 to 5.19 present sample results of RCS responses for different IDs when YY polarization is used. Specifically, we consider single-bit, two-bit, three-bit, and six-bit deletions. All results demonstrate the successful formation of RCS curves depending on the extracted resonators.
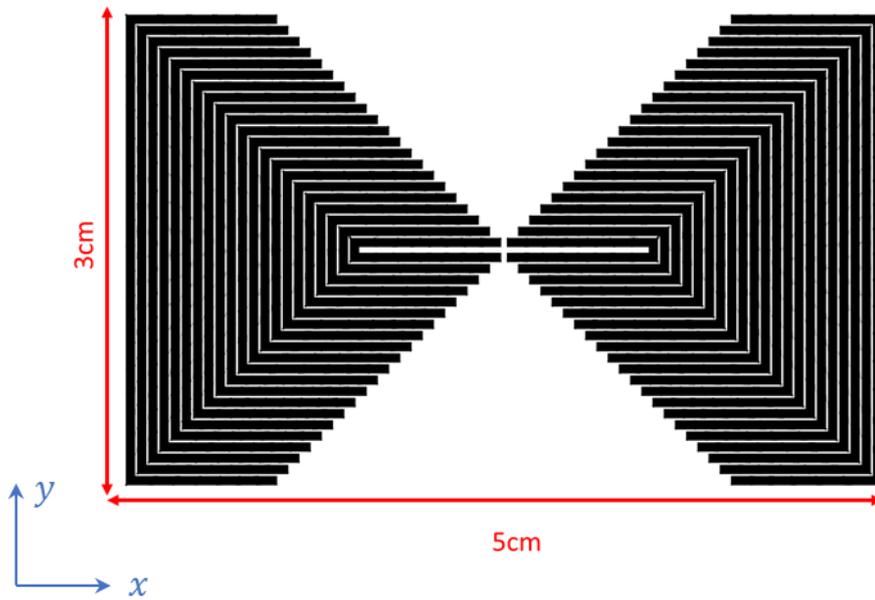
Figure 5.20. 20-bit reduced hourglass tag with ID word '11111111111111111111'
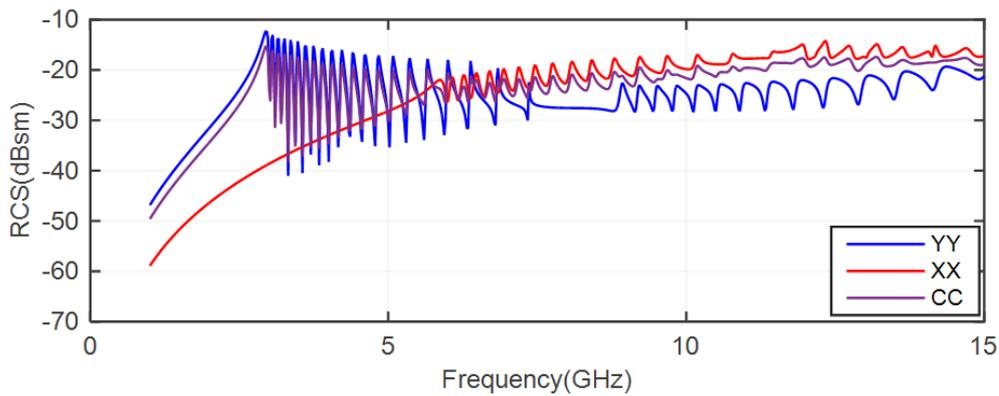
Figure 5.21. RCS of the 20-bit reduced hourglass tag with ID word '11111111111111111111'

Based on the results for the 20-bit hourglass tag, we emphasize the following.

- Despite a size reduction is applied from the 10-bit design to the 20-bit design, the obtained RCS level and peak-to-dip values are excellent.
- At the same time, the tag covers a very small area, especially in comparison to the designs considered in Chapter 3 and 4.
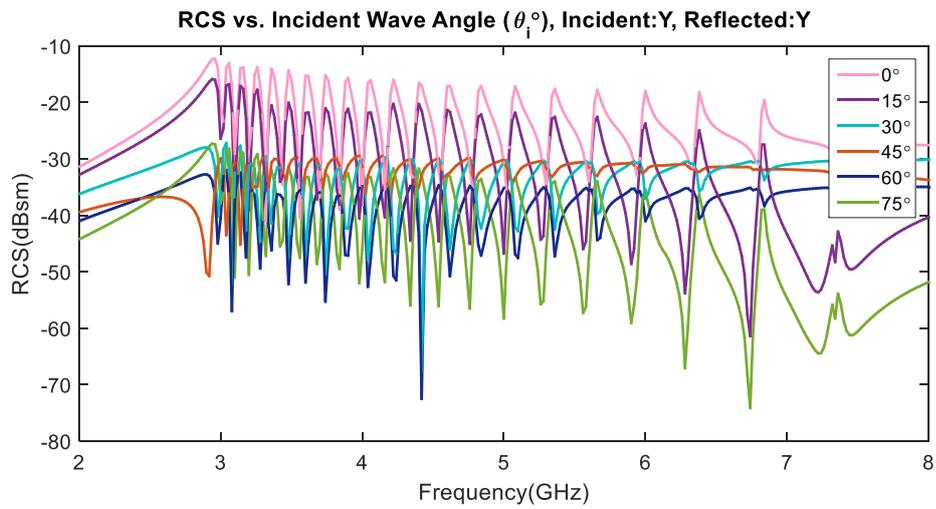
Figure 5.22. RCS of the 20-bit reduced hourglass tag with ID word '11111111111111111111' for different angles of incidence in bistatic configurations
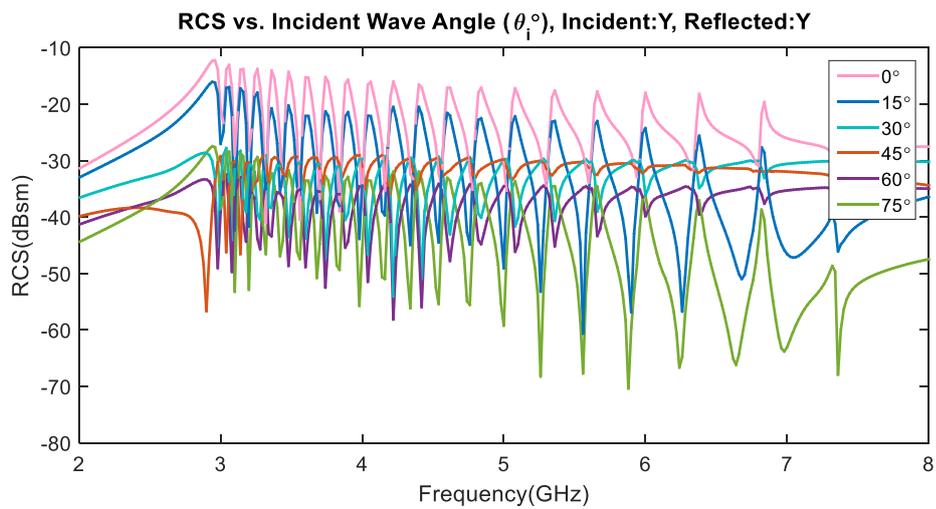
Figure 5.23. RCS of the 20-bit reduced hourglass tag with ID word '11111111111111111111' for different angles of incidence in monostatic configurations

Dimensions of the 20-bit hourglass tag are further reduced to obtain the design in Figure 5.20. The covered area of this reduced tag is 15 cm^2, whereas the original one is 32.4 cm^2, corresponding to double data capacity per unit area. Figure 5.21 shows the RCS response of the reduced tag. Figure 5.22 presents the RCS responses of the
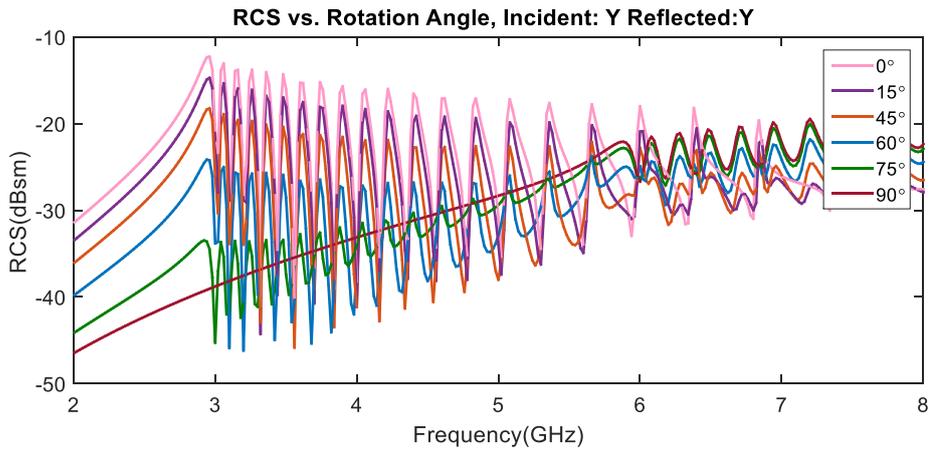
Figure 5.24. RCS of the 20-bit reduced hourglass tag with ID word '11111111111111111111' for different rotation angles at normal incidence
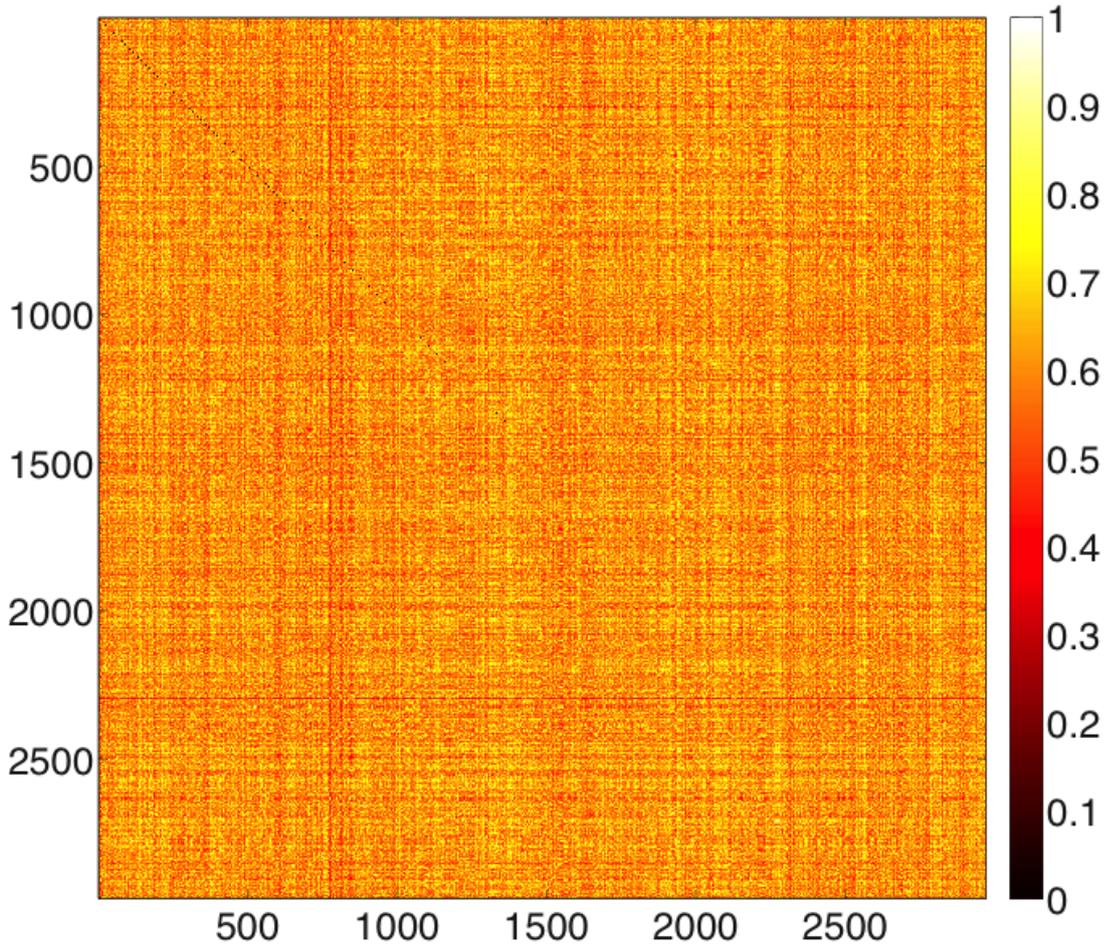
Figure 5.25. Correlation coefficient matrix for the reduced hourglass tag in Figure 5.20

same tag for different incidence wave angles when YY polarization is used. In this case, simulations are performed for bistatic configurations, where the incidence and receiving angles are θ and $(180^{\circ} - \theta)$ respectively. Similar analyses are conducted for monostatic configurations, where the incidence and receiving angles are the same, leading to the results presented in Figure 5.23. It can be observed that when the incidence angle exceeds 45°, the RCS response of the tag starts to degrade. Specifically, incidence angle should be in the interval of $0° - 45°$ for a practical usage. Figure 5.24 presents RCS responses of the tag when it is rotated in different angles (while it is lying in the same plane), where the incidence and received waves are again Y polarized. For this 20-bit reduced hourglass tag, an ID library is generated as described in Section 3.3. Following the stages in the given block diagram, a master tag is constructed in order to generate tags with different IDs. For this 20-bit reduced hourglass tag, an ID library is generated as described in Section 3.3. Following the stages in the given block diagram, a master tag is constructed in order to generate tags with different IDs. Each generated tag is simulated and the corresponding RCS response is computed. Almost 603,000 simulations are carried out in order to compute the electromagnetic responses of 3000 different ID words. After identifying highly distinguishable ones (via correlation comparisons), a database of reliable selections is generated. Figure 5.25 presents the correlation coefficient matrix for 3000 generated tags. The resulting ID library consists of 1511 highly distinguishable tags, while 1489 tags are discarded and placed in the reserve database.

5.2. Performance Comparisons of Chipless RFID Tags (Figure of Merit)

Considering chipless RFID tags, there are various figures that describe their performances, such as size, capacity, occupied bandwidth, etc. There are two main criteria to determine the performance of chipless tags [46]. The first is obtaining maximum data capacity with minimum size. The second is occupying minimum bandwidth to obtain the largest data capacity. Then, figure of merit values can be calculated based on these criteria to define the performances of different chipless RFID tags. Two figures of merit are defined as the data density per surface (DPS) in

bit/cm^2 and the data density per frequency (DPF) in bit/GHz in the literature [46]. In order to compare the performances of different chipless tag designs discussed in this thesis and some of those proposed in the literature, their DPS and DPF values are calculated and listed in Table 5.1. In order to combine two figures of merit into a single value, we further define a "performance metric" that is the multiplication of DPS and DPF. Hence, larger performance metric values indicate better performances. In general, the design in [47] leads to a larger DPS value in comparison to the other designs. On the other hand, the design discussed in Section 5.1.1.1 gives the largest DPS value when considering all designs proposed in this study. Considering DPF values, the designs in [28] and [31] provide the largest values among all designs. On the other hand, the tag discussed in Section 3.2 and its array forms have competitive DPF values. Among all tag designs, the best performance metric value seems to be obtained with the design in [47], while it is closely followed by the 10-bit nested-U-resonator-based tag (discussed in Section 5.1.1.1). We emphasize that figures of merit listed in Table 5.1 do not include detectability and distinguishability, which must be considered in practical applications. As shown in this thesis, hourglass structures provide excellent RCS levels and peak-to-dip separations, which make them suitable for real-life chipless RFID systems.

Table 5.1. *Figures of merit for different chipless RFID tag designs*

Design	Capacity (bit)	DPS (bit/cm2)	DPF (bit/GHz)	Area (cm2)	BW (GHz)	Performance Metric
2009 [25]	35	0,61	8,75	57,2	4	5,34
2005 [24]	5	0,72	5	6,94	1	3,60
2016 [31]	20	1,14	**10**	17,5	2	11,40
2012 [28]	20	1,14	**10**	17,5	2	11,40

2014 [47]	24	**3,47**	3,42	**5,76**	7	**11,87**
2015 [32]	12	1,42	0,5	8,4	6	0,71
Single	10	1,288	**9,09**	7,76	1,1	**11,71**
D12	10	0,1209	**9,09**	131,2	1,1	1,10
D2	10	0,084	**9,09**	118,5	1,1	0,76
D32	10	0,204	**9,09**	49	1,1	1,85
R1–Single	10	1,314	6,66	7,605	1,5	8,75
R1–D12	10	0,1028	6,66	97,2	1,5	0,68
R1–D2	10	0,109	6,66	91,63	1,5	0,73
R1–D32	10	0,1602	6,66	62,41	1,5	1,07
Hourglass–Single	10	**1,763**	6,25	**5,67**	1,6	11,02
Hourglass	10	0,865	6,25	11,55	1,6	5,41
Hourglass	20	0,617	8,69	32,39	2,3	5,36
Reduced Hourglass	20	1,33	4	15	5	5,32

5.3. Remarks

Based on the results presented in this chapter, our conclusions are as follows.

- In general, nested-resonator-based tags are favorable both as individual structures and in array configurations. Using only two tags leads to RCS levels similar to the U-resonator-based tag in D11 form (nine individual tags).
- Among different arrangements of nested-resonator-based tags, the hourglass configurations lead to the best results even though the number of individual tags is the same.

- YY polarization leads to the best results in terms of the base RCS levels, particularly for the hourglass configurations.

- In comparison to the 10-bit U-resonator-based tag, the hourglass geometry with a similar performance has a more compact size.

- Considering the 20-bit hourglass geometry, the reduced tag doubles the data capacity per area.

We conclude that the proposed hourglass structures are very suitable for efficient RFID systems.

CHAPTER 6

FABRICATION AND MEASUREMENT

As discussed so far, in RFID systems, chipless tags are desirable in comparison to the more common counterparts involving microchips, especially when they are produced in vast amounts. Microchips located on RFID tags restrict their usage due to additional costs, because of the existence of microchips and extra procedures to mount them on metallic tags, which in fact becomes challenging if tags are produced via inkjet printing methods. In this study, the proposed chipless tag designs are further fabricated via low-cost inkjet printing to fully demonstrate their potential as excellent components of the state-of-the-art RFID systems.

6.1. Inkjet Fabrication

Inkjet printing technique has recently become a common low-cost fabrication technique for electronic components and devices. This method does not only lower expenses, but also simplifies the fabrication processes by eliminating time-consuming procedures and materials [40]. Also, inkjet setups are widely accessible thanks to the inexpensive commercial inkjet printers that can be modified to print materials on flexible substrates. In the context of paper-based inkjet printing, absence of microchips is also attractive for green technology, since tags that contain only paper and metallic prints may be easier to recycle.

6.1.1. Inkjet Printing Process

An inkjet printer propels conductive ink onto the substrate that is moved by a reel mechanism during the printing process [41]. The head of the printer drops the ink to the predetermined points on the material [42] and the desired conductive pattern is formed. We note that an inkjet printed pattern consists of small dots of ink that typically lead to high resistance even between nearby locations.
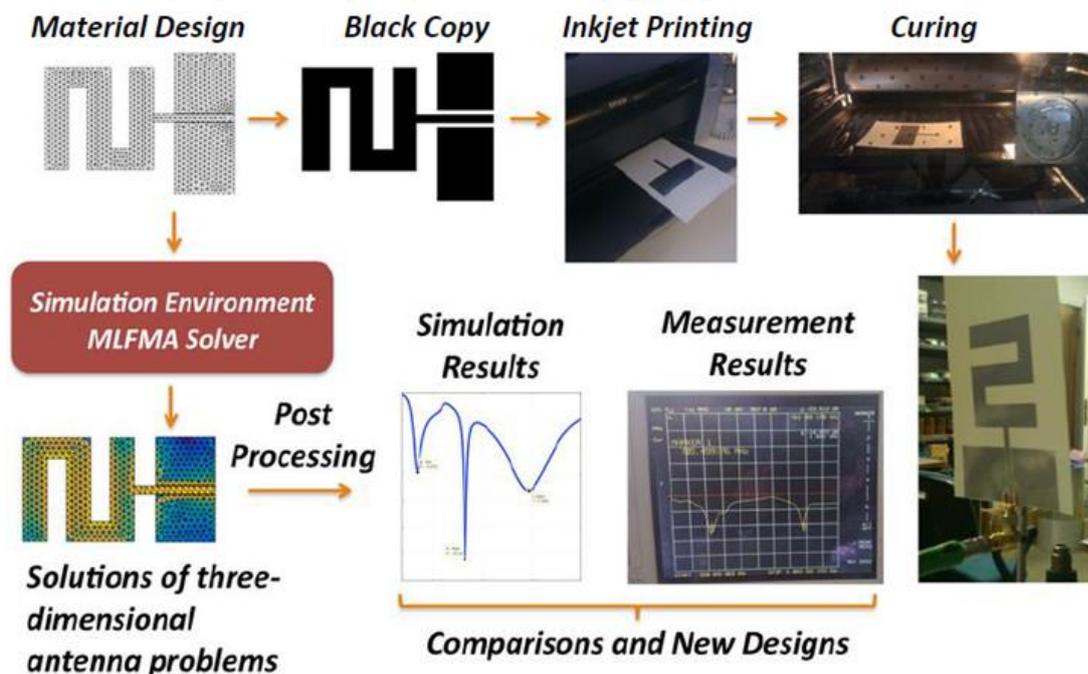
Figure 6.1. Major components of the inkjet-printing setup

In order to unite the dots into a solid layout, a curing process is necessary. In this study, heat curing is used by using a simple commercial oven. During the curing process, heat solves encapsulated nanoparticles and combines them into a uniform layer that results in significantly improved conductance [40].

Major components of the inkjet-printing setup used in this study to fabricate chipless RFID tags are presented in Figure 6.1.

6.1.2. Prototypes

In this study, two fabrication methods are employed. In the context of inkjet printing, the designed chipless RFID tags are fabricated via a commercial desktop printer, i.e., Epson C88+, which is loaded with conductive silver-based ink cartridges [40]. As the substrate, photopapers are used due to their good flexibility and inexpensive costs. The selected paper type is Canon Matte GP-501 with 10 cm × 15 cm size.
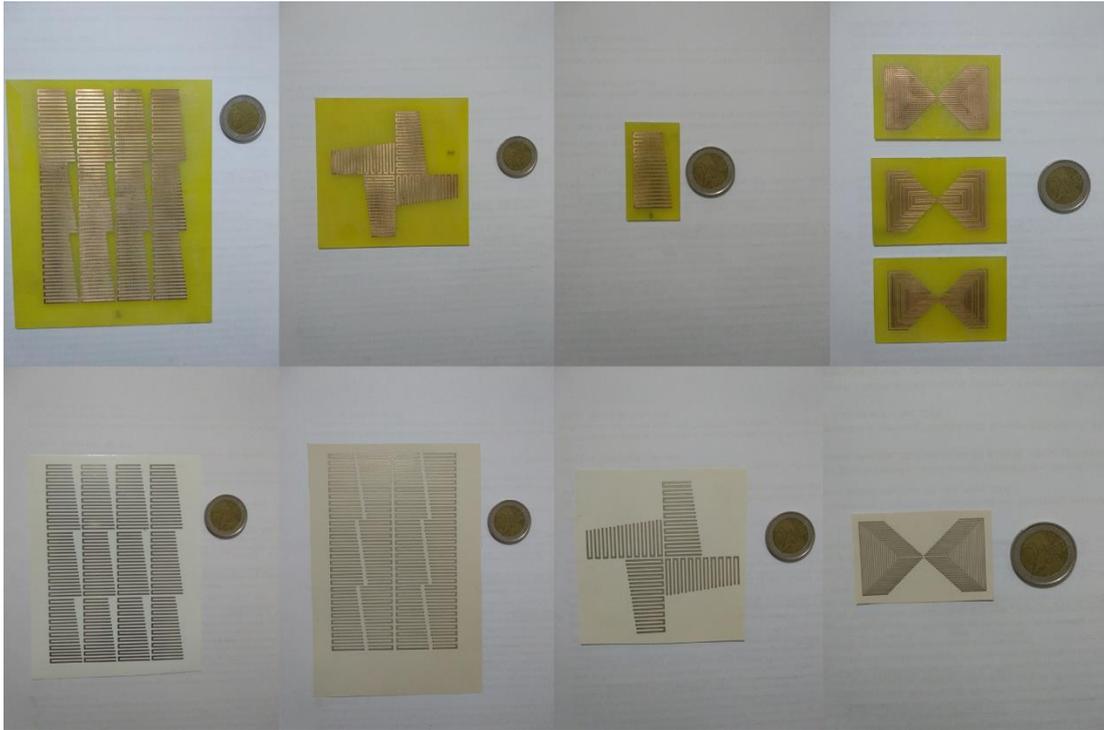
Figure 6.2. Fabricated prototypes

As a reference fabrication method, the classical PCB technique is employed. The tags are printed via an LPKF etching machine on FR4 substrates with 1.58 mm thickness. Chipless tag patterns are etched on the copper-covered sides of the PCB substrates.

Figure 6.2 presents photographs of various chipless RFID tags printed via both methods.

6.1.3. Sensitivity Analysis for Inkjet-Printed Tags

In chipless RFID systems, tags are expected to be produced in large amounts so that they must be inexpensive as much as possible. In addition, most applications need flexible and environmentally friendly tags, making inkjet printing a suitable option for fabrication. On the other hand, samples produced by inkjet printing are prone to fabrication errors more than those produced via conventional techniques. Particularly, very low-cost inkjet setups, such as used in this study, are known to lead to resolution, conductivity, and other connectivity issues. Therefore, the designed RFID tags must

be resistant to such fabrication errors. In fact, as shown below, tag structures, such as shown in Chapter 3, are quite robust from this perspective. A main issue in low-cost inkjet printing is nonuniformity caused by limited printing resolution and unbalanced material (hence conductivity) distributions. The prints may be deformed, while physical movements, tensions, and bending may further cause cracks and gaps depending on the application.

In the following results, effects of commonly encountered printing errors are analyzed [36]. Figures 6.3 to 6.5 present geometrical drawings of these error trials, as well as the corresponding RCS responses.

In Figure 6.3, we consider the performance of a single U-shaped resonator when there is a gap of width W and length L on one of the arms. Considering different lengths and widths, the resonance characteristics of the structure (RCS versus frequency) seem to be quite stable against such gaps. For example, only small frequency shifts occur as the width reaches 0.5 mm. The length of the gap is also ineffective until it reaches 0.5 mm and full disconnection occurs. Figure 6.4 presents similar results when there is a thinning (0.1 mm or 0.2 mm indentations from both sides) on one of the arms. The operation of the resonator is insensitive also to such deformations. Figure 6.5 presents another set of results, where potential cracks that may occur on the tip of an arm are investigated. Different values are tested for the width of the crack as W = 0.1, 0.2, 0.3 mm, as well as its length as L = 0.1, 1.0, 2.0 mm. RCS with respect to frequency plots in Figure 6.5 clearly show that the considered types of resonators are also stable against this kind of tip cracks.

In general, numerical results, some of which are shown here, demonstrate that tag structures based on U-shaped resonators (both in the conventional arrangements and in stacked forms to generate hourglass geometries) can be suitable to be fabricated via inkjet printing and similar techniques. Errors introduced during fabrications can be tolerated, until a total disconnection occurs such that the resonance path is completely damaged.
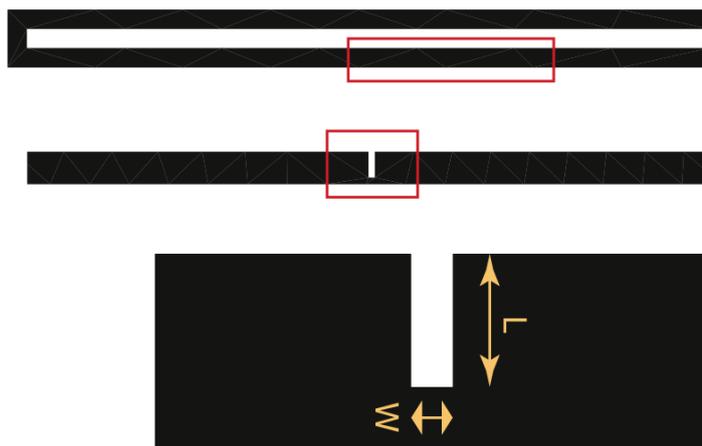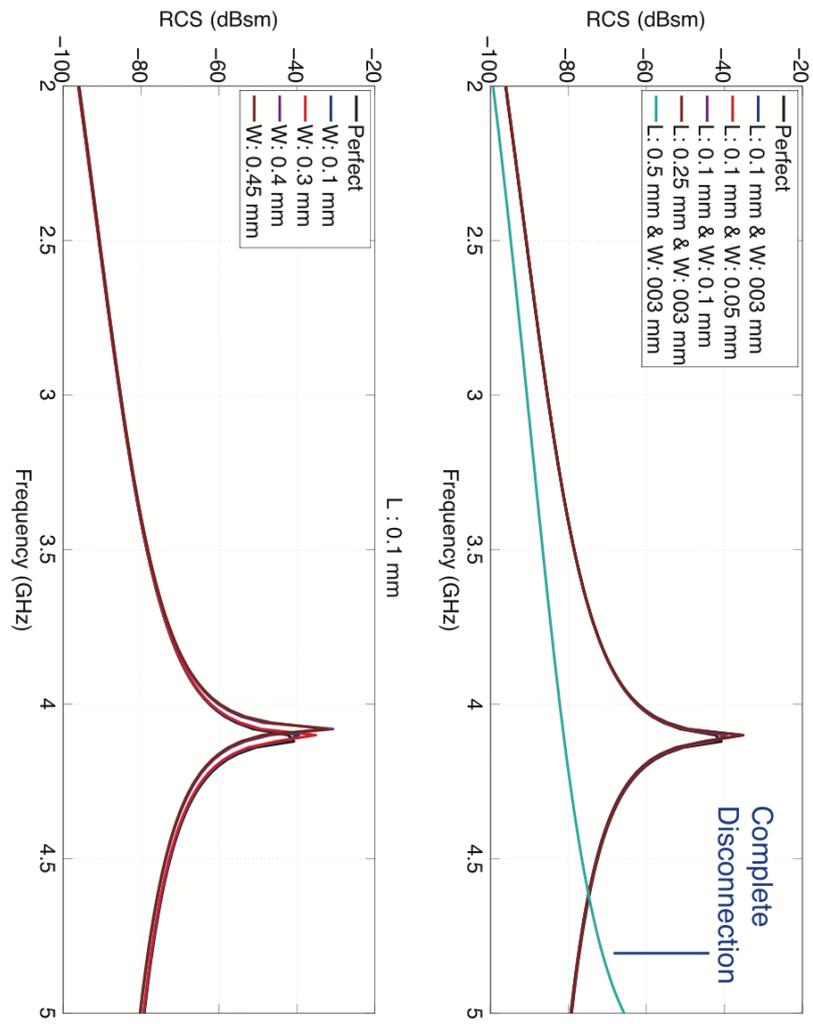
Figure 6.3. RCS response of a single U-shaped resonator when there is a gap of width W and length L
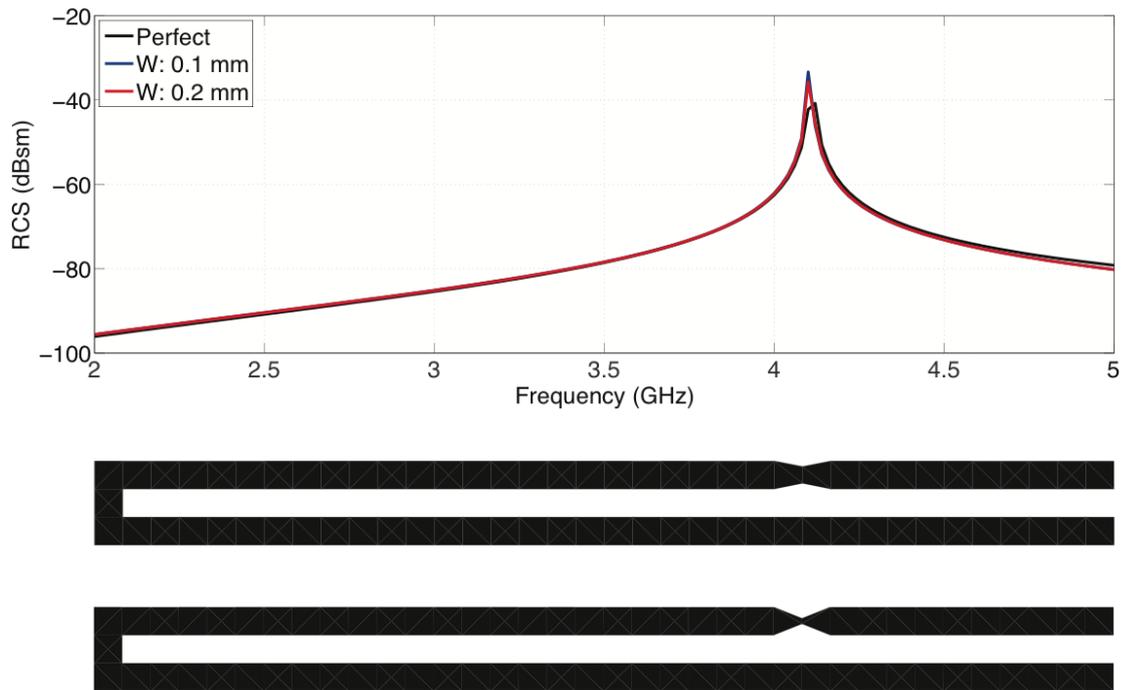
71

Figure 6.4. RCS response of a single U-shaped resonator when there is thinning on one of the arms
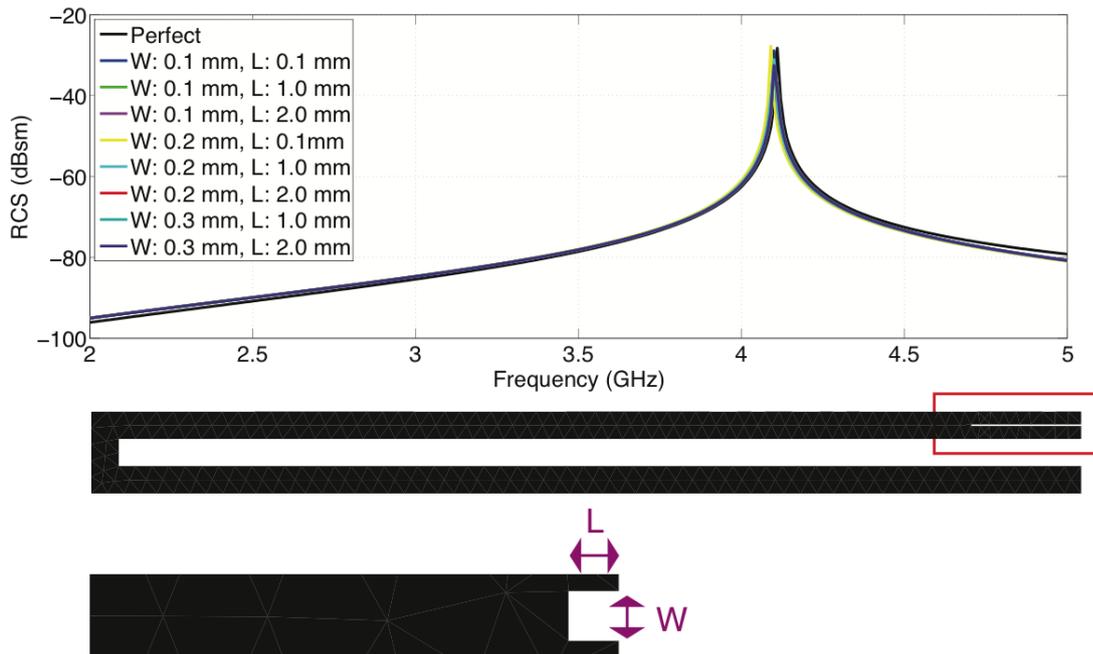

Figure 6.5. RCS response of a single U-shaped resonator when there is crack on the tip of an arm

6.2. Measurement Method

Measurements of chipless RFID tags are commonly performed with a frequency-based method due to the inherent spectral signature-based operation of these tags [13]. The tags can be considered as passive targets with specific responses with respect to frequency since there is not any communication protocol. In addition, the tags typically have longer read ranges so that the setup should support long-distance measurements [33].

Vector network analyzers (VNAs) are commonly used in test setups for characterizing frequency-based signatures of RFID tags [30]. VNA evaluates the S21 parameter which defines the ratio between the reflected signal power to the transmitted signal power with respect to frequency. Two broadband identical horn antennas having 13 dBi gain, as shown Figure 6.6, are used as TA and RA. The antennas are connected to the transmitting and receiving ports of the VNA. Transmitting and receiving waves are co-polarized with Y polarization. Tag measurements are carried out in bistatic configuration [43] by separating and isolating TA and RA.

Measurements of the proposed tags are performed in the anechoic chamber located in the Department of Electrical and Electronics Engineering at METU. In order to reduce electromagnetic couplings between TA and RA, they are separated by 50 cm distance from each other, while both are 65 cm away from the tag as shown in Figure 6.7. Antennas are placed on foam panels to balance their horizontal positions. In order to support the chipless tags and fix their distances to the antennas, a foam bar is used. The VNA is placed outside of the room and long microwave cables are used to connect it to the antennas. Figure 6.8 presents a photograph of the measurement setup.
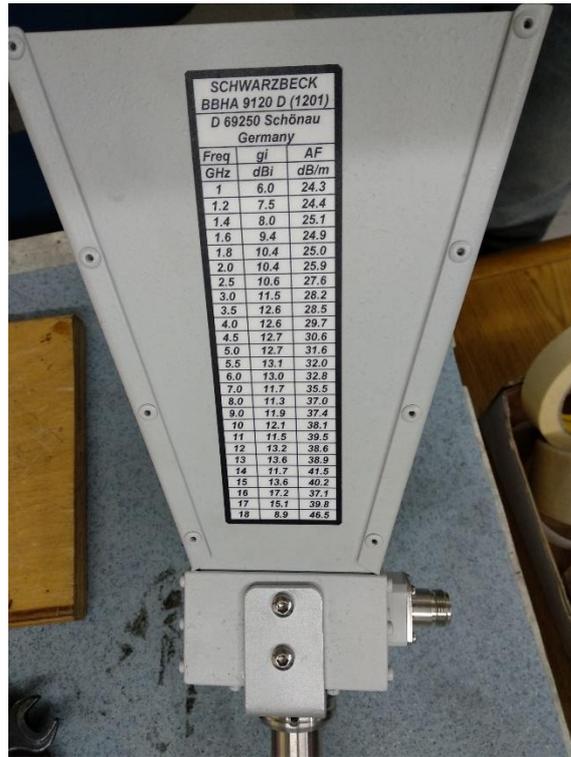
Figure 6.6. A broadband antenna used for measurements
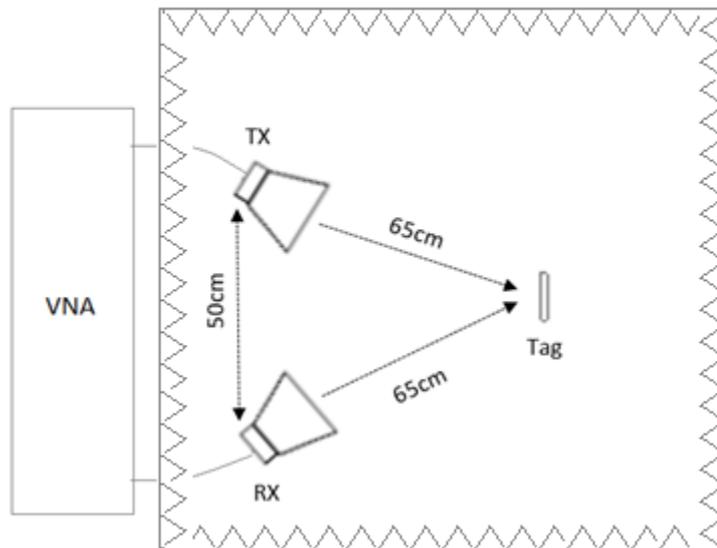
Figure 6.7. A diagram of the measurement setup

74
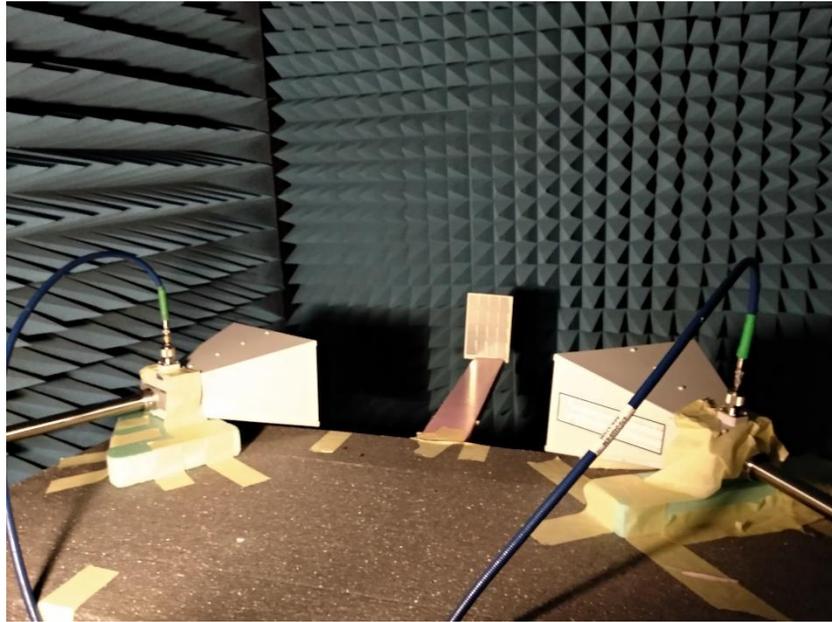
Figure 6.8. A photograph of the measurement setup

6.2.1. Calibration and Post-Processing

In order to obtain accurate results, careful calibration procedures should be applied while measuring chipless RFID tags. In this study, there are two types of calibration procedures: (i) An instrumental calibration for VNA and (ii) an environmental calibration, generally known as post-processing [28].

First, an instrumental calibration, which is also known as a full two-port calibration, is applied to VNA in order to remove systematic errors stemming from cables or connectors during the measurements. The calibration procedure is performed via an SMA calibration kit at the end of the cables that are later connected to the antennas. After a full two-port calibration, the measurement takes place, which is a three-stage procedure involving chipless-tag, empty-room, and reflecting-plate measurements as detailed below.

Figure 6.9. Signal pathway from TA to RA including the environmental components

Second, an environmental calibration procedure is applied to the measured S21 data [28], which is basically a post-processing technique that removes the effects of environmental reflections as well as electromagnetic couplings [33]. The magnitude and phase of the signal reflected from a measured tag may cause reading errors due to envir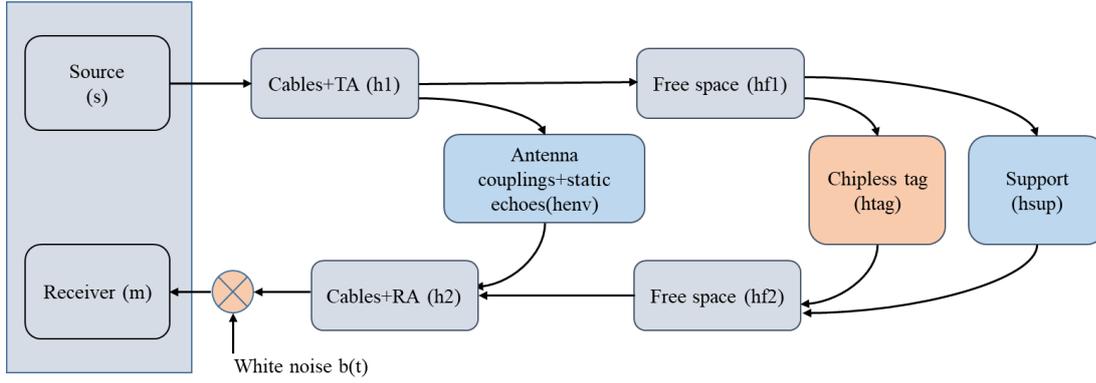onmental effects. These effects cannot be removed with the first calibration process; therefore, a sophisticated process needs to be used for accurate reading.

Figure 6.9 presents the signal pathway running from TA to RA including the environmental components [33]. By using this model, Measurement $m(t)$ depending on the input signal $s(t)$ can be written as [33]

$$m(t) = h_2 * hf_2 * (h_{tag} + h_{sup}) * h_1 * hf_1 * s(t) + \qquad (6.1)$$
$$h_2 * h_{env} * h_1 * s(t) + b(t),$$

where h_1 and h_2 represent the transfer functions of the cables and the antennas on the transmitting and receiving ports of the network analyzer, whereas hf_1 and hf_2 represent the transfer functions of the pathway along which the signal travels from the antennas to the tag or vice versa. In addition, h_{tag} is the transfer function of the tag, h_{sup} and h_{env} represent the transfer functions of the tag support and direct couplings

76

between the antennas, respectively, and * denotes the convolution operation [33]. Finally, $b(t)$ defines the white noise added to the system.

Then, $S21$ can be obtained by using $m(t)$ in (6.1) as

$$S21(f) = TF[h_2 * hf_2 * (h_{tag} + h_{sup}) * h_1 * hf_1 + h_2 * h_{env} * h_1] + B(f), \qquad (6.2)$$

where TF represents Fourier transform. This function relates the S21 with the components of the channel model. This way, we obtain $S21$ in frequency domain as

$$S21(f) = H_2 \cdot Hf_2 \cdot (H_{tag} + H_{sup}) \cdot H_1 \cdot Hf_1 + H_2 \cdot H_{env} \cdot H_1 + B(f), \qquad (6.3)$$

where capitalized variables represent Fourier transforms of the corresponding variables. White noise $B(f)$ can be eliminated by taking the average of few measurement data; thus, it can be omitted.

In order to satisfy communication symmetry rule, H_1 and H_2 terms should be identical, as well as Hf_1 and Hf_2 terms. This way, H_1 and H_2 terms can be simplified into H_1. Likewise, Hf_1 and Hf_2 terms can be simplified into Hf_1. Then, (6.3) can be simplified into

$$S21 = H_1^2 \cdot Hf_1^2 \cdot (H_{tag} + H_{sup}) + H_1^2 \cdot H_{env}. \qquad (6.4)$$

To obtain H_{tag}, a calibration process including a three-stage measurement process based on (6.4) is necessary. First, a tag-free setup is considered while leaving all other components, including the tag support, in their place to obtain

$$S21_{empty} = H_1^2 \cdot Hf_1^2 \cdot H_{sup} + H_1^2 \cdot H_{env}. \qquad (6.5)$$

Likewise, a second measurement is carried out after placing the tag under test to the setup. We obtain

$$S21_{tag} = H_1^2 \cdot Hf_1^2 \cdot (H_{tag} + H_{sup}) + H_1^2 \cdot H_{env}. \qquad (6.6)$$

Then, the subtraction value of $S21_{tag} - S21_{empty}$, which represents the effects of antenna couplings, echoes, as well as reflections from the tag support, is obtained as

$$S21_{tag} - S21_{empty} = H_1^2 \cdot Hf_1^2 \cdot H_{tag}. \tag{6.7}$$

The subtraction term removes the coupling and reflection effects; however, it is not sufficient to eliminate Hf_1 (free-space effects) and H_1 (antenna and cable effects). Therefore, a third measurement with a known H_{ref} is required. For this purpose, a rectangular conducting plate is placed instead of the tag and we obtain [44]

$$S21_{ref} = H_1^2 \cdot Hf_1^2 \cdot (H_{ref} + H_{sup}) + H_1^2 \cdot H_{env}. \tag{6.8}$$

Using the expression above, we derive

$$H_1^2 \cdot Hf_1^2 = \frac{S21_{ref} - S21_{empty}}{H_{ref}}. \tag{6.9}$$

Finally, by substituting (6.7) into (6.9), we obtain

$$H_{tag} = \frac{S21_{tag} - S21_{empty}}{S21_{ref} - S21_{empty}} H_{ref}. \tag{6.10}$$

Far-field RCS is defined as

$$\sigma = \lim_{R \to \infty} \left[4\pi R^2 \frac{|E_s|^2}{|E_i|^2} \right], \tag{6.11}$$

which can be written in terms of $S21$ as [43]

$$\sigma = 4\pi R^2 |S21|^2. \tag{6.12}$$

By substituting (6.10) in (6.12), we arrive at the expression for the RCS of the measured tag as

$$\sigma_{tag} = \left[\frac{S21_{tag} - S21_{empty}}{S21_{ref} - S21_{empty}} \right]^2 \sigma_{ref}. \qquad (6.13)$$

σ_{ref} can be calculated numerically via any simulation environment using the dimensions of the conducting plate.

Consequently, via the three-stage measurement procedure, we can obtain the RCS of the tag.

6.2.2. Measurement Results and Remarks

Figures 6.10 to 6.21 present measured RCS responses of various chipless RFID tag prototypes. RCS responses of the tags are calculated with the measured S21 parameters using (6.14). RCS response of the reference conductor plate is obtained numerically via MLFMA for more accurate results. Finally, calculated RCS responses of the tags are normalized (frequency shift) in order to include effective dielectric effects for both PCB and inkjet substrates. Specifically, in order to normalize RCS responses, their frequency values are shifted by multiplying with approximately 0.65 ($\varepsilon_{r_{eff}} \cong 2.37$) and 0.85 ($\varepsilon_{r_{eff}} \cong 1.38$) for FR4 and Canon Matte GP-501 respectively. Measured RCS responses are compared with simulation results obtained for Y polarization under normal incidence.
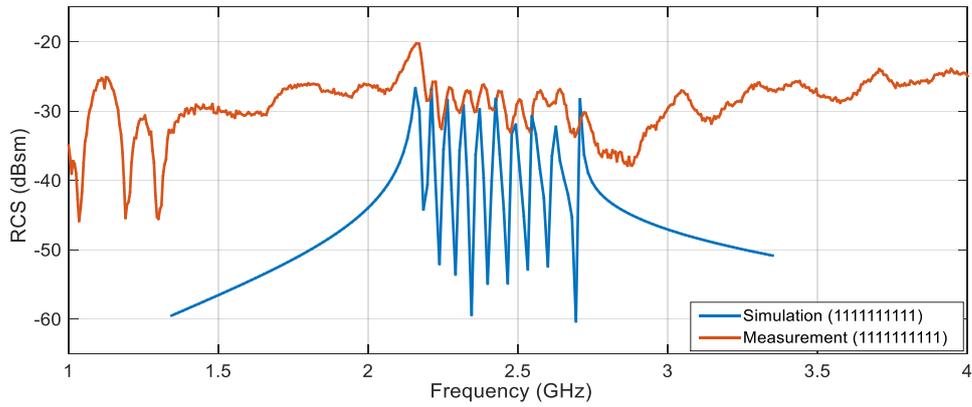
Figure 6.10. Measurement (PCB) and simulation results for the 10-bit U-shaped (full)
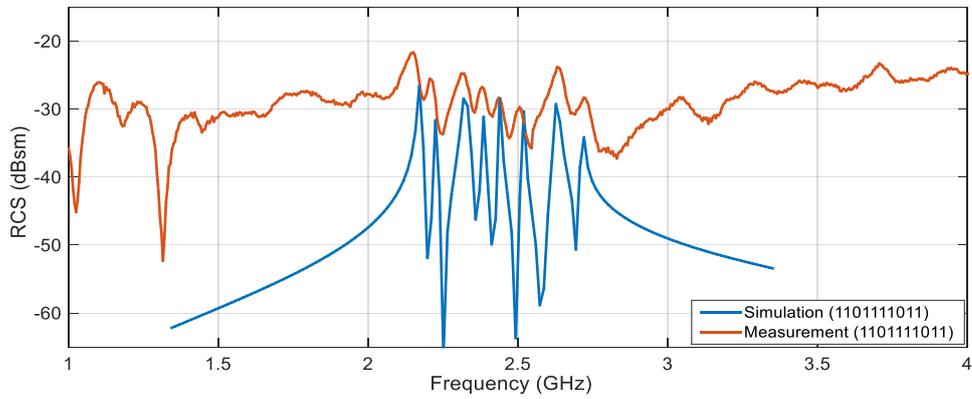
Figure 6.11. Measurement (PCB) and simulation results for the 10-bit U-shaped tag (two bits are deleted)

Figure 6.12. Comparison of measurement (PCB) and simulation results for the 10-bit U-shaped tags

Figure 6.13. Measurement (PCB) and simulation results for the 10-bit R1 tag (full)

Figure 6.14. Measurement (PCB) and simulation results for the 10-bit R1-D12 tag (full)

Figure 6.15. Measurement (PCB) and simulation results for the 10-bit R1-D32 tag

Figure 6.16. Measurement (PCB) and simulation results for the 20-bit hourglass tag (full)
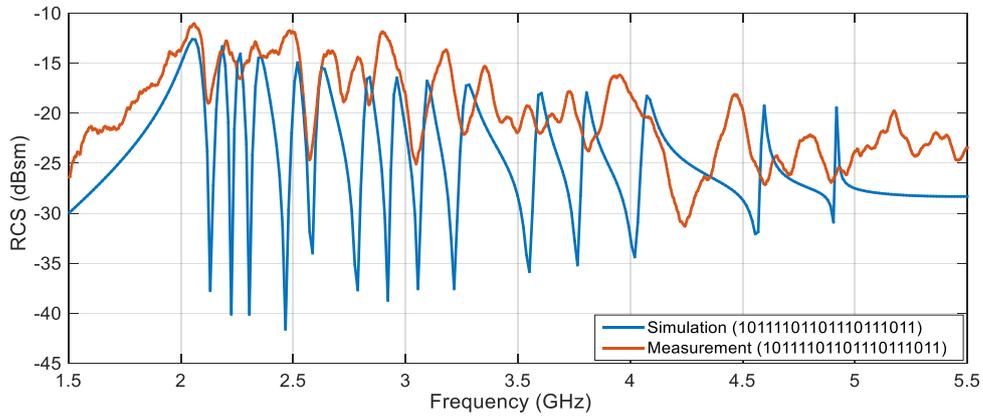
Figure 6.17. Measurement (PCB) and simulation results for the 20-bit hourglass tag with an ID word
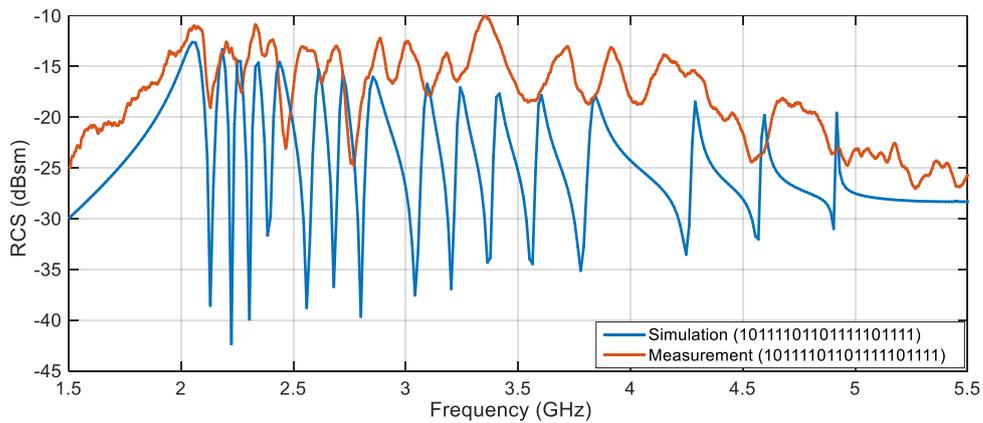
Figure 6.18. Measurement (PCB) and simulation results for the 20-bit hourglass tag with an ID word

82
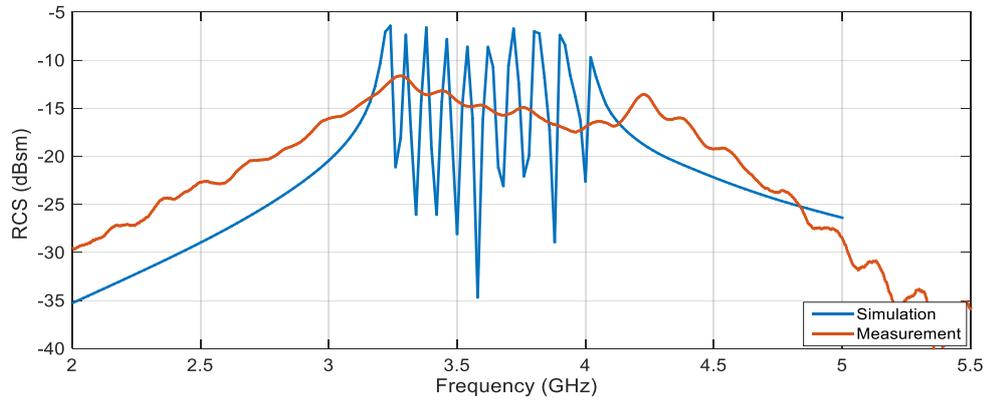
Figure 6.19. Measurement (inkjet-printed) and simulation results for the 10-bit U-shaped D12 tag (full)
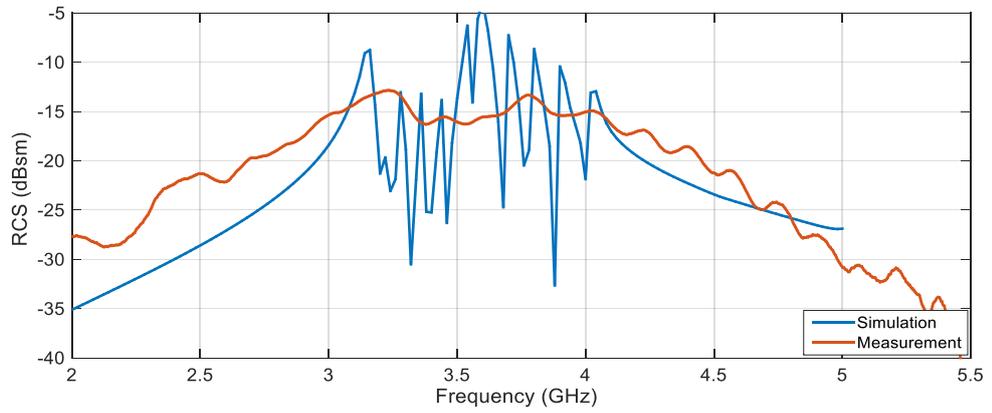
Figure 6.20. Measurement (inkjet-printed) and simulation results for the 10-bit U-shaped D2 tag (full)
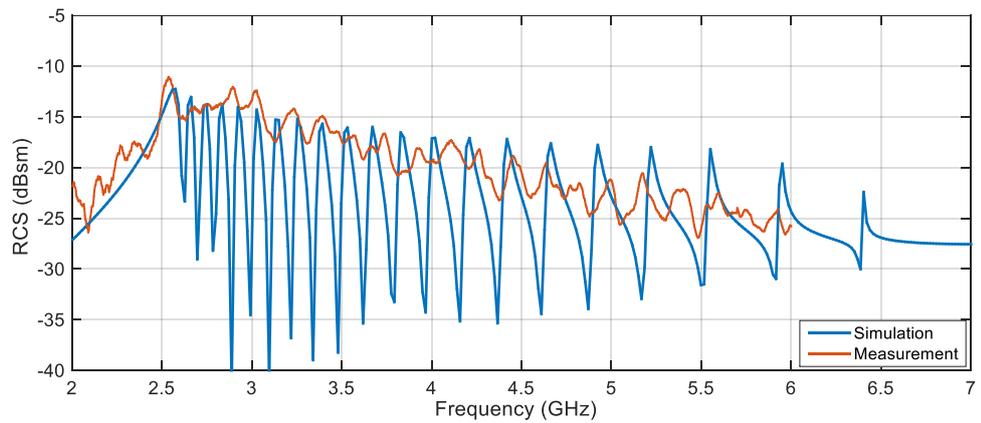
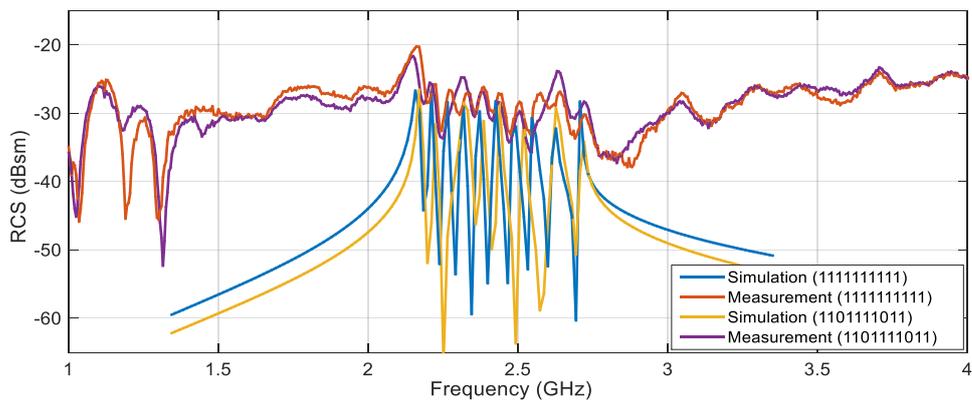Figure 6.21. Measurement (inkjet-printed) and simulation results for the 20-bit hourglass tag (full)

83
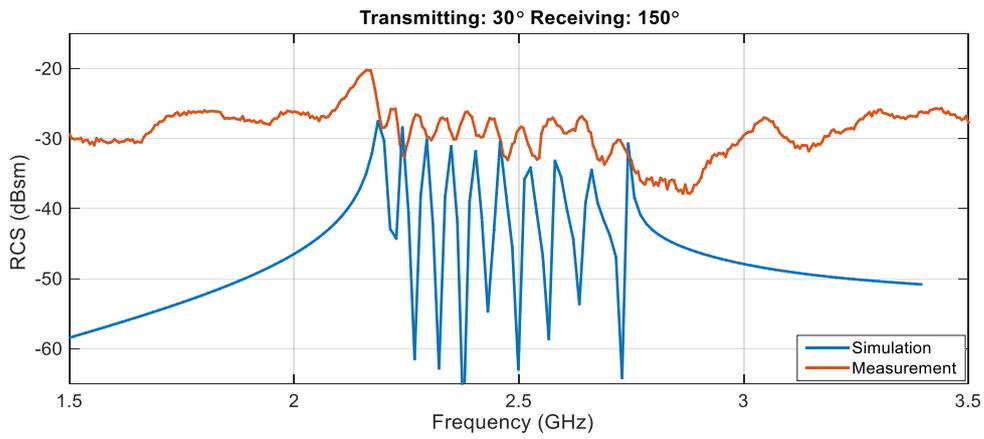
Figure 6.22. Measurement (PCB) and simulation results for the 10-bit U-shaped tag (full)
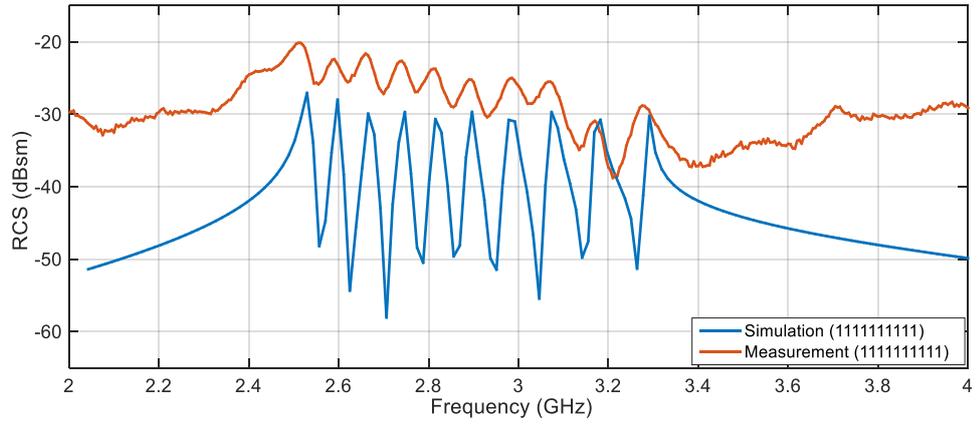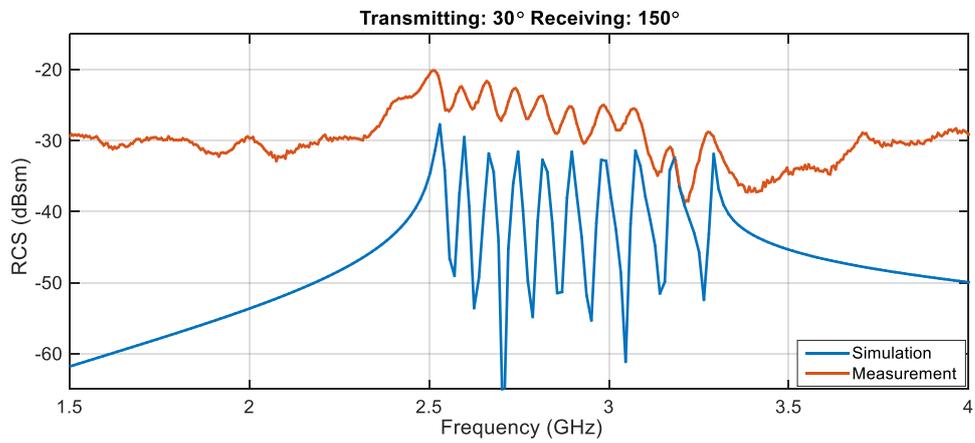

Figure 6.23. Measurement (PCB) and simulation results for the 10-bit R1 tag (full)
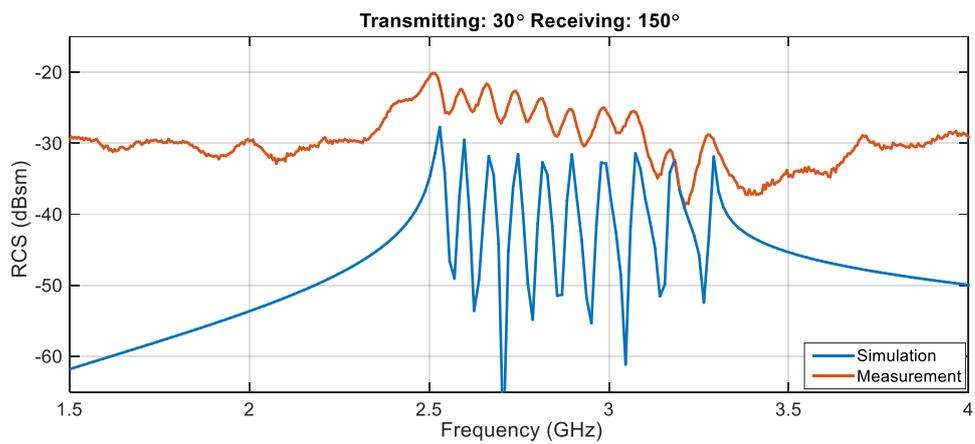
Figure 6.24. Measurement (PCB) and simulation results for the 10-bit R1-D12 (full)
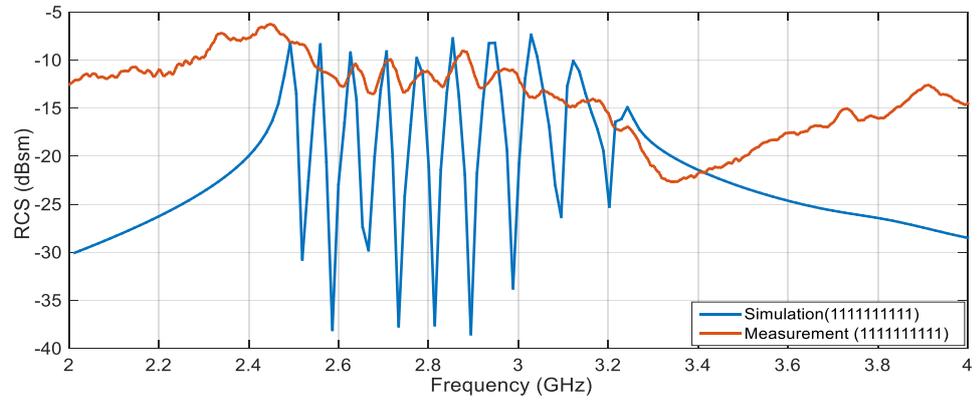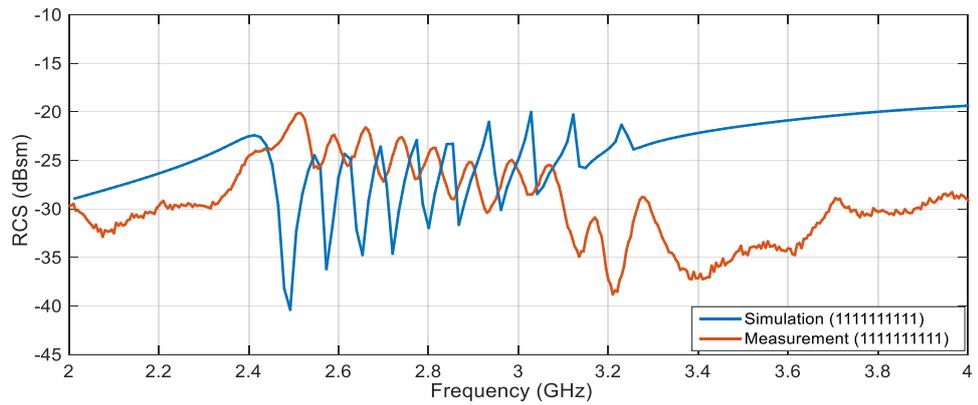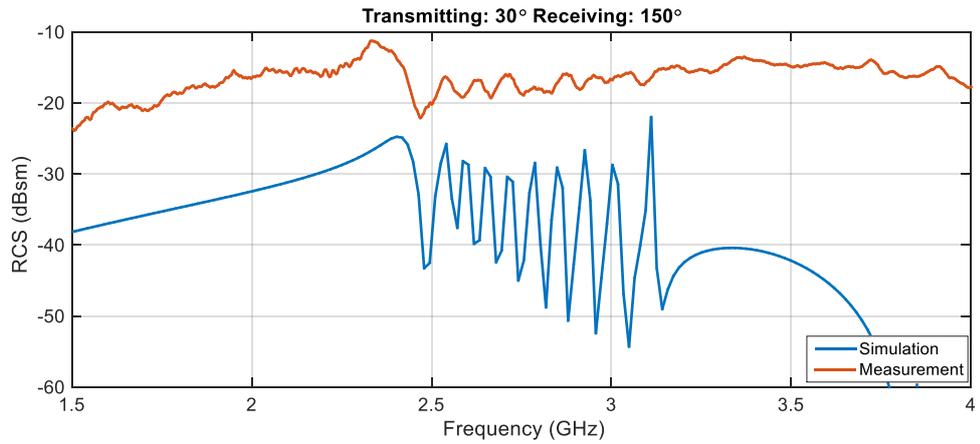
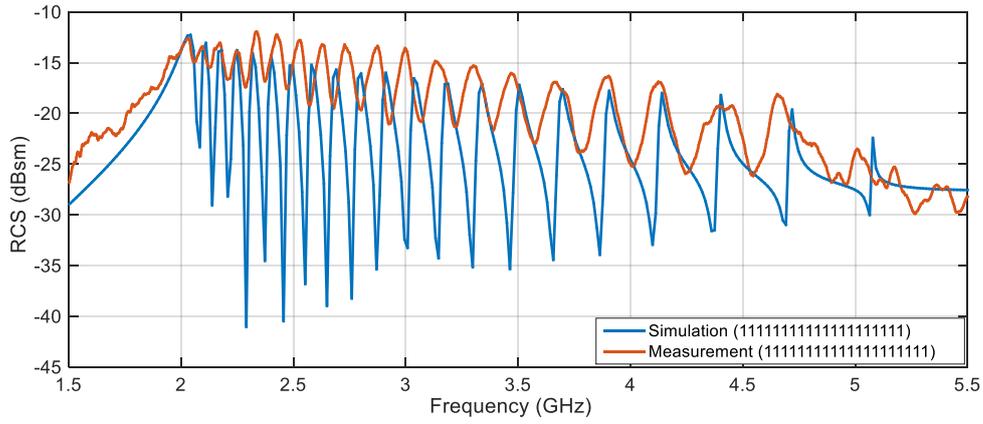Figure 6.25. Measurement (PCB) and simulation results for the 10-bit R1-D32 tag (full)
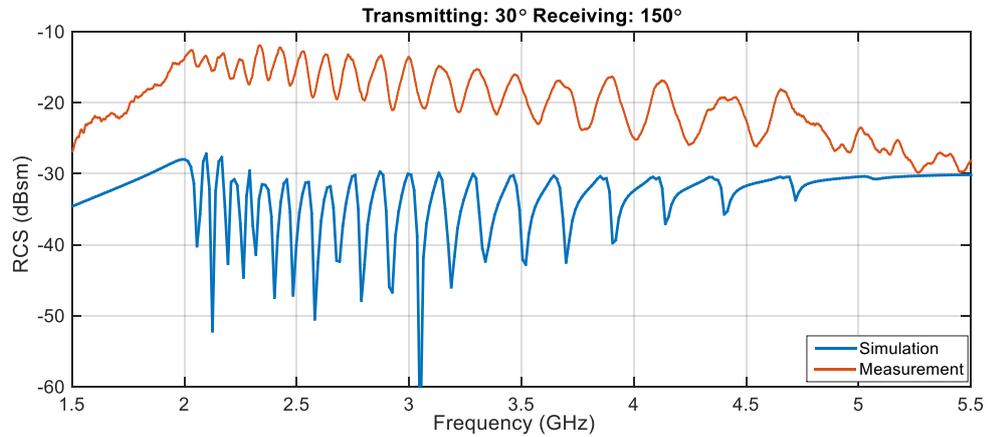
Figure 6.26. Measurement (PCB) and simulation results for the 20-bit hourglass tag (full)

Secondly, some of the tags are simulated under 30° incidence illumination for Y polarization, which may be more consistent with the measurement setup. Figures 6.22 to 6.26 present these simulation results in comparison to the measured RCS responses.

Our observations on the measurement results are as follows.

- Measured RCS response of the 10-bit U-shaped tag fabricated on PCB is consistent with the corresponding simulation result. All resonance peaks are clearly distinguishable in the overall response. Moreover, tags with different

85

IDs have specific measurement responses enabling the detection and identification of the encoded ID words.

- Measured RCS responses of the reduced tags fabricated on PCBs are similar to the simulated responses. On the other hand, high-frequency peaks are not clearly observed for the array configurations since quality of resonances decreases as the frequency increases [33].

- For inkjet-printed R1-D12 and R1-D22 tags, resonance peaks are not clearly observed, most probably due to fabrication issues. Despite all efforts to reduce the resistivity of samples via heat curing, the inkjet-printed prototypes still have insufficient conductivity that may deteriorate their reflectivity. On the other hand, the measured RCS responses still have oscillatory characteristics as in the simulation results.

- Considering the 20-bit hourglass tags fabricated on PCB, resonance peaks and missing peaks are highly distinguishable for different ID words. These results confirm the superior performance of the hourglass design in comparison to the standard ones based on U-shaped resonators. It is also remarkable that the inkjet-printed hourglass tag gives promising results.

CHAPTER 7

CONCLUSION

In this thesis, design, simulation, and fabrication of low-cost chipless RFID tags are presented. All aspects of frequency-based chipless tags are focused in the context of various designs in detail. Performances of existing chipless RFID tags are improved in terms of readability and reliability with new approaches.

A typical chipless RFID tag design starts by constructing a prototype with a resonator sequence. Data encoding procedure is based on absence-presence of resonators, which simplifies the overall process by correlating the physical structure with the encoded binary data directly. Calculated frequency-dependent RCS responses of the tags characterize their IDs.

Routine of a chipless RFID system is discussed in detail. For RFID applications, achieving the highest data capacity is important, while the generated ID library should be reliable for error-free identification of the tags. In order to avoid tags with similar responses, an elimination procedure is defined and high-quality ID libraries are generated for both conventional and novel designs.

In order to improve the performances of chipless RFID tags, their array configurations are presented with diverse numerical analyses. In comparison to a single tag, array configurations enhance tag readability by providing higher RCS levels and prevent misreading with more powerful resonances. Various array scenarios improve the base RCS level by almost 20 dB. On the other hand, array configurations are not compact and they bring a trade-off between compactness and performance.

As a major contribution of this thesis, a novel hourglass-shaped chipless tag design is presented. The design provides remarkable high-quality resonances and strong RCS responses, while being compact and suitable for practical applications.

Proposed tag designs are fabricated via two different technologies. In addition to the classical PCB fabrication, where tag patterns are etched on FR4, a very low-cost inkjet-printing setup is used to fabricate flexible prototypes. As detailed, the tag patterns are directly printed on photograph papers using commercial printers loaded with silver ink cartridges. Therefore, this fabrication method enables flexible, lightweight, low-cost, and environmentally friendly tags. However, it brings its own disadvantages, e.g., printouts have low resolution, leading to deformations of the printed resonators. Also, conductivity issues cause low performances in the RCS responses. Measurements show that inkjet-printed tags provide promising responses, while further improvements are needed to make them practical.

Chipless RFID tags are inexpensive solutions to item-level tagging for state-of-the-art and future application areas. The main motivation of this study is to bring new approaches to such existing contactless identification technologies.

Finally, future works can be listed as follows.

- The inkjet printing and curing process must be improved in order to make inkjet-printed tags practical.
- To test the designed tags in practical scenarios, measurements should be performed for tags attached on various types of objects such as water bottles, packaged foods, and metal tools, etc. In addition, measurements should be performed in noisy environments to assess the actual performances of the designed tags.
- Reducing the sizes of the tags is always open to research, while this is a quite challenging task in the context of chipless RFID systems.

REFERENCES

[1] D. McFarlane, S. Sarma, J. Chirn, C. Wong, and K. Ashton, "Auto ID systems and intelligent manufacturing control," *Engineering Applications of Artificial Intelligence*, vol. 16, pp. 365–376, Jun. 2003.

[2] J. Visich, S. Li, B. Khumawala, and P. Reyes, "Empirical evidence of RFID impacts on supply chain performance," *International Journal of Operations & Production Management*, vol. 29, pp. 1290–1315, Nov. 2009.

[3] K. Finkenzeller, *RFID Handbook*. Wiley, 2003.

[4] D. M. Dobkin, *The RF in RFID: Passive UHF RFID in Practice*. Elsevier, 2007.

[5] M. Bellis, "The history and use of bar codes," *ThoughtCo*, Mar. 2019. [Online]. Available at: https://www.thoughtco.com/bar-codes-history-1991329 (accessed Aug. 2019).

[6] P. Trujillo, "Barcodes: the ultimate guide to barcodes," *WaspBuzz,* Apr. 2015. [Online]. Available at: http://www.waspbarcode.com/buzz/barcode/ (accessed Aug. 2019).

[7] S. Preradovic and N. C. Karmakar, "Chipless RFID: Bar code of the future," *IEEE Microw. Mag.*, vol. 11, pp. 87–97, Dec. 2010.

[8] M. Karkkainen and J. Holstrom, "Wireless product identification: Enabler for handling efficiency, customization and information sharing," *Supply Chain Manag.: An Int. J.*, vol. 7, pp. 242–252, Oct. 2002.

[9] H. Stockman, "Communication by means of reflected power," *Proceedings of the IRE*, vol. 36, pp. 1196–1204, Oct. 1948.

[10] J. Landt, "The history of RFID," *IEEE Potentials*, vol. 24, pp. 8–11, Oct. 2005.

[11] D.C. Twist, "The impact of radio frequency identification on supply chain facilities," *Journal of Facilities Management*, vol. 3, pp. 226–239, Sep. 2005.

[12] P. Harrop and R. Das, "Printed and chipless RFID forecasts, technologies & players 2011–2021," IDTechEx, https://www.idtechex.com/en/research-report/printed-and-chipless-rfid-forecasts-technologies-and-players-2011-2021/254 (Accessed Aug. 2019).

[13] V. D. Hunt, A. Puglia, and M. Puglia, *RFID: A Guide to Radio Frequency Identification*. Wiley, 2007.

[14] K. V. S. Rao, "An overview of backscattered radio frequency identification system (RFID)," *Asia Pacific Microwave Conference*, vol. 3, pp. 746–749, Dec. 1999.

[15] K. V. Rao and P. V. Nikitin, "Theory and measurement of backscattering from RFID tags," *IEEE Antennas Propag. Mag.*, vol. 48, pp. 212–218, Dec. 2006.

[16] N. C. Karmakar and G. F. Swiegers, "Multiresonator-based chipless RFID system for low-cost item tracking," *IEEE Trans. Microw. Theory Tech.*, vol. 57, pp. 1411–1419, May 2009.

[17] R. Das and P. Harrop, "RFID forecasts, players and opportunities 2009–2019," IDTechEx Rep., Apr. 2009.

[18] R. Das, "Chipless RFID: The end game," IDTechEx, Feb. 2006. [Online]. Available at: https://www.idtechex.com/en/research-article/chipless-rfid-the-end-game/435 (Accessed Aug. 2019).

[19] N. C. Karmakar, E. M. Amin, and J. K. Saha, *Chipless RFID Sensors*. Wiley, 2016.

[20] C. S. Hartmann, "A global SAW ID tag with large data capacity," in *Proc. IEEE Ultrasonics Symp.*, pp. 65–69, Oct. 2002.

[21] S. Shretha, J. Vemagiri, M. Agarwal, and K. Varahramyan, "Transmission line reflection and delay-based ID generation scheme for RFID and other applications," *Int. J. Radio Freq. Identification Technol. Appl.*, vol. 1, pp. 401–416, 2007.

[22] J. McVay, A. Hoorfar, and N. Engheta, "Space-filling curve RFID tags," in *Proc. 2006 IEEE Radio and Wireless Symp.,* pp. 17–19, Apr. 2006.

[23] H. Sagan, *Space-Filling Curves*. Springer-Verlag, 1994.

[24] I. Jalaly and D. Robertson, "Capacitively-tuned split microstrip resonators for RFID barcodes," *2005 European Microwave Conference*, vol. 2, Oct. 2005.

[25] S. Preradovic, I. Balbin, N. C. Karmakar, and G. F. Swiegers, "Multiresonator-based chipless RFID system for low-cost item tracking," *IEEE Trans. Microw. Theory Tech.*, vol. 57, pp. 1411–1419, Apr. 2009.

[26] S. Preradovic and N. Karmakar, "Design of fully printable planar chipless RFID transponder with 35-bit data capacity," *2009 European Microwave Conference,* pp. 13–16, Sept. 2009.

[27] I. Balbin and N. C. Karmakar, "Phase-encoded chipless RFID transponder for large-scale low-cost applications," *IEEE Microw. Wireless Compon. Lett.*, vol. 19, pp. 509–511, Aug. 2009.

[28] A. Vena, E. Perret, and S. Tedjini, "A fully printable chipless RFID tag with detuning correction technique," *IEEE Microw. Wireless Compon. Lett.*, vol. 22, pp. 209–211, Mar. 2012.

[29] A. Vena, E. Perret, and S. Tedjini, "RFID chipless tag based on multiple phase shifters," *2011 IEEE MTT-S International Microwave Symposium*, Jun. 2011.

[30] A. Vena, E. Perret, and S. Tedjini, "Chipless RFID tag using hybrid coding technique," *IEEE Trans. Microw. Theory Tech*, vol. 59, pp. 3356–3364, Nov. 2011.

[31] J. Havlicek, M. Svanda, J. Machac, and M. Polivka, "Improvement of reading performance of frequency domain chipless RFID transponders," *Radioengineering*, vol. 25, pp. 219–229, Apr. 2016.

[32] L. Xu and K. Huang, "Design of compact trapezoidal bow-tie chipless RFID tag," *Int. J. Antennas Propag.*, vol. 2015, pp. 1–7, May 2015.

[33] A. Vena, E. Perret, and S. Tedjini, *Chipless RFID based on RF Encoding Particle*. Elsevier, 2016.

[34] Avionics Department of the Naval Air Warfare Center Weapons Division, Radar Cross Section. *Electronic Warfare and Radar Systems Engineering Handbook*, 2003.

[35] Ö. Ergül and L. Gürel, *The Multilevel Fast Multipole Algorithm (MLFMA) for Solving Large-Scale Computational Electromagnetics Problems.* Wiley, 2014.

[36] E. Çetin, M. B. Şahin, and Ö. Ergül, "Numerical study of chipless tags for radio-frequency-identification (RFID) applications," *Advanced Electromagnetics*, vol. 8, pp. 10–17, Feb. 2019.

[37] E. Çetin, M. B. Şahin, and Ö. Ergül, "Array strategies for improving the performances of chipless RFID tags," in *Proc. IEEE Antennas and Propagation Soc. Int. Symp.*, pp. 2015–2016, Jul. 2018.

[38] E. Çetin, M. B. Şahin, and Ö. Ergül, "Design of highly distinguishable chipless tag for radio-frequency-identification applications," *URSI-Turkey Scientific Symp.*, Sep. 2018.

[39] I. Panchenko, "Three-sigma rule," *Encyclopedia of Mathematics*, Dec. 2018. [Online]. Available at: http://www.encyclopediaofmath.org/index.php?title=Three-sigma_rule&oldid=43551 (Accessed Aug. 2019).

[40] F. Mutlu, C. Önol, B. Karaosmanoğlu, and Ö. Ergül, " Inkjet-printed cage-dipole antennas for radio-frequency applications," *IET Microwaves, Antennas & Propagation*, vol. 11, pp. 2016–2020, Nov. 2017.

[41] G. Tarapata, D. Paczesny, and K. Kawecki, "Characterization of inkjet printing HF and UHF antennas for RFID applications," in *Proc. SPIE*, pp. 32–38, Oct. 2013.

[42] E. Tekin, P. J. Smith, and U. S. Schubert, "Inkjet printing as a deposition and patterning tool for polymers and inorganic particles," *Soft Matter*, vol. 4, pp. 703–713, Feb. 2008.

[43] C. A. Balanis, *Antenna Theory, Analysis and Design*. Wiley-Interscience, 2005.

[44] W. Wiesbeck and D. Kähny, "Single reference, three target calibration and error correction for monostatic, polarimetric free space measurements," in *Proc. IEEE*, vol. 79, pp. 1551–1558, Oct. 1991.

[45] R.A. Fisher, *Statistical Methods for Research Workers*, 13th Edition. Hafner Publishing, 1967.

[46] C. Herrojo, F. Paredes, J. Mata-Contreras, and F. Martin, "Chipless-RFID: A Review and Recent Developments, " *Sensors,* vol 19, 3385, Aug. 2019.

[47] R. Rezaiesarlak, and M. Manteghi, "Complex-natural-resonance-based design of chipless RFID tag for high density data", *IEEE Trans. Antennas Propag.*, vol. 62, pp. 898–904, Feb. 2014.